Benchmarking of the MIT High Temperature Gas-Cooled Reactor TRISO-Coated Particle Fuel Performance Model

by

Michael A. Stawicki

SUBMITTED TO THE DEPARTMENT OF NUCLEAR SCIENCE AND ENGINEERING IN PARTIAL FULFILLMENT OF THE REQUIREMENTS FOR THE DEGREES OF

MASTER OF SCIENCE IN NUCLEAR SCIENCE AND ENGINEERING
AND
BACHELOR OF SCIENCE IN NUCLEAR SCIENCE AND ENGINEERING
AT THE
MASSACHUSETTS INSTITUTE OF TECHNOLOGY

May 2006
[June 2006]

Signature of Author _____

Michael A. Stawicki
Department of Nuclear Science and Engineering
May 5, 2006

Certified by _____

Ronald G. Ballinger
Professor of Nuclear Science and Engineering
Associate Professor of Materials Science and Engineering
Thesis Supervisor

Accepted by _____

Andrew C. Kadak
Professor of the Practice of Nuclear Science and Engineering
Thesis Reader

Accepted by _____

Jeffrey A. Coderre
Associate Professor of Nuclear Science and Engineering
Chairman, Departmental Committee on Graduate Students

Benchmarking of the MIT High Temperature Gas-Cooled Reactor TRISO-Coated Particle Fuel Performance Model

by

Michael A. Stawicki

Submitted to the Department of Nuclear Science and Engineering on May 5, 2006 in partial fulfillment of the requirements for the degrees of Master of Science in Nuclear Science and Engineering and Bachelor of Science in Nuclear Science and Engineering

ABSTRACT

MIT has developed a Coated Particle Fuel Performance Model to study the behavior of TRISO nuclear fuels. The code, TIMCOAT, is designed to assess the mechanical and chemical condition of populations of coated particles and to determine the failure probability of each of the structural coating layers. With this, the code determines the overall particle failure rate. TIMCOAT represents a significant advancement over earlier codes as it includes a pyrocarbon crack induced particle failure mechanism, which applies probabilistic fracture mechanics.

As part of the International Atomic Energy Agency (IAEA) Coordinated Research Program (CRP) on coated particle fuel technology, a code benchmark has been developed by the Idaho National Laboratory (INL). The benchmark includes simple analytic studies and more complex simulations of TRISO particles from past and future experiments. For each study a large variety of particle parameters are specified.

This thesis reports TIMCOAT's results from the benchmark study. As this was a blind benchmark, no other results are available for comparison. However, TIMCOAT is able to independently calculate several of the parameters specified by the benchmark, and comparisons are made between results obtained using IAEA parameters and TIMCOAT calculated parameters.

The material properties which describe the effects of irradiation on pyrolytic carbon are the focus of the comparison. The rates of irradiation induced creep and swelling calculated by TIMCOAT and the rates provided in the benchmark differed by a factor of two to four in some cases and led to differences in particle failure rate by several orders of magnitude. In addition, varying the uncertainties in these and other parameters was found to have a large impart on the failure probability.

It is concluded that accurate modeling of TRISO particles depends on having very high accuracy data describing material properties and a very good understanding of the uncertainties in those measurements.

Thesis Supervisor: Ronald G. Ballinger
Title: Professor of Nuclear Science and Engineering and Associate Professor of Materials Science and Engineering

Acknowledgements

I would like to offer special thanks to my advisor, Professor Ronald Ballinger, for affording me the opportunity to work on this project and for his guidance and support throughout the course of the endeavor; and to Professor Andrew Kadak for his assistance in reviewing my work and his continued tutelage during my time at MIT.

I acknowledge the efforts of those who came before who worked to create and improve TIMCOAT: Dr. Jing Wang who received his PhD for the initial development of the code, Jane Diecker who began work on integrating TIMCOAT's chemistry models, and Chaiyod Soontrapa who completed the first series of code optimizations.

Appreciation is also extended to the Nuclear Science and Engineering Department at MIT and the Nuclear Regulatory Commission for their part in funding this project.

Finally, I offer a note of personal gratitude to my parents, Al and Mary Stawicki, and my fiancé Dr. Robin Chan for their love, support, and encouragement.

Far and away the best prize that life offers is the chance to work hard at work worth doing.

~ Theodore Roosevelt, Speech in New York September 7, 1903

Table of Contents

Table of Figures

Table of Tables

1 Introduction

At the current time it can be said we are in the midst of a nuclear renaissance. Nuclear technologies are already an important source of electric power, but as governments and the public continue to become interested in developing an inexpensive, safe, and environmentally friendly method to generate electricity, there has been renewed interest in nuclear power. One of the advanced systems being considered is the High Temperature Gas-cooled Reactor (HTGR) as it seems to have the potential to meet these criteria. HTGRs use ceramic coated fuel particles embedded in a graphite matrix. Before any HTGR system can be deployed, however, acceptable performance characteristics of these ceramic coated fuel particles must first be demonstrated. To this end, research groups in several countries have begun to develop performance models to predict the behavior of these particles. In conjunction with the International Atomic Energy Agency Coordinated Research Program (IAEA-CRP), the Idaho National Laboratory (INL) has developed a series of benchmark cases [1] to facilitate comparisons between the models of each of the research participants.

This thesis describes the results of these benchmark cases obtained by the MIT fuel performance model. As a precursor, a brief description of HTGRs and ceramic coated fuel is provided before a detailed description of the MIT model.

1.1 Review of High Temperature Gas-cooled Reactors

Two types of HTGRs began to be developed in the 1950s and reemerged in the 1980s. One type, the block type reactor, uses prismatic blocks which contain the fuel as well as cooling channels and slots for control absorbers and instrumentation. The fuel consists of ceramic microspheres approximately 1 mm in diameter pressed into compacts as shown in Figure 1-1. The other type of reactor, The Pebble Bed Reactor (PBR), uses these same fuel microspheres embedded in 6 cm graphite spheres or "pebbles" each containing about 15,000 microspheres. This arrangement is shown in Figure 1-2. The PBR is somewhat unique among reactor systems in that the pebbles flow through the core during operation. Fresh, un-irradiated or recycled pebbles are dropped into the top or the core vessel, and

used pebbles are extracted from the bottom. Coolant does not flow through channels but rather through the bulk of the vessel with control absorbers and instrumentation at the core periphery.

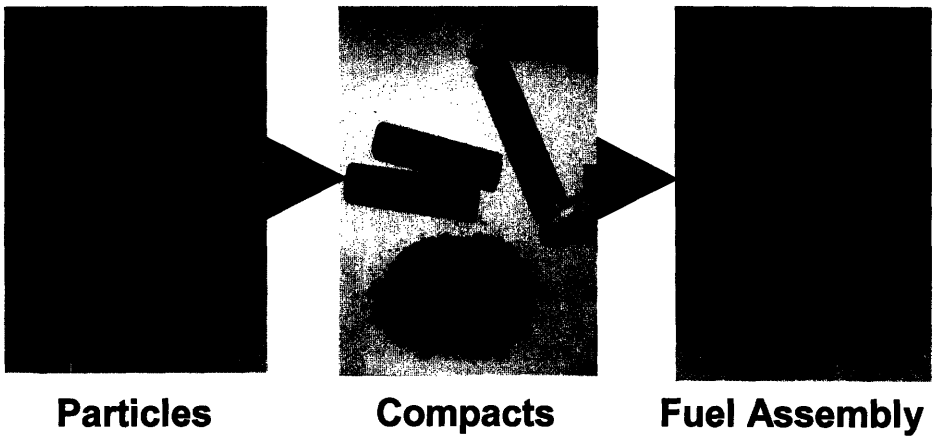

Figure 1-1: Illustration of General Atomics Prismatic Block HTGR Fuel

Both of these HTGR systems share a set of common design criteria intended to enhance passive safety characteristics. Helium, as a single phase noble gas, is used as coolant because of its favorable chemical and neutronic properties. Fuel is contained in coated microspheres, as mentioned, which are supposed to be able to contain all radiotoxic fission products up to a temperature of approximately 1600°C. This temperature is selected, since the reactor is designed such that the fuel temperature will not exceed 1600°C during any transient. This is done by limiting the power density to 3 – 4 MW/m^3 and by ensuring decay heat can be removed by passive mechanisms such as natural convection and radiation. Graphite is used for all core structures and as matrix material because its temperature limit is far above 1600°C. The reactor is also able to shut down using only free falling control rods [2].

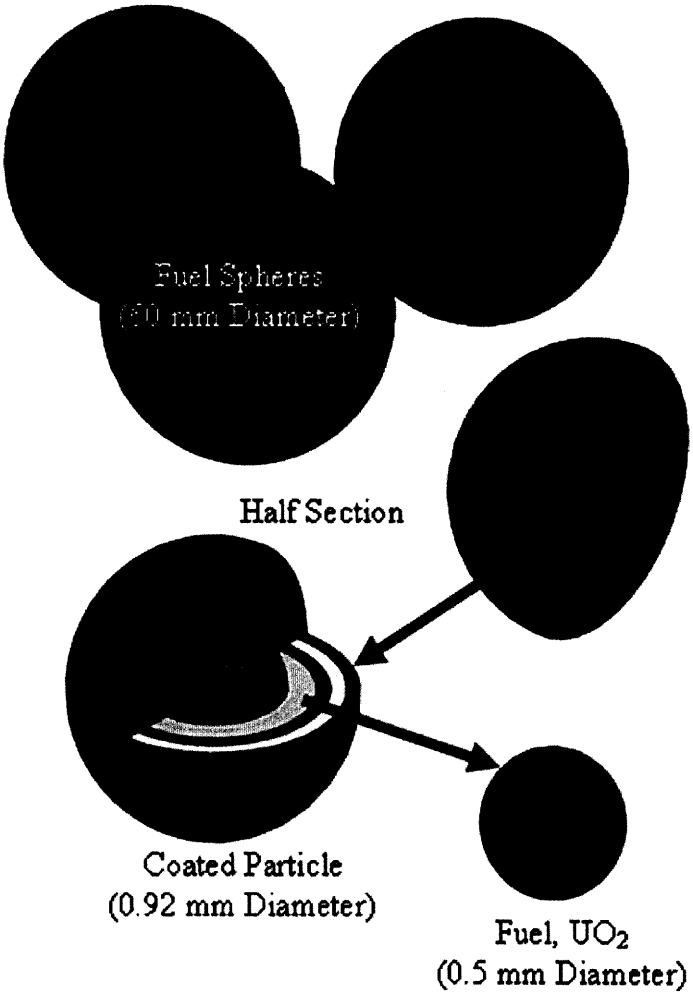

Figure 1-2: Illustration of PBR HTGR Fuel

Both experimental and commercial HTGRs are currently under development. The PBR is being developed by ESKOM of South Africa, British Nuclear Fuels (BNFL) of the United Kingdom, and the Institute of Nuclear Energy Technology, a part of Tsinghua University in Beijing, China. The block type reactor is being considered by a consortium of General Atomics in the United States, MINATOM in Russia, Framatome in France, and Fuji Electric in Japan. In addition, numerous other programs and testing facilities exist in about 10 countries.

1.2 Coated Fuel Particles

Both of the HTGR systems discussed in Section 1.1 use ceramic coated particles to contain the fuel. The purpose of these particles is twofold. They not only contain fissile isotopes, which produce energy, but are also intended as a barrier to the release of fission products into the environment. The typical fuel particle has five components. At the center is a fuel kernel typically UO_2 or UCO. Surrounding this kernel is a low density pyrolytic carbon buffer layer intended to provide a porous medium to absorb fission products. Around that are three near isotropic structural layers. The inner and outer layers are constructed of a high density pyrolytic carbon, the IPyC and OPyC, respectively. Between these PyC layers is a layer of silicon carbide (SiC), which serves as the pressure vessel for the particle. These particles are called tri-isotropic or TRISO particles. The name refers to the three isotropic structural layers, the IPyC/SiC/OPyC. Figure 1-3 shows a micrograph of such a particle, and Table 1-1 describes the properties of each layer in further detail.

To access the performance of the TRISO design, it is necessary to know the failure probability of each of the three structural layers. Before knowing this, the mechanisms by which each of the layers may fail must be understood. These mechanisms are the subject of the next section.

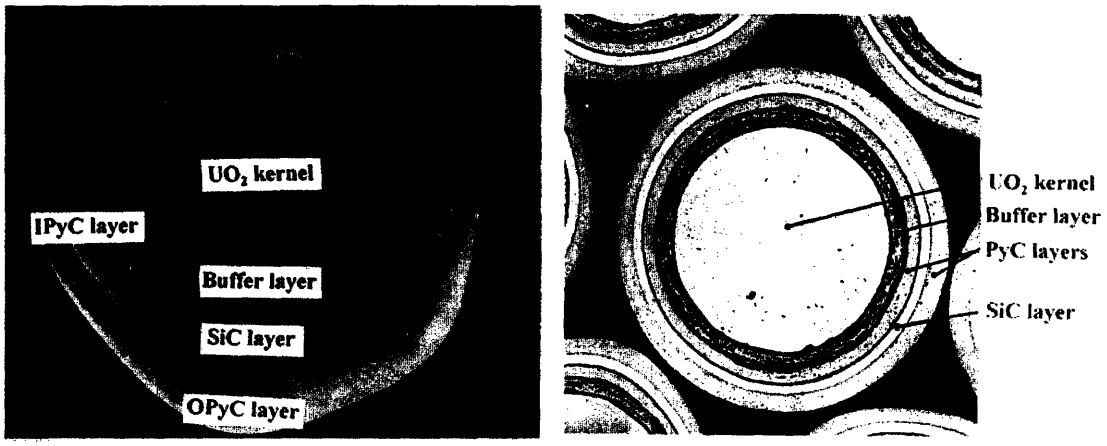

Figure 1-3: Micrograph of a typical TRISO Particle [2]

Table 1-1: Properties of Coated Particle Layers [4]

LAYER	DESCRIPTION
Fuel Kernel	The kernel is typically 300 – 600 μm in diameter and contains UO_2 or UCO. During the nuclear fission process, the kernel produces a mixture of radioactive fission products. Among the fission products are gaseous species that cause stresses in the coatings, as well as solid metallic species that chemically interact with the coatings. The fuel kernel swells with increasing burn-up of the fuel.
Pyrolytic Carbon Buffer Layer	This layer is in direct contact with the kernel. The density of this layer is in the range of 0.9 – 1.1 g/cm^3, compared with theoretical density of 2.26g/cm^3 for pyrocarbon. The porous buffer layer is an absorber of fission recoils and provides free volume to accommodate fission products and kernel swelling. It also serves as a mechanical separation between the kernel and the structural coating layers.
IPyC	This is the first of the three structural layers and has a density of 1.8 – 2.0g/cm^3. The layer forms the first barrier against the fission gas release from the fuel kernel and resists migration of actinides and fission products. The IPyC layer is a practically impenetrable barrier for fission gases like Krypton and Xenon and the fission product Iodine, but it becomes pervious for Cesium and Strontium at high (higher than normal operational) temperatures. It does not stop Silver.
SiC	The SiC layer has a density of about 3.20g/cm^3, which is very close to its theoretical density. This layer provides retention of all fission products under normal operating conditions. It must remain intact to prevent the release of radioactive material from the particle. SiC is attractive because it has a higher mechanical strength than dense PyC layers, and it is highly stable under fast neutron irradiation. Unfortunately, at temperatures above 1600°C, SiC will be corroded by Palladium and other rare earth elements as well as become porous to Cesium, Strontium, and Silver. In addition, at temperatures in the region of 2000 - 2200°C, thermal decomposition of SiC takes place.
OPyC	This layer protects the SiC layer from being damaged during the fuel manufacturing process. It also compresses the SiC layer as it shrinks during fast neutron irradiation.

1.3 Failure Mechanisms for Coated Particles

Failure mechanisms for TRISO particles can be broadly classified into two categories, mechanical mechanisms and chemical mechanisms. Mechanical mechanisms are those mechanisms in which failure of a structural layer is the result of a stress that exceeds a material strength failure criterion either due to crack initiation and propagation or due to overloading. Chemical mechanisms refer to those that involve corrosion, decomposition, or other weakening of the structural layers due to elements that build up inside the particle during irradiation. These then induce a mechanical failure. The specific mechanisms that occur in each category are discussed below.

Mechanical Failures:

1.) Over Pressure Failures – during the irradiation of TRISO particles, fission products build up inside the kernel. Some of these fission products are gaseous and migrate into the buffer and out to the structural layers. As the pressure of these gases increase over the life of the particle, they will induce increasing tensile stresses in the structural layers. If the mean tensile stress in any one of the layers exceeds the strength of that layer, the layer fails. This is referred to as an over pressure failure.

2.) Cracking Induced Failures – Early in the irradiation history, pyrocarbon layers shrink in both radial and tangential directions. The shrinkage of the pyrocarbon helps compress the SiC and prevent over pressure failures. As irradiation continues, however, reorientation on the pyrocarbon structure causes it to swell in the radial direction but continue to shrink in the tangential direction. As a result, the pyrocarbon layers can crack, and these cracks can lead to very high local stress concentrations in the silicon carbide layer even while the net stress in the SiC is compressive. This stress concentration cracks and fails the SiC layer.

Chemical Failures:

1.) Fission Product Attack – As fission products are built up and released from the kernel, they migrate to the structural layers and corrode them [5]. The level of corrosion is dependent on the amount of free oxygen and the temperature of the

microsphere. Corrosion is enhanced at higher temperatures. This corrosion thins the effected structural layer and reduces its strength. As a result of this thinning, the existing tensile stresses in the layer are now sufficient to fail it.

2.) Amoeba Effect – The thermally driven migration of the fuel kernel toward the hot side of the microsphere is referred to as the Amoeba Effect [6]. It occurs over time and is more severe at higher temperatures and thermal gradients. For oxide fuels, oxygen reacts with PyC to form CO, which is transported to the cold side of the microsphere causing the kernel to migrate toward to hot side. If this effect is severe enough, the kernel can physically collide with and breach the structural layers as shown in Figure 1-4 .

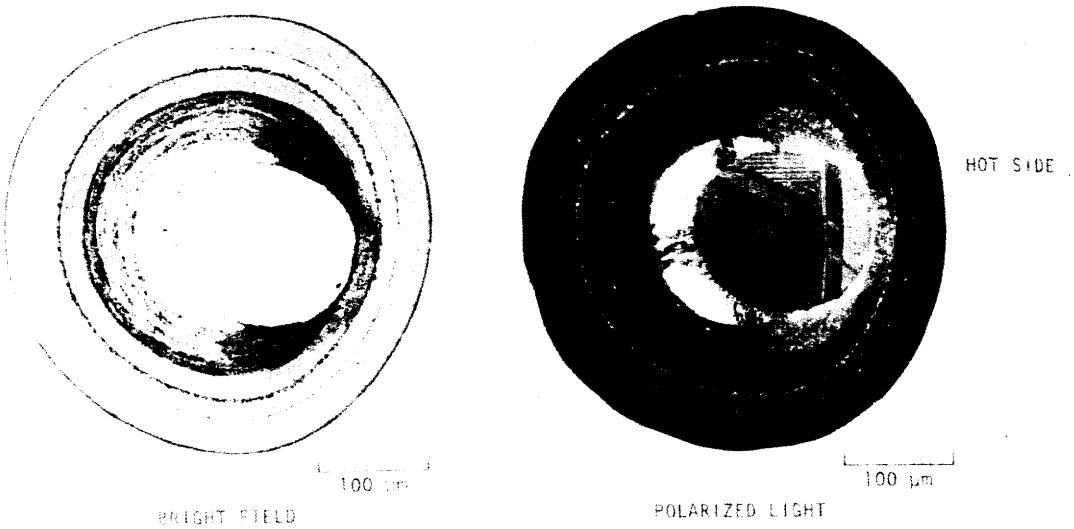

Figure 1-4: Amoeba Effect [7]

In addition to these four failure mechanisms, manufacturing defects and imprecision inherent in the tools used in the manufacture process can either lead to gross particle failure or the substantial weakening of one of the structural layers. It is possible to identify additional mechanisms related to the conditions that would prevail under certain types of HTGR transients, but this information is not pertinent to this thesis. More detail can be found in reference [4]. For the purposes of the INL benchmarking study, only the first two mechanical failure mechanisms, over-pressurization and PyC cracking, are considered. These mechanisms are modeled in the MIT coated particle performance model named TIMCOAT.

2 MIT Coated Particle Performance Model – TIMCOAT

The TIMCOAT code was designed specifically to model TRISO fuel performance in HTGR systems. It is a stochastic program that first calculates the conditions a sample TRISO particle would encounter given a set of input parameters that describe the particle and HTGR system. It then calculates the mechanical and chemical response of the particle to that environment. The mechanical models in TIMCOAT are well developed, while chemical model development is just beginning. As such, only the mechanical models are used in this benchmarking program. Once the code determines the response of the particle, it compares the state of the particle to a set of failure conditions to determine if the particle has failed. It then samples another particle and repeats this process to determine the failure probability of each of the three structural layers.

2.1 Inputs

TIMCOAT requires the user to specify input parameters relating to the TRISO particle and to the HTGR system. A complete list of the needed input parameters is found in Table 2-1, and a sample input file is included in Appendix I. A standard deviation can be supplied for most of the parameters in the table. The standard deviations are used by the model to develop distributions for the value of each particular parameter. The distributions used are presented in Table 4-1.

Table 2-1: TIMCOAT Input Parameters

Parameter	Units	Parameter	Units
IPyC Characteristics		**Fuel Kernel Characteristics**	
IPyC BAF		Fuel Type	
IPyC Coating Rate	μm/min	Oxygen to Uranium Ratio	Atom Ratio
IPyC Crystallite Length	μm	Carbon to Uranium Ratio	Atom Ratio
IPyC Weibull Modulus		U-235 Enrichment	Weight %
IPyC Characteristic Strength	MPa m^3/Weibull Modulus	Kernel Theoretical Density	g/cc
IPyC Density	g/cc	Kernel Density	g/cc
IPyC Thickness	μm	Kernel Diameter	μm
SiC Characteristics		**PyC Buffer Layer Characteristics**	
SiC Weibull Modulus		Buffer Theoretical Density	g/cc
SiC Characteristic Strength	MPa m^3/Weibull Modulus	Buffer Density	g/cc
SiC Fracture Toughness	MPa $\mu m^{1/2}$	Buffer Thickness	μm
SiC Density	g/cc	**General Properties of Dense PyC**	
SiC Thickness	μm	PyC Modulus of Elasticity	MPa
SiC Modulus of Elasticity	MPa	PyC Poisson's Ratio	
SiC Poisson's Ratio		PyC Poisson's Ratio In Creep	
SiC Coefficient of Thermal Expansion	K^{-1}	PyC Coefficient of Thermal Expansion	K^{-1}
OPyC Characteristics		PyC Creep Coefficient	(MPa 10^{25} n/m^2)$^{-1}$
OPyC BAF		PyC Swelling Strain Rate	(ΔL/L) 10^{25} n/m^2
OPyC Coating Rate	μm/min	**Irradiation Conditions in HTGR System**	
OPyC Crystallite Length	μm	Irradiation Duration	EFPD
OPyC Weibull Modulus		End of Life Burnup	% FIMA
OPyC Characteristic Strength	MPa m^3/Weibull Modulus	End of Life Fluence	10^{25} n/m^2
OPyC Density	g/cc	Irradiation Temperature	C
OpyC Thickness	μm	Internal Pressure	MPa
Numeric Modeling Parameters		Ambient Pressure	MPa
Elapsed Time	Days		
Time Step	Days		

2.2 Simulation Types and Modes

TIMCOAT allows three different types of simulations to be run. The simplest is a constant power, constant temperature simulation. In this type of simulation the user enters an average irradiation temperature, an end of life fluence, a burnup, an irradiation time, and a time step. The code then assumes that fluence and burnup accumulate at a constant rate over the irradiation time and calculates the conditions in the particle at each time step. This method of simulation is the fastest to setup and is useful for parametric studies interested in the effects of varying material properties on the stress distributions in a normalized particle. It does not, however, allow to user to simulate to effects of temperature and power level variation. It also does not allow the user to alter the time step over the irradiation history to reduce calculation time.

The next more complex simulation type is the irradiation test. This method requires the user to supply an additional input file that specifies full power days, temperature, burnup, and fluence at any increment the user chooses. The code then calculates the conditions in the particle at these increments. This method is needed when temperatures and powers are not constant, and it has the additional advantage of allowing the user to adjust the time step to improve calculation efficiencies. This is particularly advantageous when simulating particles that have large end of life fluences. This is the method of simulation that is used for all of the benchmarks.

The third mode of simulation is designed specifically for the simulation of PBRs. It requires the user not only to provide an irradiation history as with the second method but also a power shape in the PBR system. This method is not used in this thesis and will not be discussed further. Additional information can be found in reference [8].

In addition to these three simulation types, the code can be run in several modes. If the user is interested in the detailed stress distributions in a nominal particle, then the code can be run in the nominal mode in which the standard deviations on all the parameters are ignored. If the user wishes to simulate a population of particles, then the code is run in sampling mode where it samples particle parameters from the input distributions in the traditional Monte Carlo sense. The user also has the option to enable or disable the failure evaluation portion of the model and to choose which failure mechanisms to consider [4].

2.3 Model Structure

Once the user provides the necessary input parameters and specifics a simulation type and mode, the code begins to execute. Assuming the user wishes to study the failure probability of a population of particles, the code first samples a particle and power history, then determines the power density and neutron flux the particle is exposed to in the next time step. It then determines the temperature distribution in the particle, the accumulated fast neutron fluence, and the quantity of fission gases released from the fuel

kernel. This information is then passed to a mechanical model that determines the stress distribution in the particle and any dimensional or material property changes due to chemical effects. The stress distributions are then passed to the failure model that determines if the particle fails. If so, simulation on this particular particle stops and another particle is sampled. If not, the particle is advanced to the next time step. Figure 2-1 shows a flowchart of this procedure.

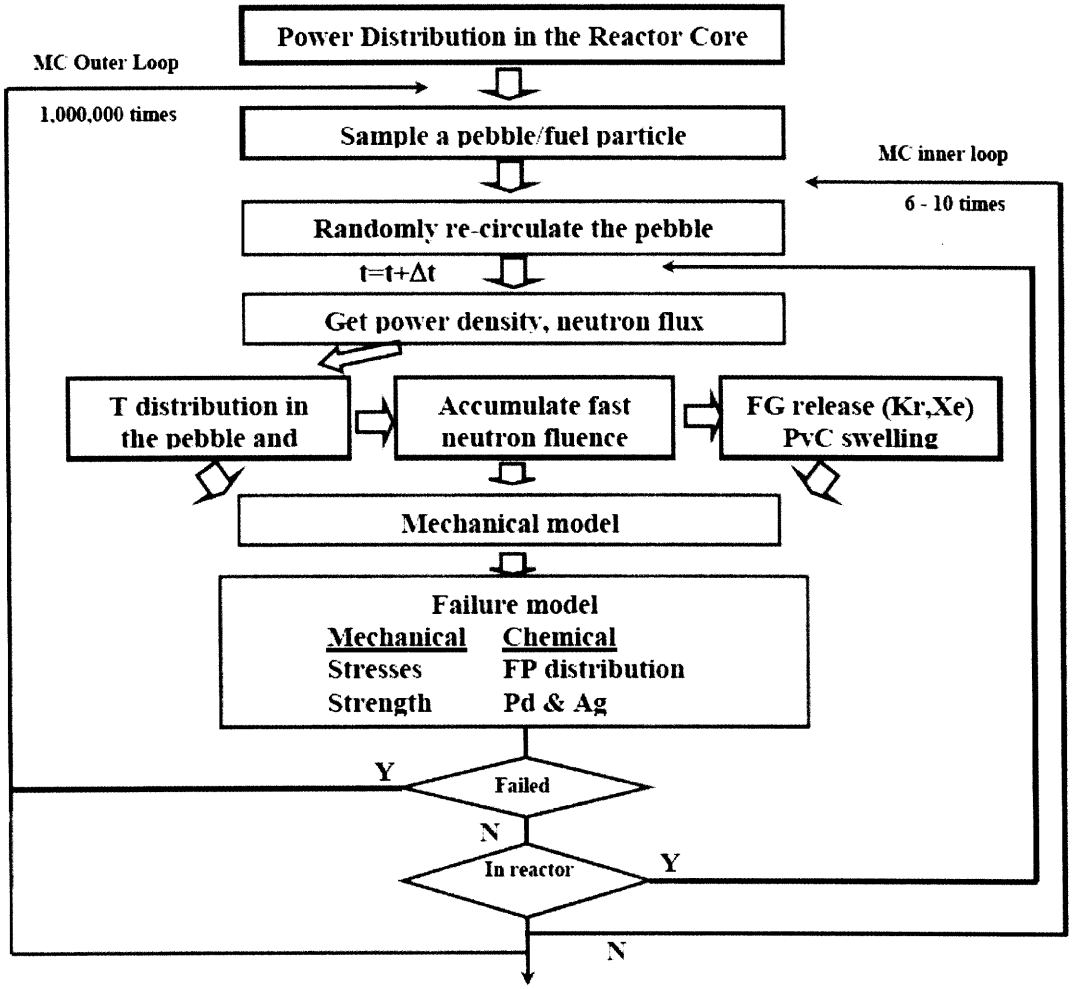

Figure 2-1: Flowchart for TIMCOAT Modeling Procedure [8]

If the user wishes a more simplified version of the code to run, the appropriate loops and components can be easily deactivated by adjusting flags in the input file. A complete derivation of all the models used in TIMCOAT can be found in reference [4].

2.4 Output

The output generated by the code depends on whether a nominal particle is being considered to determine its physical behavior under irradiation or if a population of particles is being simulated to determine failure probabilities. A brief summary of the output parameters that are generated for each of the three structural layers is given in Table 4-5.

Table 2-2: TIMCOAT Output Parameters

Output Parameter	Function Of	Format
Nominal Particle		
Radial and Tangential Stress	Fast neutron fluence	Table
Radial and Tangential Strain	Fast neutron fluence	Table
Displacement	Fast neutron fluence	Table
Swelling Rates	Irradiation EFPD	Table
Irradiation Temperature, Pressure	Time	Table
Burnup and Fluence	Time	Table
Sampled Population of Particles		
Complete listing of input parameters for each failed particle	Index	Table
Maximum Radial and Tangential Stress	Population Average	Table
Minimum Radial and Tangential Stress	Population Average	Table
Failure Probability	Population Average	Table
Failure Cause for each failure	Index	Table
Time, Stress, Fluence, Burnup at failure	Parameter bounds	Histogram
Time to SiC Failure after each PyC Failure	Fast neutron fluence	Histogram

3 IAEA-CRP Normalized Coated Particle Benchmarks

The IAEA-CRP benchmark program for normalized coated particle fuel performance is in three parts and consists of a total of 11 cases. A normalized particle refers to one whose parameters are the mean value of the input distributions. Therefore, results from these particles are deterministic and no uncertainties are calculated. The first part consists of simple analytical calculations on simplified, un-irradiated, coated particles to test tangential stress calculations in the layers. The second part again tests simplified, coated particles and is designed to test the modeling of various mechanical properties of the pyrocarbon layers. The third part models TRISO particles under a variety of temperature and irradiation conditions. In each of these three parts, failure probabilities are not calculated. It is assumed that the particle does not fail under the given conditions, and the corresponding stress distributions in the layers are calculated. Failure probabilities will be the subject of Section 4 which includes an additional two parts.

Each case specifies a metric of comparison, which is a single parameter or several parameters from the model that are to be explicitly reported. Results for each metric from each of these three parts will be presented and discussed in turn. For reference, input parameters for each of the 11 cases can be found in Appendix I and corresponding irradiation histories can be found in Appendix II.

3.1 Part 1: Analytical Mechanical Benchmark Cases

This portion of the benchmark consists of three cases. All three consider a single normalized, un-irradiated particle. Each of the cases is described and then data for the metric of comparison is given.

3.1.1 Description of Cases

Case 1: Elastic SiC – a particle consisting of a fuel kernel, a pyrocarbon buffer and only a single structural layer, SiC, is modeled. The particle is not under any thermal stress and is subject to a constant internal and external pressure. The gradient

between these pressures creates tensile stresses in the SiC layer. The metric of comparison in this case is the maximum tensile stress in the SiC.

Case 2: Simple BISO – the particle modeled in this case is identical to the particle modeled in case 1 except that the single structural layer is now IPyC instead of SiC. Again, the metric of comparison is the maximum tangential stress in the IPyC layer.

Case 3: IPyC / SiC Composite – a particle with a fuel kernel, a buffer and two structural layers, an IPyC and SiC, is considered here. Again there are no thermal stresses and the particle is subject to constant internal and external pressures. The metric of comparison is the maximum tangential stress in each of the two structural layers.

The dimensions of each of these particles are provided in diagrams in Appendix III.

3.1.2 Results

The radial and tangential stresses as a function of radial location in the structural layers are presented in Figure 3-1, Figure 3-2 and Figure 3-3 for Case 1, 2, and 3, respectively. The specific comparison metrics are shown in Table 3-1.

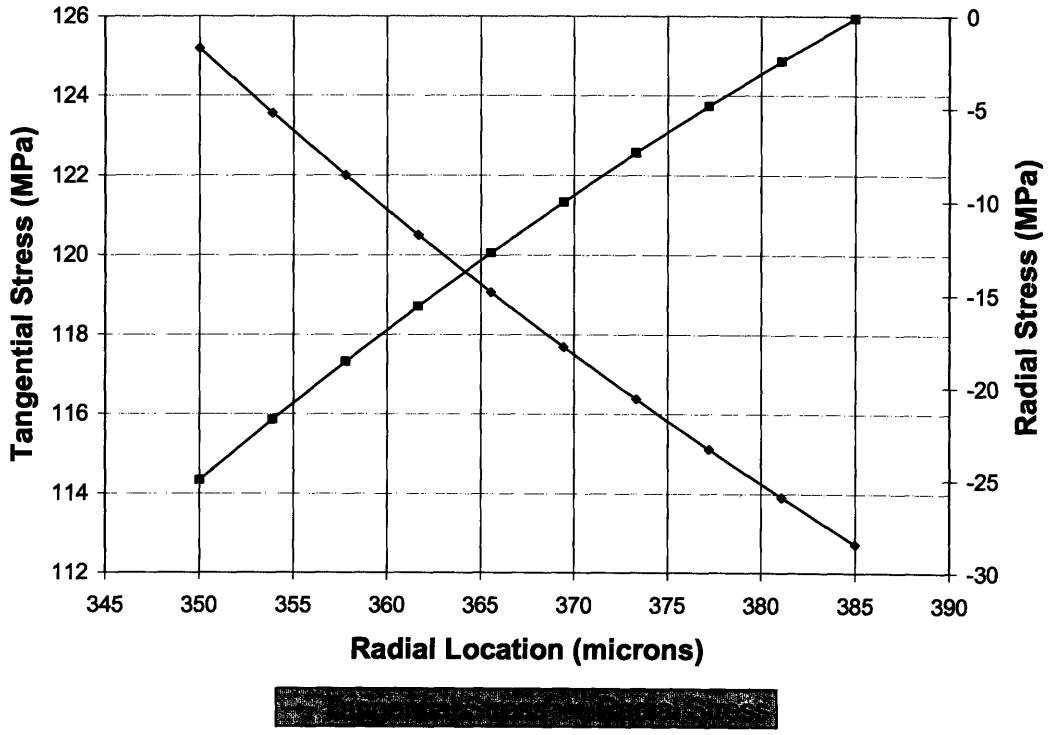

Figure 3-1: Radial and Tangential Stresses in SiC for Case 1

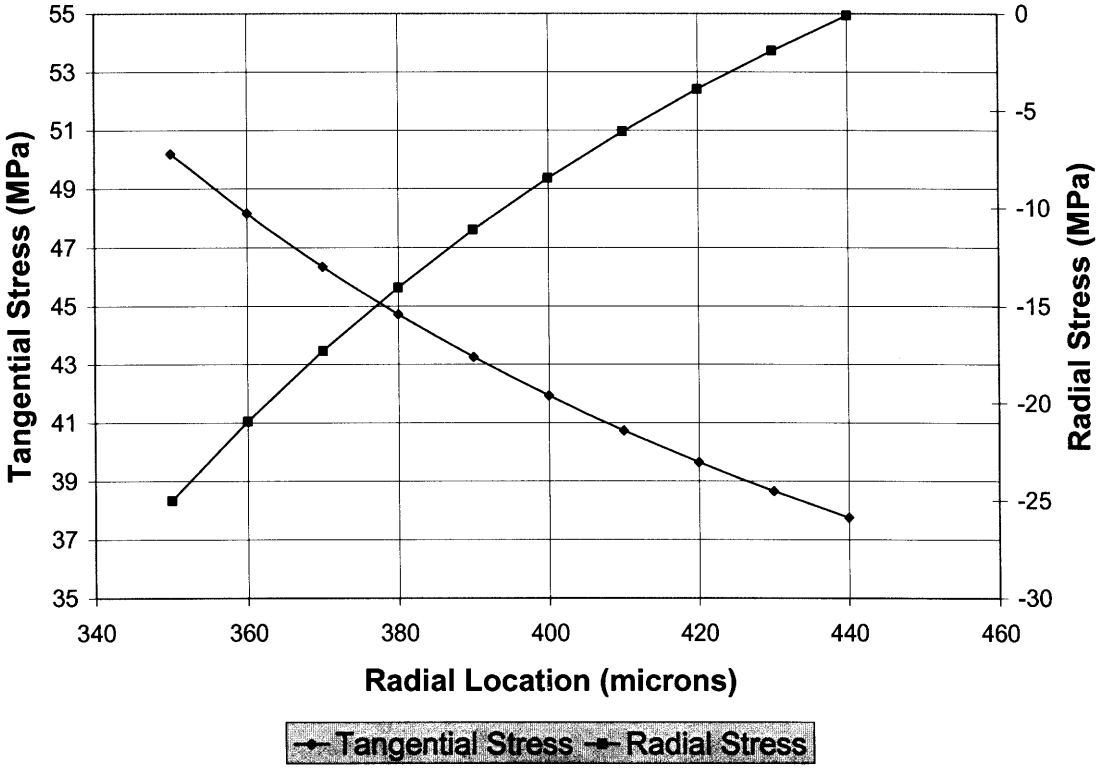

Figure 3-2: Radial and Tangential Stresses in IPyC for Case 2

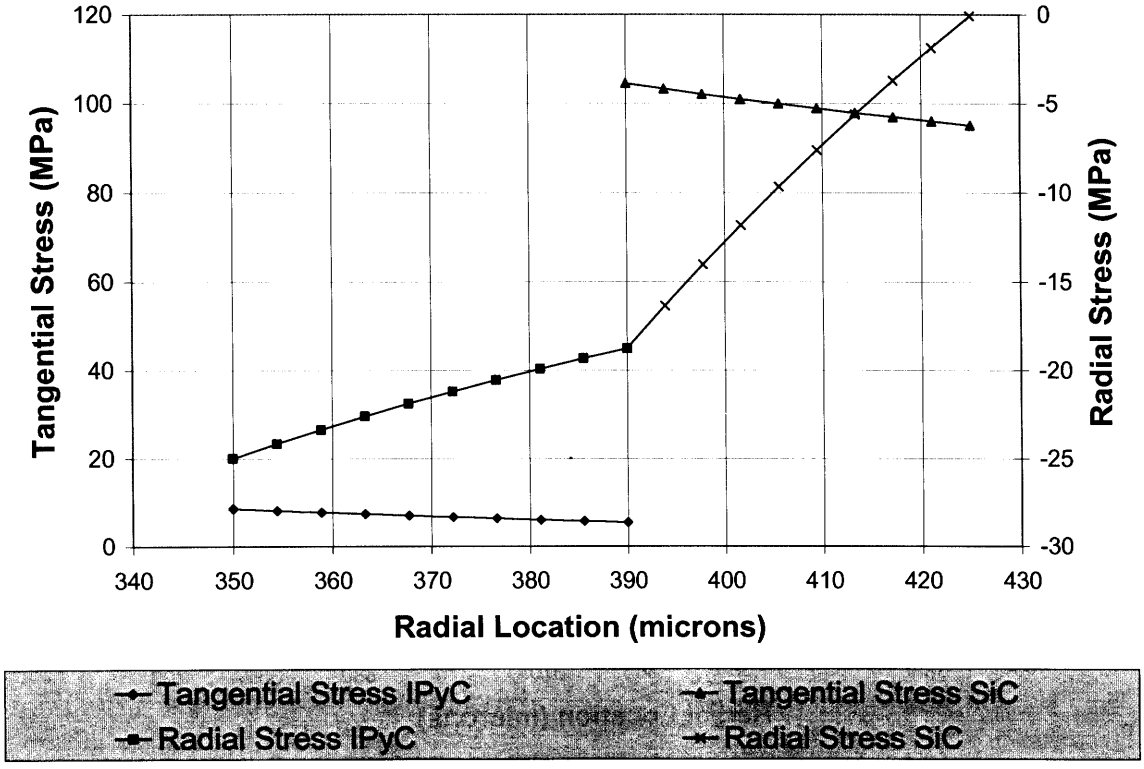

Figure 3-3: Radial and Tangential Stresses in IPyC and SiC for Case 3

Table 3-1: Comparison Metrics for Cases 1, 2 and 3

Case	Comparison Metric	Stress (MPa)
1	Maximum Tangential Stress in SiC	125.2
2	Maximum Tangential Stress in IPyC	50.20
3	Maximum Tangential Stresses in IPyC and SiC	IPyC: 8.701 SiC: 104.5

Case 1 is elastic SiC, so it is simple to analytically calculate the stresses so as to confirm the results of the code. The radial and tangential stresses, σ_r and σ_t, in a thick shell can be calculated as follows [9]:

$$\sigma_r = \frac{2A}{3} + \frac{B}{2r^3} \qquad \sigma_t = A - \frac{\sigma_r}{2}$$

Where r is the radial position in the particle and A and B are constants that come from applying boundary conditions on the radial stress,

$$\sigma_r(r_i) = -P_i \qquad \sigma_r(r_o) = -P_o$$

$$A = -\frac{3}{2}\frac{P_i r_i^3 - P_o r_o^3}{r_i^3 - r_o^3} \qquad B = 2(P_i - P_o)\frac{r_i^3 r_o^3}{r_i^3 - r_o^3}$$

P_i and P_o refer to the internal and external pressures, respectively, and r_i and r_o refer to the inner and outer radii of the layer. The stresses from these calculations are compared to those from TIMCOAT in Table 3-2. They are in perfect agreement.

Table 3-2: Comparison of Analytical and TIMCOAT Calculations Case 1

	Radial (MPa)		Tangential (MPa)	
Radial Position (μm)	TIMCOAT	Analytical	TIMCOAT	Analytical
350.000	-25.000	-25.000	125.190	125.190
353.889	-21.735	-21.735	123.558	123.558
357.778	-18.611	-18.611	121.995	121.995
361.667	-15.620	-15.620	120.500	120.500
365.556	-12.754	-12.754	119.067	119.067
369.444	-10.008	-10.008	117.694	117.694
373.333	-7.375	-7.375	116.378	116.377
377.222	-4.850	-4.850	115.115	115.115
381.111	-2.426	-2.426	113.903	113.903
385.000	-0.100	-0.100	112.740	112.740

3.1.3 Discussion

These first three cases are sufficiently simple that it is possible to predict the nature of the results a priori. It is expected that the radial stresses will be equal to the prevailing pressure at the inner surface and then decrease in magnitude through the structural layers to equal the lower external pressure at the outer surface. If the structural layers were planer or cylindrical, then the stresses would decrease linearly through the layer as the cross-sectional area at each location would be constant. As the structural layers are spherically shaped, however, the cross-sectional area increases through the layer, and so it is expected that the rate of decrease of stress in going from the inner surface to the outer surface decreases. These two phenomena are clearly seen in Figure 3-1and Figure 3-2.

An important assumption that TIMCOAT makes is shown Figure 3-3. The radial stress between the outer surface of the IPyC and the inner surface of the SiC is continuous. This boundary condition is set in the code for computational efficiency. It is an assumption that the code makes that is not necessarily physically accurate. In situations were the layers might become debonded or lose integrity during irradiation, it would not be expected that the radial stresses from one layer to the next be continuous. Accordingly, this assumption introduces some error into the code's calculations that is not presently quantifiable.

With regard to the tangential stresses, it should be the case that they be largest in magnitude where the radial stresses are largest and that they exhibit the same concavity as the radial stresses. This is consistent with the three figures.

3.2 Part 2: Pyrocarbon Mechanical Response Benchmark Cases

The next four cases in the benchmarking program study the variation of stress distributions in pyrocarbon due to irradiation effects. Under irradiation, pyrocarbon experiences dimensional changes and because PyC is a heterogeneous mixture of anisotropic graphite crystallites, its behavior is complicated. There are two important phenomena, irradiation induced swelling and irradiation induced creep.

Irradiation induced swelling in PyC is dominated by two mechanisms, densification and microstructure reorientation. PyC layers are manufactured by a vapor deposition process that deposits thin planes of material on the fuel microsphere. As the PyC is irradiated, coalescence of vacancies and voids shrinks the PyC parallel to the deposition plane; this is densification. Interstitial defects cause crystallites to reorient and grow perpendicular to the plane; this is reorientation. During the manufacture process, thermal shrinkage cracks form and are preferentially aligned parallel to the coating plane. These cracks provide space for initial reorientation, and so when PyC is first irradiated, only densification is observed and the material experiences a net decrease in volume. As the dose to the material increases, the competition between densification and reorientation results in increased porosity parallel to the coating plane and the shrinkage rate drops, eventually to zero. After this point, additional irradiation results in an increasing rate of swelling perpendicular to the coating plane both as a result of reorientation and the porosity being generated. Consequently, the PyC volume shrinkage stops, and the volume begins to increase until differential strains result in disintegration [10]. Figure 3-4 illustrates this process. In the figure the circles represent voids, and the bars represent graphite crystallites.

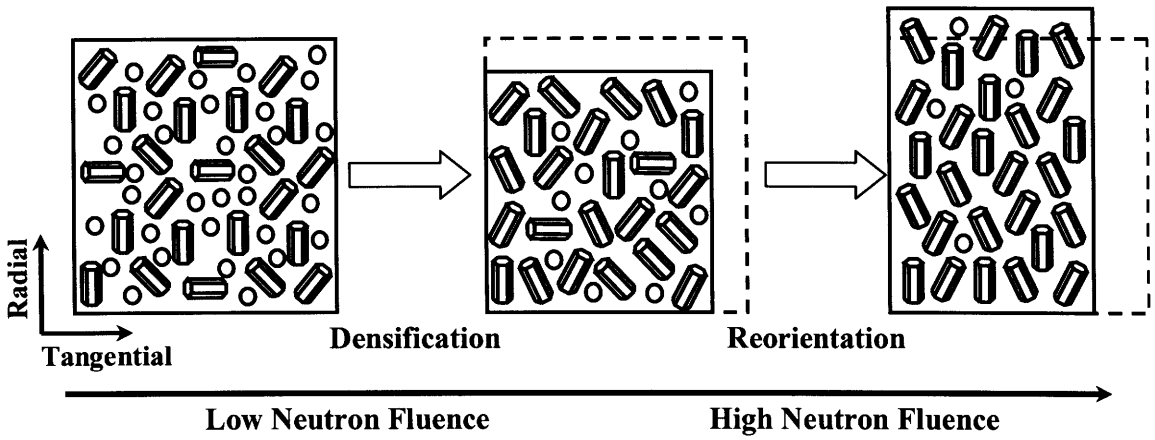

Figure 3-4: Illustration of Irradiation Induced Dimensional Changes in PyC [4]

This swelling behavior is, in general, a function of PyC density, anisotropy, temperature, and the fast neutron fluence. A new correlation must be developed to model the swelling behavior each time one of these parameters changes. TIMCOAT examines a set of experimental results presented in reference [11], known as CEGA-002820, to create a database for the dependence of the swelling rate on each of these parameters. It interpolates between points in this database to develop a radial and tangential swelling correlation for every individual particle that is modeled. Where appropriate, however, the benchmark cases specify a correlation to be used, and TIMCOAT has been adapted to use these correlations. It was noticed, however, that the results obtained with the benchmark correlation and with the TIMCOAT database differ in some cases, and so both results will be presented.

The other important irradiation induced dimensional effect in PyC is creep, which refers to the time dependent deformation of the PyC under a constant stress as a result of irradiation damage to its structure. Creep is described by two parameters. The creep coefficient specifies the fractional radial deformation per unit stress per unit fluence and the Poisson's ratio in creep is used in describing the corresponding tangential deformation. TIMCOAT is capable of calculating both of these parameters from information found in CEGA-002820 in a similar fashion that it calculates swelling. Again, the benchmark cases specify these two parameters when needed, and these can be

used to replace the TIMCOAT calculations. As with swelling, differences were noticed between the two sets of parameters, and results for both are provided.

3.2.1 Description of Cases

The four cases in this part of the benchmark all consider the same type of particle and conditions. The particle consists of a fuel kernel, a low density buffer, and two structural layers, an IPyC and a SiC. The particles are subject to constant internal and external pressures, a constant temperature and a constant fast neutron flux. It is assumed that no fissions occur in the particle and that, therefore, the burnup in the particle is zero. The cases differ only in how the irradiation creep and swelling are handled. For all cases the metrics of comparison are plots of the maximum tangential stress in the IPyC and SiC as a function of fast neutron fluence. The remainder of the input parameters for these cases is in Appendix I, irradiation histories are located in Appendix II, and dimensional sketches are presented in Appendix III.

Case 4a) No Creep / Constant Swelling

Table 3-3: PyC Irradiation Properties for Case 4a

Parameter	Units	IAEA Value
Radial Swelling Correlation	$(\Delta L/L)/10^{25}$ n/m^2	-0.005x
Tangential Swelling Correlation	$(\Delta L/L)/10^{25}$ n/m^3	-0.005x
Creep Coefficient	(MPa 10^{25} n/m^2)$^{-1}$	0
Poisson's Ratio In Creep		0

It is noted that the swelling correlation is given as a function of "x" which refers to the fast neutron fluence (10^{25} neutrons / m^2) for energies greater then 0.18 MeV. This usage of "x" will remain consistent throughout this thesis. No TIMCOAT calculated values are used here.

Case 4b) Constant Creep / No Swelling

Table 3-4: PyC Irradiation Properties for Case 4b

Parameter	Units	IAEA Value	Calculated Value
Radial Swelling Correlation	$(\Delta L/L)/10^{25}$ n/m^2	0	
Tangential Swelling Correlation	$(\Delta L/L)/10^{25}$ n/m^3	0	
Creep Coefficient	(MPa 10^{25} n/m^2)$^{-1}$	2.71E-04	IPyC: 1.36E-04
Poisson's Ratio In Creep		0.5	

The calculated values in Table 3-4 refer to values determined by TIMCOAT from its database drawn from information presented in CEGA-002820. A blank cell in the calculated values column indicates that the IAEA Value is being used.

Case 4c) Constant Creep / Constant Swelling

Table 3-5: PyC Irradiation Properties for Case 4c

Parameter	Units	IAEA Value	Calculated Value
Radial Swelling Correlation	$(\Delta L/L)/10^{25}$ n/m^2	-0.005x	
Tangential Swelling Correlation	$(\Delta L/L)/10^{25}$ n/m^3	-0.005x	
Creep Coefficient	(MPa 10^{25} n/m^2)$^{-1}$	2.71E-04	IPyC: 1.36E-04
Poisson's Ratio In Creep		0.5	

Case 4d) Constant Creep / Fluence Dependent Swelling

Table 3-6: PyC Irradiation Properties for Case 4d

Parameter	Units	IAEA Value	Calculated Value
Radial Swelling Correlation	$(\Delta L/L)/10^{25}$ n/m^2	1.36334E-03x^3 -7.77024 E-03x^2 +2.00861E-02x -2.22642E-02	1.40357 E-03x^3 -9.12192 E-03x^2 +2.31797 E-02x -2.34047 E-02
Tangential Swelling Correlation	$(\Delta L/L)/10^{25}$ n/m^3	-3.53804E-04x^3 +1.69251E-03x^2 +2.63307E-03x -1.91253E-02	-6.01503E-04x^3 +2.53955E-03x^2 +2.35463E-03x -1.97986E-02
Creep Coefficient	(MPa 10^{25} n/m^2)$^{-1}$	2.71E-04	IPyC: 1.36E-04
Poisson's Ratio In Creep		0.5	

3.2.2 Results and Discussion Case 4a

Figure 3-5 displays the tangential stresses in the IPyC and SiC layers as a function of fast neutron fluence. The maximum tangential stresses occurred at the inner surfaces of the two layers. The stress in the IPyC layer starts out as a tensile stress and increases in magnitude during irradiation. The stress in the SiC layer begins as a tensile stress and then becomes compressive during irradiation.

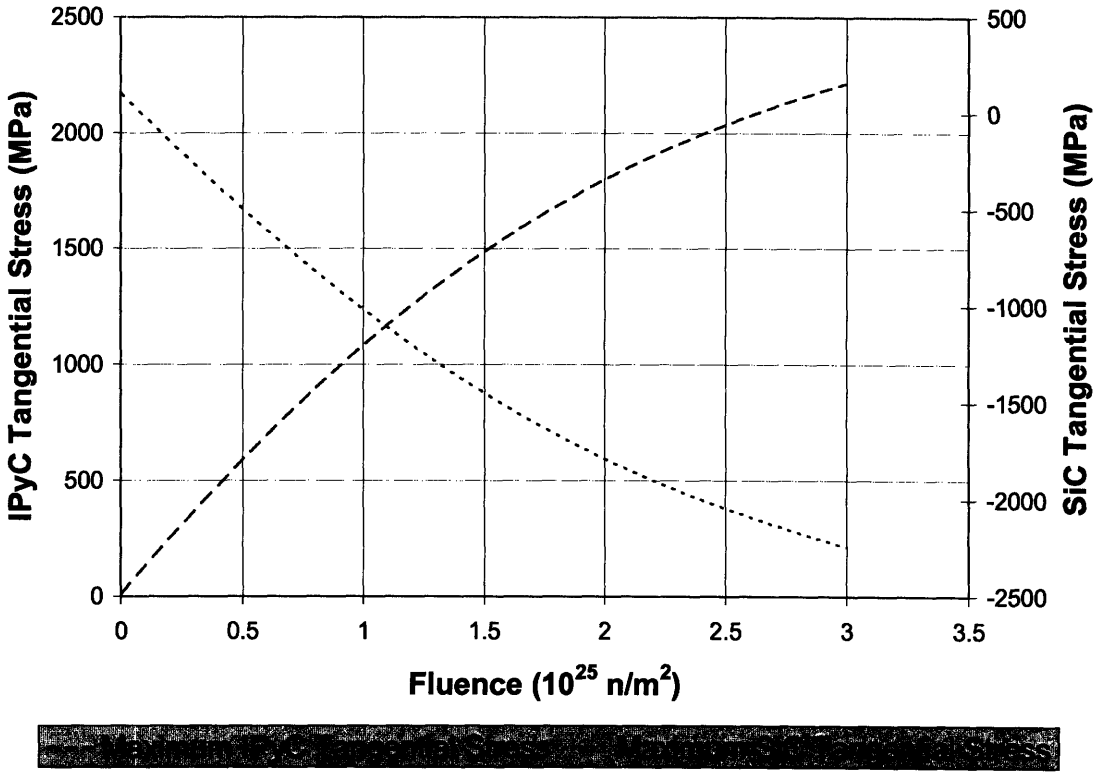

Figure 3-5: Maximum Tangential Stresses in IPyC and SiC Layers for Case 4a

The behavior of these stresses bears some analysis. At the beginning of the irradiation cycle, there are no tangential stresses in the IPyC or SiC layer. As the irradiation proceeds, the IPyC begins to shrink uniformly due to the assumed model of irradiation induced swelling. This shrinkage would lead to a decrease in the radius of the IPyC. Remember, however, that Young's modulus of the SiC is almost an order of magnitude larger then that of the IPyC, so the SiC can be thought of as rigid, holding the IPyC and preventing it from shrinking. This force holding the IPyC at a larger radius creates tension, and as it continues to shrink over the irradiation period, the magnitude of this tension increases. Correspondingly, because of the bond between the SiC layer and the IPyC layer, the shrinkage of the IPyC pulls the inner surface of the SiC layer toward the center of the particle, resulting in an increasing compressive stress. By modeling the swelling in this particle as a uniform rate of shrinkage, the effects of the densification mechanism are expressed. As there is no relaxation in the shrinkage as the cycle progresses, the reorientation mechanism is suppressed.

Figure 3-6 shows the radial stress at the IPyC/SiC interface as a function of fast neutron fluence. The stress is tensile and increases in magnitude with fluence. The maximum value of 400.6 MPa occurs at the end of the simulation. This behavior is consistent with the continued shrinkage of the IPyC attempting to pull away from the SiC layer.

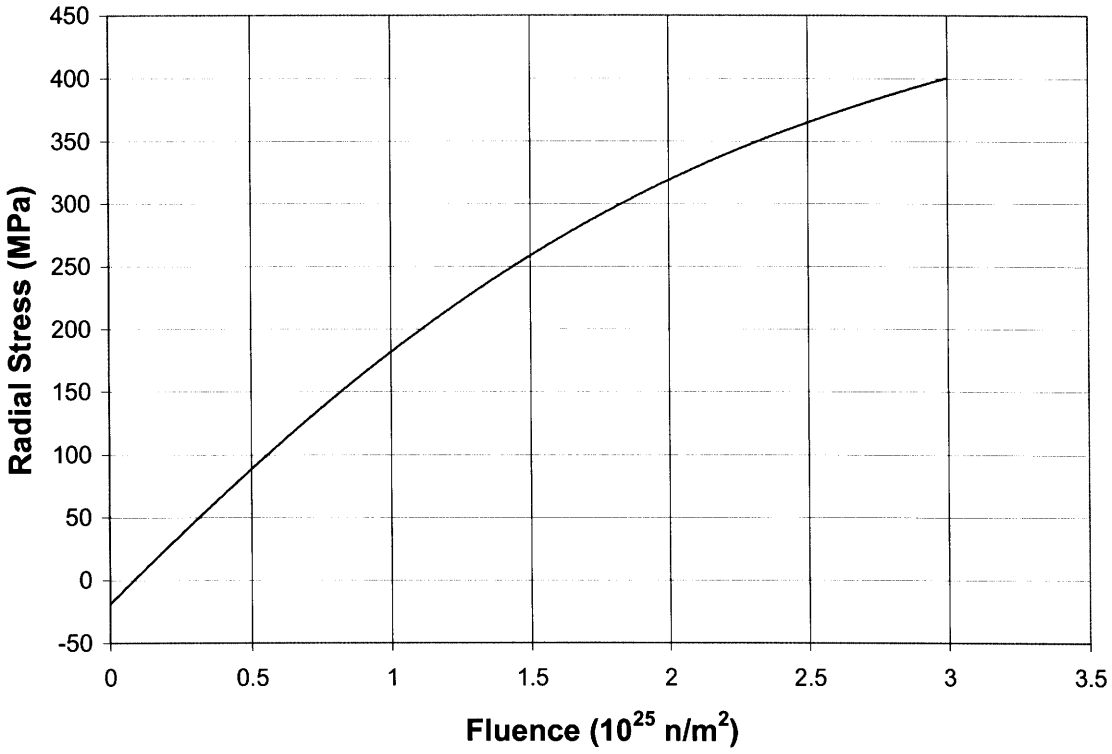

Figure 3-6: Radial Stress at the IPyC/SiC Interface for Case 4a

3.2.3 Results and Discussion Case 4b

Figure 3-7 shows the tangential stresses at the inner surfaces of the two structural layers both for the IAEA recommended value of the creep coefficient and the TIMCOAT calculated value. For this particular case, it is difficult to identify a cross-section in one of the layers that has the maximum stress throughout irradiation, so the inner surface was selected instead as indicated by the benchmark. The stress distributions are different than those found in Case 4a. The PyC in this particle is modeled as being susceptible to irradiation creep but not swelling. The creep allows the PyC to slowly deform under the high internal pressure. As a result, the stress in the IPyC decreases rapidly until the tangential compressive stress is equal to the outward force of the internal pressure. The

effect in the SiC layer is opposite. As the IPyC expands by creep, it presses against the SiC thereby increasing the tensile stress in the SiC layer. As is expected, the increase in the stress in the SiC stops once the IPyC has come to equilibrium. This behavior uncovers an unexpected effect of the internal pressure. As the internal pressure causes creep that places the IPyC into compression, it can offset the effects of swelling shown in Case 4a and actually help to relax the stresses in the IPyC layer.

Table 3-4 indicates that the creep coefficient calculated by TIMCOAT is almost exactly half what is specified in the IAEA benchmarks. The benchmark document, which can be found in Appendix IV, states that the creep coefficient for this case is a factor of two larger than the value found in the literature. This gives confidence in TIMCOAT's calculations. The reason for doubling the coefficient was not given and as will be discussed in Section 4.1.2, using such a large coefficient proves to be problematic in later cases. As such, results for the TIMCOAT calculated value are shown in Figure 3-7 as well. It is seen in the figure that the smaller creep coefficient implies a longer relaxation time but the same asymptotic stresses.

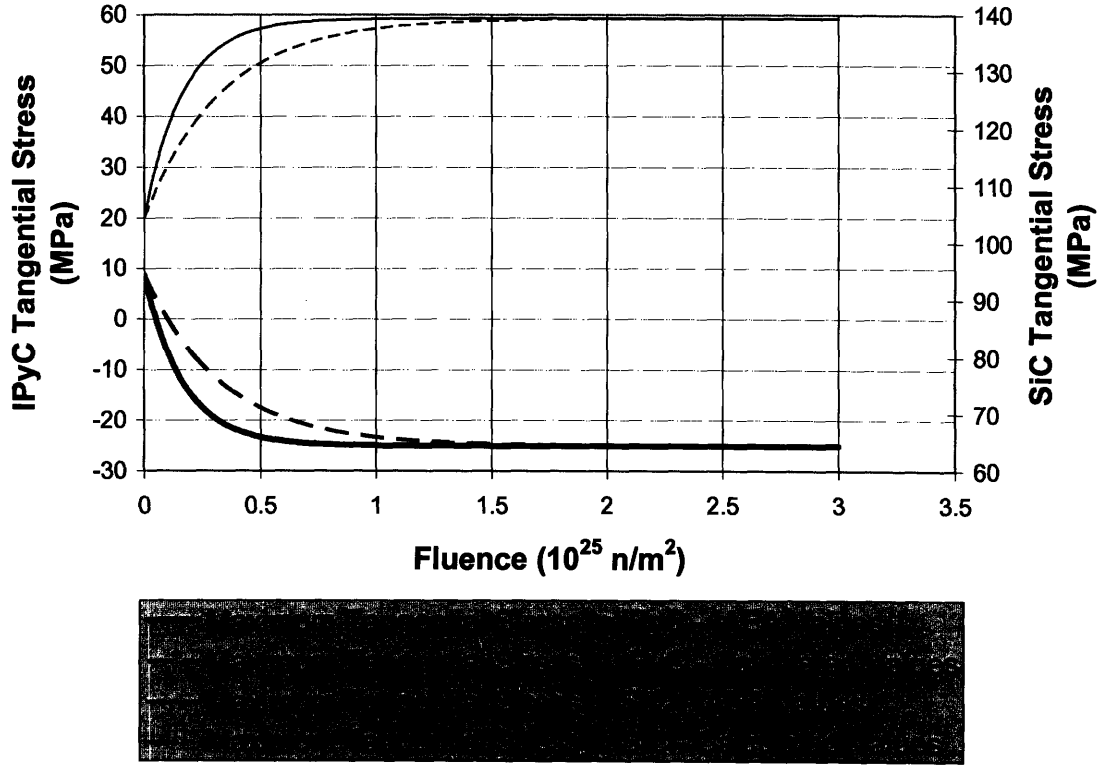

Figure 3-7: Inner Surface Tangential Stresses in IPyC and SiC Layers for Case 4b

Figure 3-8 shows how the effects of irradiation creep propagate through the IPyC layer over the course of the irradiation. The curves in the figure track the radial stresses in successive evenly distributed shells of the IPyC. It is seen that the effect of the creep on the radial stress is also to cause an equilibration with the internal pressure of 25 MPa over the course of the irradiation.

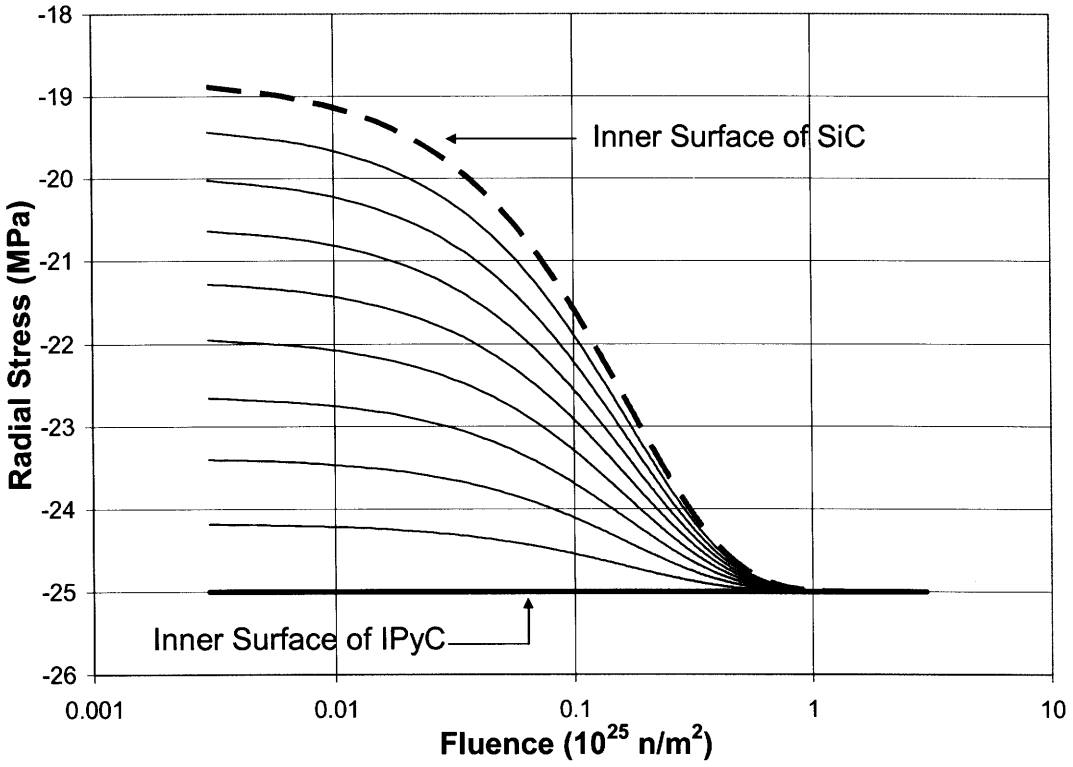

Figure 3-8: Radial Stress Profile in IPyC Layer for Case 4b

3.2.4 Results and Discussion Case 4c

In this case the IPyC is assumed to be affected by both irradiation swelling and creep. Figure 3-9 shows the tangential stresses at the inner surface of the two structural layers for both the IAEA specified creep coefficient and the TIMCOAT calculated one. First, consider the general behavior of the stress in the IPyC. At the beginning of the irradiation cycle, the stress rises rapidly. Consulting the results in Case 4a, this is easily attributed to the densification associated with low fluence swelling. At fluences of about 0.5 and 0.8×10^{25} n/m^2 for the IAEA and TIMCOAT calculated parameters, respectively,

the stress reaches a maximum, and then begins to decline. From the results in Case 4b, this decline is attributable to the stress relaxation caused by creep. The stress in the SiC layer is determined by the changes taking place in the IPyC as described in Sections 3.2.2 and 3.2.3. The swelling places the SiC into compression, and the creep restores the tensile stress.

It is very important to note the differences between the stress behaviors that are caused by varying the creep coefficient. Recall that the TIMCOAT calculated creep coefficient is half that of the value prescribed in the benchmark document. Figure 3-9 shows that when the creep coefficient is halved, the maximum stress in IPyC layer is doubled. This is significant when considering failure mechanisms for the IPyC layer. Using a smaller creep coefficient increases the probability of cracking the IPyC early in the irradiation history. For the SiC layer, halving the creep coefficient about doubles the compressive stress in the layer. From Figure 3-9 it is seen that for the smaller coefficient, once the tangential stress becomes compressive, it remains that way throughout the irradiation. For the larger coefficient, however, the stress again becomes tensile toward the end of the cycle. This is significant as the strength of the SiC layer decreases with irradiation damage, and the end of life tensile stress could lead to an increased probability of direct SiC layer failure. It is reasonable to conclude then that the difference in these creep coefficients could have a significant effects in the relative importance of different mechanisms of particle failure and on the overall probability of particle failure.

Figure 3-10 shows the radial stress profile in the IPyC layer as a function of fast neutron fluence. The behavior of the stresses follows the same pattern as the tangential stresses in the IPyC.

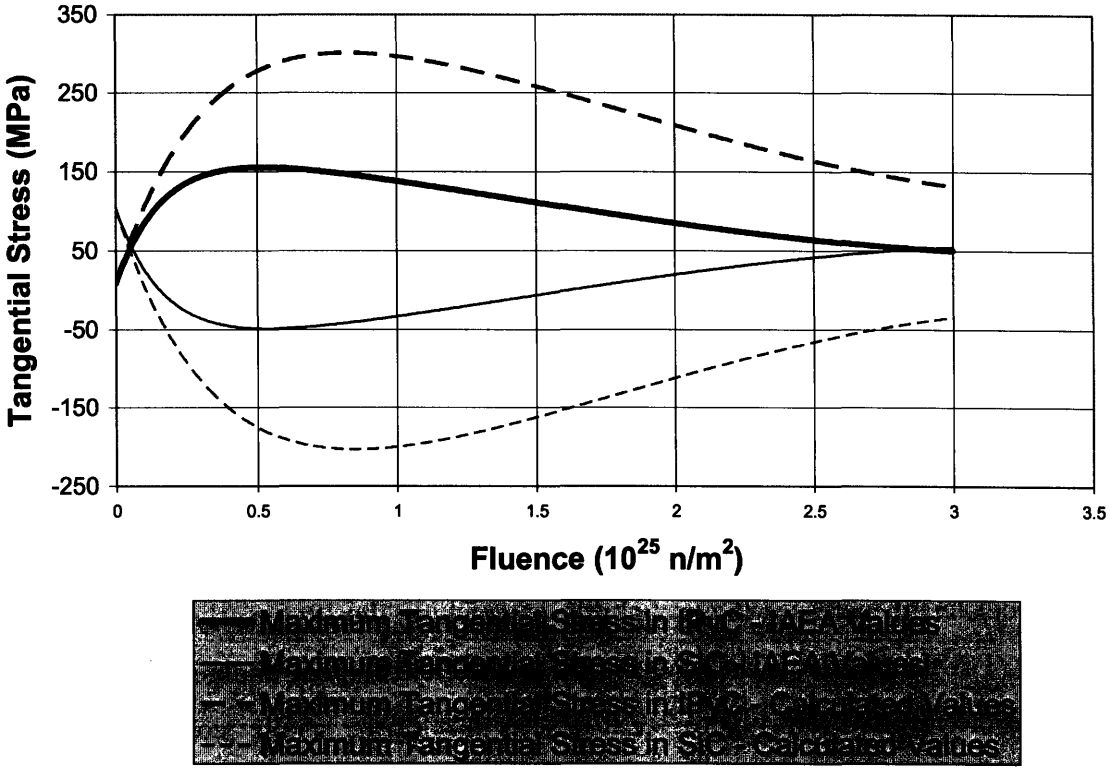

Figure 3-9: Inner Surface Tangential Stresses in IPyC and SiC Layers for Case 4c

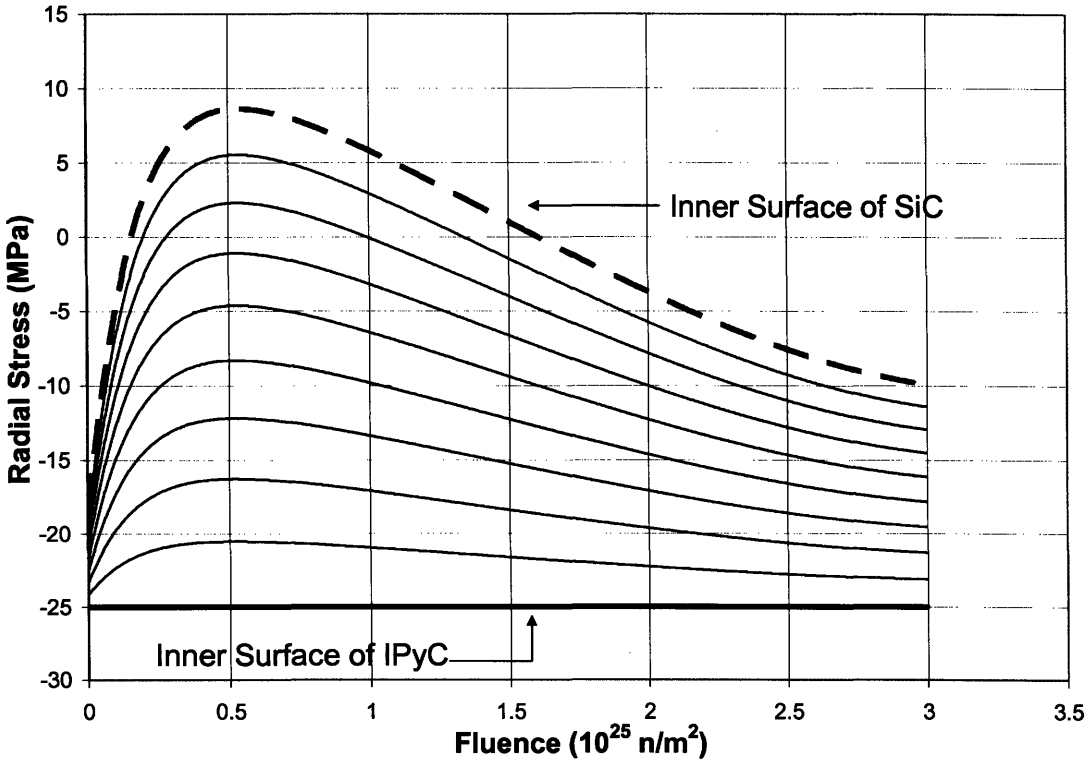

Figure 3-10: Radial Stress Profile in IPyC Layer for Case 4c

3.2.5 Results and Discussion Case 4d

This case differs from Case 4c only in that the swelling rate is not constant and not isotropic but, rather, depends on fluence. Figure 3-11 shows this dependence for the swelling correlation given in the benchmark document as well as for the TIMCOAT determined correlation. The two correlations are in very good agreement at low fluences and then begin to diverge slightly toward the end of the irradiation history. It is difficult to determine if this divergence reflects a substantive difference in the assumed swelling behavior or is simply an artifact of different interpolation procedures. This is noted here as it will become significant in cases that run to higher fluences.

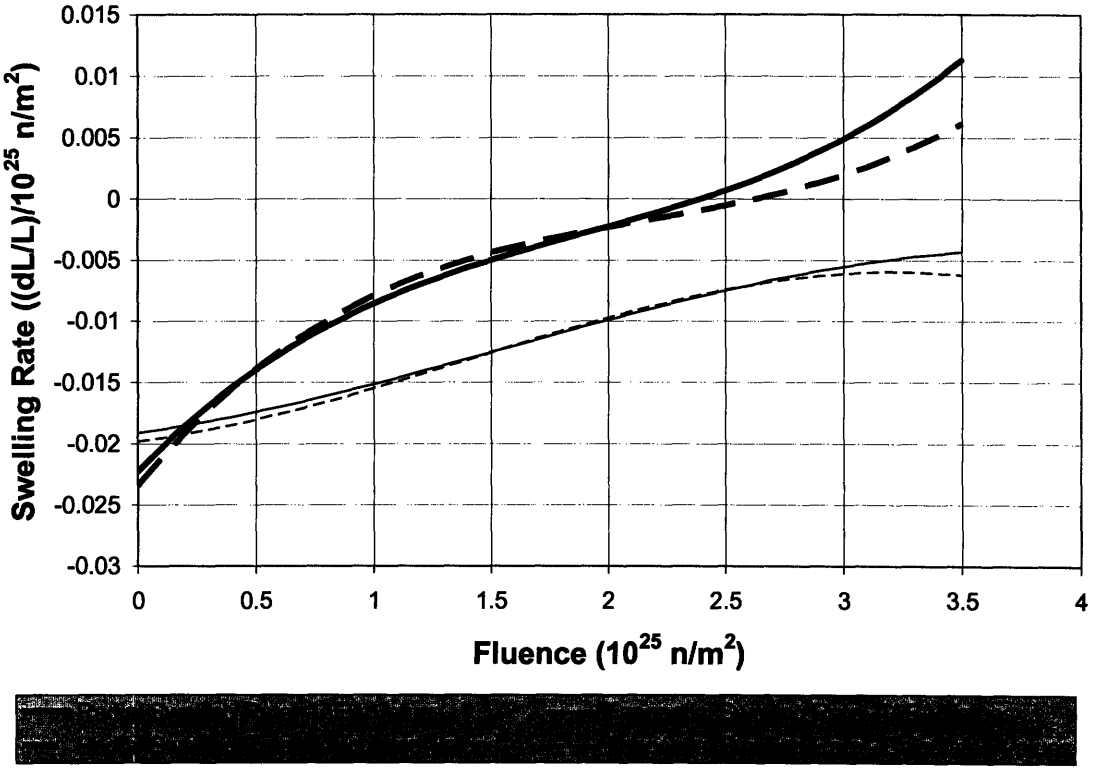

Figure 3-11: Radial and Tangential Swelling Rates for Case 4d

Using these two sets of swelling correlations and the combination of creep coefficients indicated in Table 3-6, the tangential and radial stresses at the inners surfaces of the two structural layers presented were obtained. These results are shown in Figure 3-12 and Figure 3-13.

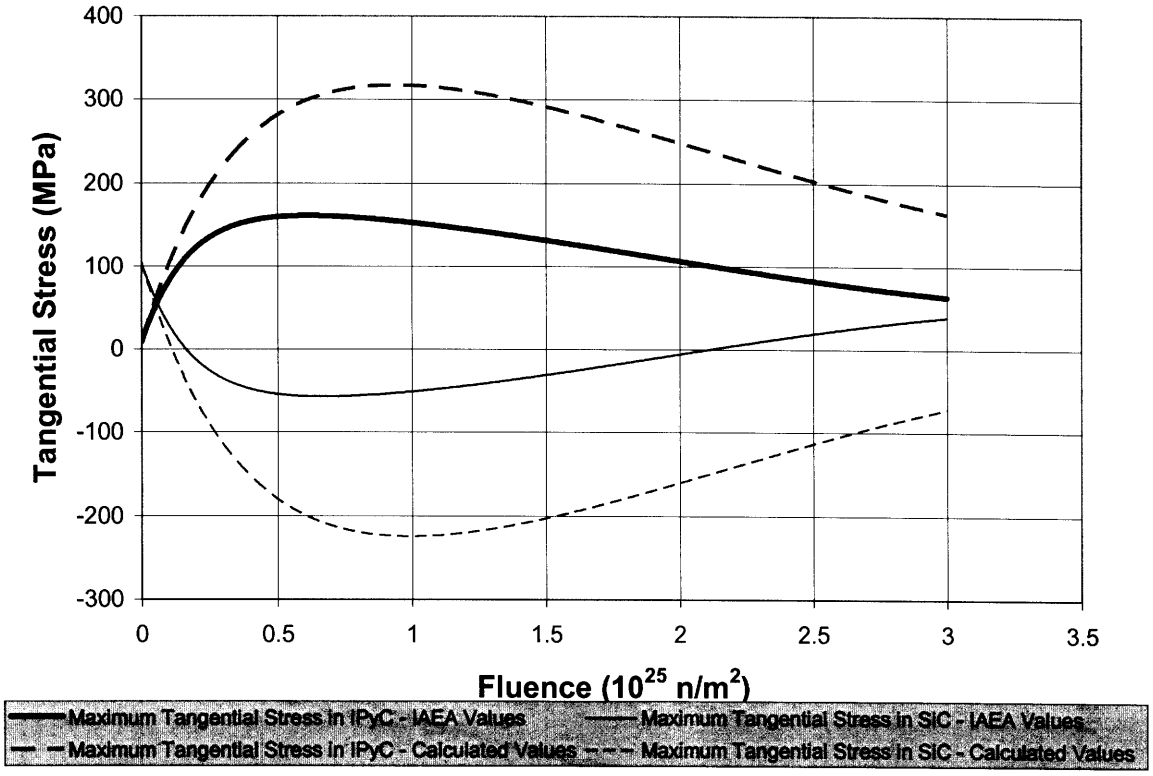

Figure 3-12: Inner Surface Tangential Stresses in IPyC and SiC Layers for Case 4d

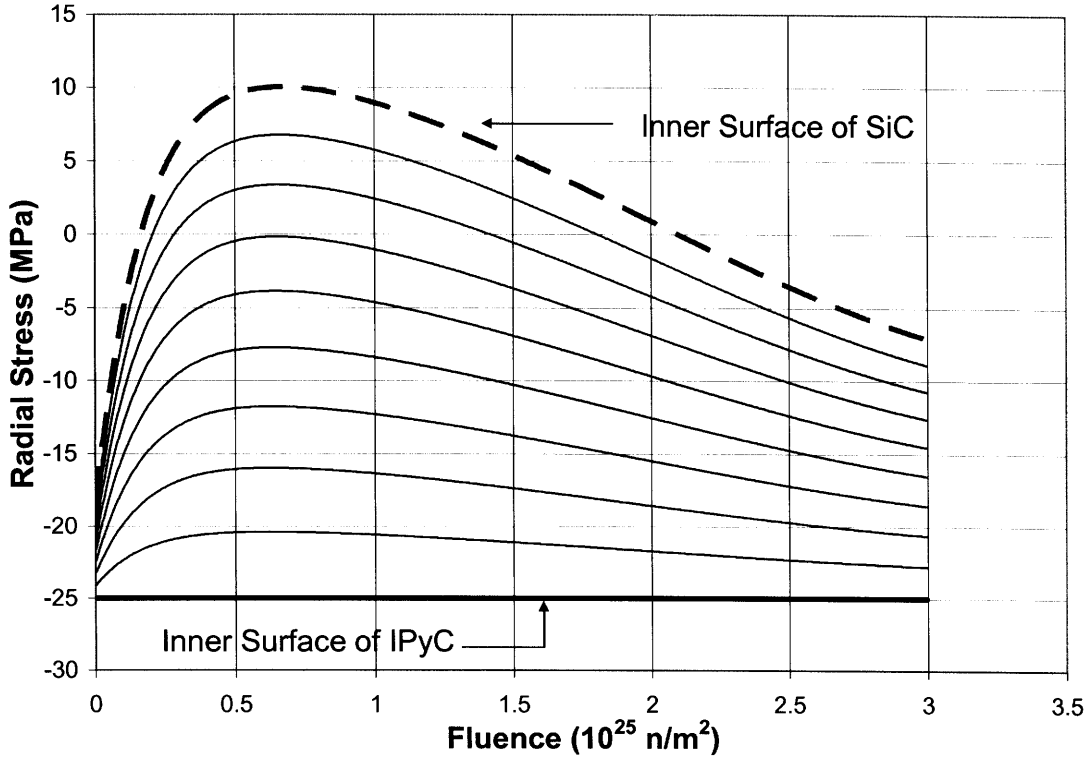

Figure 3-13: Radial Stress Profile in IPyC Layer for Case 4d

The results of this case are very similar to those found in Case 4c. The IAEA and TIMCOAT calculated curves differ because of the differing creep coefficients and slightly smaller end of cycle swelling. As compared with the uniform, isotropic swelling in Case 4c, the larger shrinkage rate at the beginning of the irradiation cycle led to a higher peak tensile tangential stress in the IPyC layer and a larger peak compressive tangential stress in the SiC layer. The reversal of the dimensional changes from shrinkage to swelling at the end of the cycle had little effect on the tangential stresses. In both cases 4c and 4d the stress in the two structural layers changes about the same amount from their peak to end of life values. This indicates the dominance of the creep mechanism at higher fluences. The behavior of the radial stresses is similar to that found in Case 4c and is otherwise unremarkable.

3.3 Part 3: Nominal TRISO Benchmark Cases

The next four cases in the benchmark study look at coated particles with three structural layers, IPyC/SiC/OPyC. As in Part 2, single, normalized particles are considered. The effects of varying kernel diameter and PyC anisotropy are examined as well as the effects of varying temperatures and pressures during irradiation. In all four cases, the metrics of comparison are the maximum tangential stress in the IPyC and SiC layers as a function of fast neutron fluence. Again, results using both values from the benchmark document and TIMCOAT calculations are presented. In addition to the TIMCOAT calculated swelling and creep, which was discussed in Part 2, TIMCOAT calculated PyC Poisson's ratios in creep will be added. These ratios are dynamic with respect to fast neutron fluence and are drawn from data presented by Kaae [12]. Kaae indicates that the value of the Poisson's ratio appears to depend on the effective creep strain which can be related to the fast neutron fluence.

3.3.1 Description of Cases

The input parameters listed in the benchmark document for cases 5 through 8 can be found in Appendix I, and the irradiation histories are located in Appendix II. Dimensional diagrams are shown in Appendix III. For cases 5 – 7 the TRISO particle is

assumed to be irradiated at a constant temperature and neutron flux with internal pressure in the particle and burnup in the kernel accumulating linearly over the irradiation cycle. In case 8, the particle is assumed to be irradiated under a constant flux, but the temperature is cycled. Table 3-7, Table 3-8 and Table 3-9 summarizes the PyC properties used for cases 5, 6 and 7 respectively.

Case 5) TRISO Particle with 350 μm Kernel

Table 3-7: PyC Irradiation Properties for Case 5

Parameter	Units	IAEA Value	Calculated Value
Radial Swelling Correlation	$(\Delta L/L)/10^{25}$ n/m^2	See Table 3-6	
Tangential Swelling Correlation	$(\Delta L/L)/10^{25}$ n/m^3		
Creep Coefficient	(MPa 10^{25} n/m^2)$^{-1}$	2.71E-04	1.36E-04
Poisson's Ratio In Creep		0.5	x < 0.3: 0.5 – x/3 x > 0.3: 0.4

The properties of the PyC in case 5 are identical to those in case 4d. Accordingly, the swelling correlations are the same.

Case 6) TRISO Particle with 500 μm Kernel

Table 3-8: PyC Irradiation Properties for Case 6

Parameter	Units	IAEA Value	Calculated Value
Radial Swelling Correlation	$(\Delta L/L)/10^{25}$ n/m^2	See Table 3-6	
Tangential Swelling Correlation	$(\Delta L/L)/10^{25}$ n/m^3		
Creep Coefficient	(MPa 10^{25} n/m^2)$^{-1}$	2.71E-04	1.36E-04
Poisson's Ratio In Creep		0.5	x < 0.3: 0.5 – x/3 x > 0.3: 0.4

Again, the properties of the PyC in case 6 are identical to those in case 4d.

Case 7) TRISO Particle with High Anisotropy

Table 3-9: PyC Irradiation Properties for Case 7

Parameter	Units	IAEA Value	Calculated Value
Radial Swelling Correlation	$(\Delta L/L)/10^{25}$ n/m^2	+7.27026E-04x^3 -5.05553E-03x^2 +1.83715E-02x -2.12522E-02	+1.29933E-03x^3 -9.28014E-03x^2 +2.58697E-02x -2.32152E-02
Tangential Swelling Correlation	$(\Delta L/L)/10^{25}$ n/m^3	-8.88086E-04x^3 +5.03465E-03x^2 -3.42182E-03x -1.79113E-02	-5.44594E-04x^3 +2.5893E-03x^2 +1.02187E-03x -1.98942E-02
Creep Coefficient	(MPa 10^{25} n/m^2)$^{-1}$	2.71E-04	1.36E-04
Poisson's Ratio In Creep		0.5	x < 0.3: 0.5 – x/3 x > 0.3: 0.4

Case 8) TRISO Particle with Cyclic Temperature

This case is intended to model the temperature and pressure history a TRISO particle would encounter in flowing through and being recycled in a PBR but it still only considers a normalized particle. The temperature in the particle is increased linearly from 600°C to 1000°C, then dropped immediately back to 600°C, and cycled again in this fashion a total of 10 times. To avoid singularities in the rate of temperature change during simulation, this drop was spread over a small time. The corresponding internal pressure in the particle followed a similar pattern of cyclical gradual rise followed by immediate drop. The pressure and temperature history inputs used for this case are shown in Figure 3-14. Fast neutron fluence and burnup are assumed to accumulate linearly over time. This is an approximation, as realistically fissions would stop during the cooling phase as the particle is recycled to the top of the PBR.

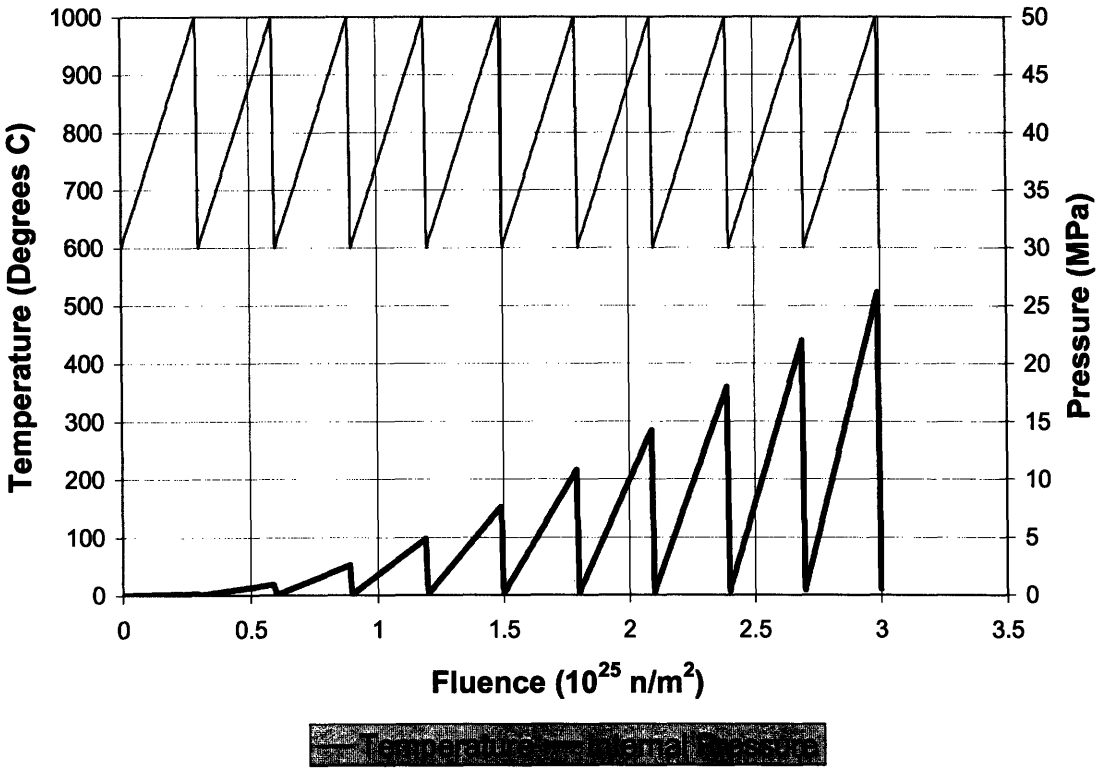

Figure 3-14: Temperature and Internal Pressure Histories for Case 8

Table 3-10 gives the PyC materials properties for this case. Unlike in all previous cases where the irradiation induced creep coefficient is a constant over the cycle, the varying temperatures here lead to a varying creep coefficient as shown in Figure 3-15. As in previous cases the creep coefficient chosen in the benchmark documents is about twice that of the TIMCOAT calculated value.

Table 3-10: PyC Irradiation Properties for Case 8

Parameter	Units	IAEA Value	Calculated Value
Radial Swelling Correlation	$(\Delta L/L)/10^{25}$ n/m^2	+4.03266E-04x^3 -2.25937E-03x^2 +9.82884E-03x -1.80613E-02	+6.4176E-04x^3 -4.230376E-03x^2 1.32541E-02x -1.89504E-02
Tangential Swelling Correlation	$(\Delta L/L)/10^{25}$ n/m^3	-4.91648E-04x^3 +2.32979E-03x^2 +1.71315E-03x -1.78392E-02	-3.43626E-04x^3 +9.65679E-04x^2 +4.77559E-03x -1.95471E-02
Creep Coefficient	(MPa 10^{25} n/m^2)$^{-1}$	See Figure 3-15	
Poisson's Ratio In Creep		0.5	x < 0.3: 0.5 – x/3 x > 0.3: 0.4

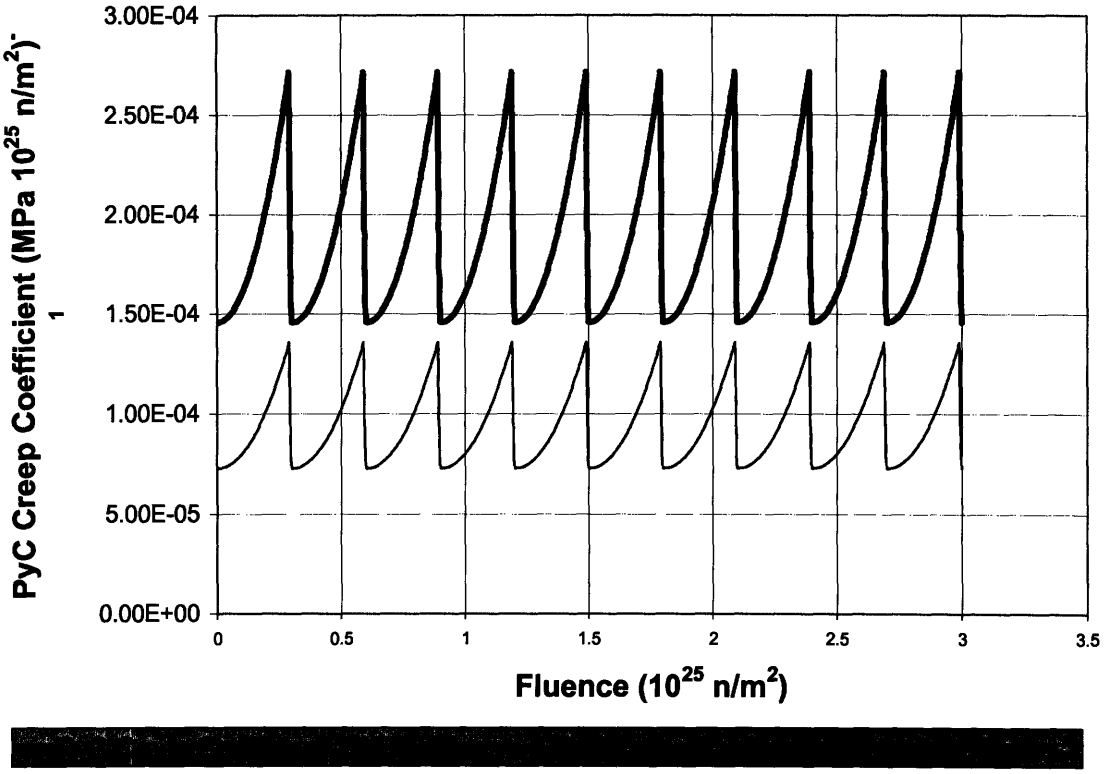

Figure 3-15: PyC Creep Coefficient for Case 8

3.3.2 Results and Discussion Case 5

The absolute maximum tangential stresses in the IPyC and SiC layers were found to occur at inner surfaces of the layers. Three separate combinations of PyC material properties were consider for this case. The first was all IAEA values and the second was IAEA values with TIMCOAT swelling rate and creep coefficient values. These first two combinations are consistent with the pattern of data presented in the Section 3.2 and appear in Figure 3-16. As before, the smaller creep coefficient leads to a larger peak tensile stress in the IPyC and a larger peak compression in the SiC. The swelling rates are the same as those shown in Figure 3-11 and are responsible for little variability between these two results. It is noted that with the addition on an OPyC layer, the SiC layer is now in compression over the entire irradiation cycle.

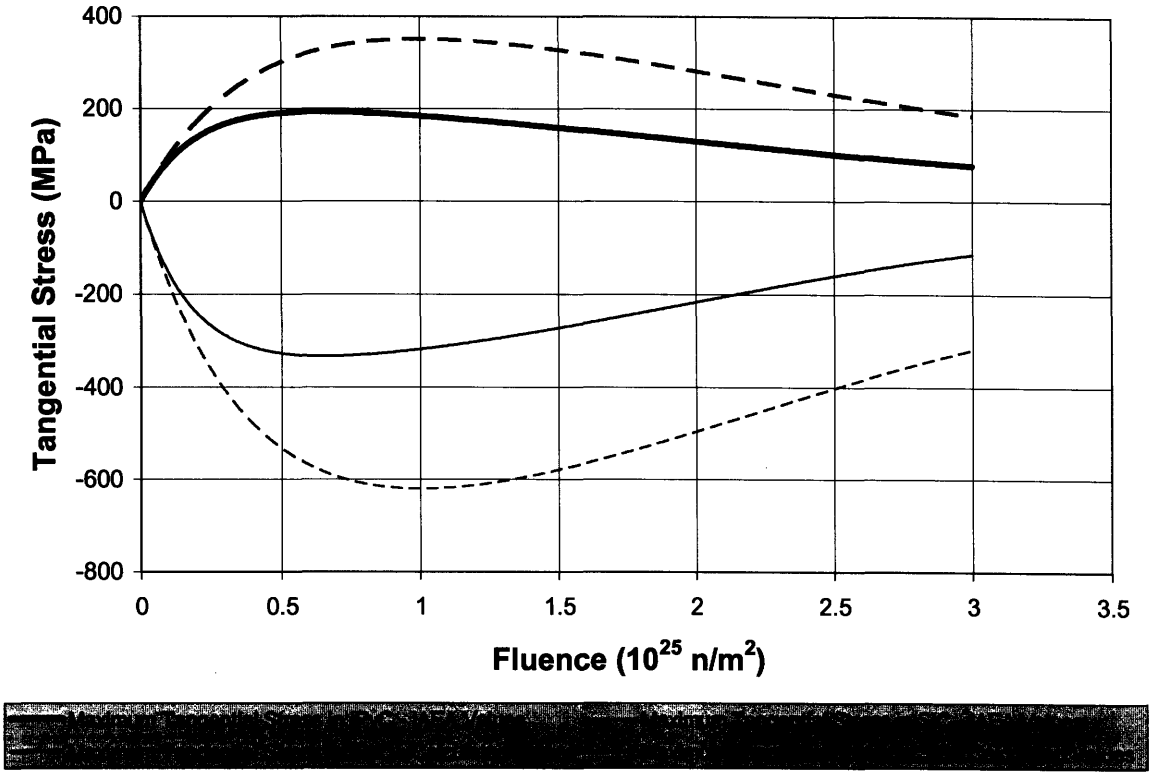

Figure 3-16: Maximum Tangential Stresses in IPyC and SiC Layers for Case 5 (Calculated Values include TIMCOAT calculated swelling rates and creep coefficient)

The third combination of PyC properties considered adds the TIMCOAT calculated variable Poisson's ratio in creep to the second combination. While variable, this ratio is always smaller than the benchmark specified value of 0.5. As seen in Figure 3-17 this smaller Possion's ratio in creep allows for greater relaxation of the tangential stresses in the IPyC layer. As a result, the peak stress is smaller and the end of cycle stress begins to approach the benchmark properties value. With this combination of parameters it can be hypothesized that if particle failure probabilities are considered, results from the TIMCOAT set of parameters would compare more closely to the IAEA parameter results at higher fluences than at lower fluences. This should be kept in mind when considering later cases where failure probabilities are calculated.

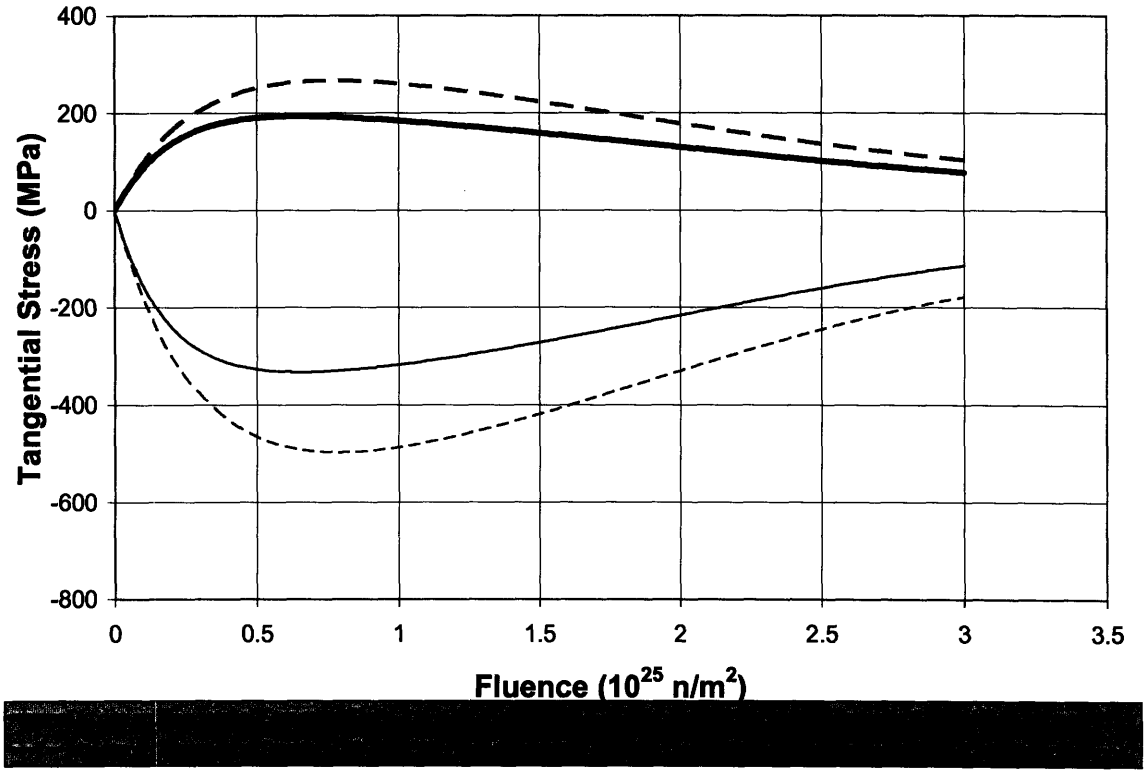

Figure 3-17: Maximum Tangential Stresses in IPyC and SiC Layers for Case 5 (Calculated Values include TIMCOAT calculated swelling rates, creep coefficient and variable Poisson's ratio in creep)

The reader is reminded that for all subsequent cases, "calculated values" refer to those values obtained when TIMCOAT calculated parameters are used for the PyC swelling rate, creep coefficient and Poisson's ratio in creep.

3.3.3 Results and Discussion Case 6

Case 6 differs from Case 5 only in that the size of the fuel kernel is increased from 350 μm to 500 μm while the thickness of the four coating layers remains constant. Again, the maximum tangential stresses in the IPyC and SiC layers, presented in Figure 3-18, occur at the inner surfaces of the layers. Contrasting these results with those in Figure 3-17 reveals the effects of the larger kernel. For both IAEA and Calculated values, the larger kernel reduces peak stresses in the two layers by about 15 MPa. At first this might seem counter intuitive. As the radius of each of these layers is increased, so should tension for a constant internal pressure. Recall, however, that the dominate effect in determining the

peak stress is the interaction between the SiC and PyC layers, not the effect of the internal pressure. Increasing the radius for a constant PyC shrinkage rate early in the cycle implies that the fractional dimensional change will be reduced, and so the peak stress will be reduced. At the end of the cycle, the IAEA values still show the stress about 15 MPa less with the larger kernel. For the TIMCOAT values, however, the difference is now only 8 MPa. This is an effect of the small Poisson's ratio, which increases the rate of stress relaxation for the larger volume of PyC.

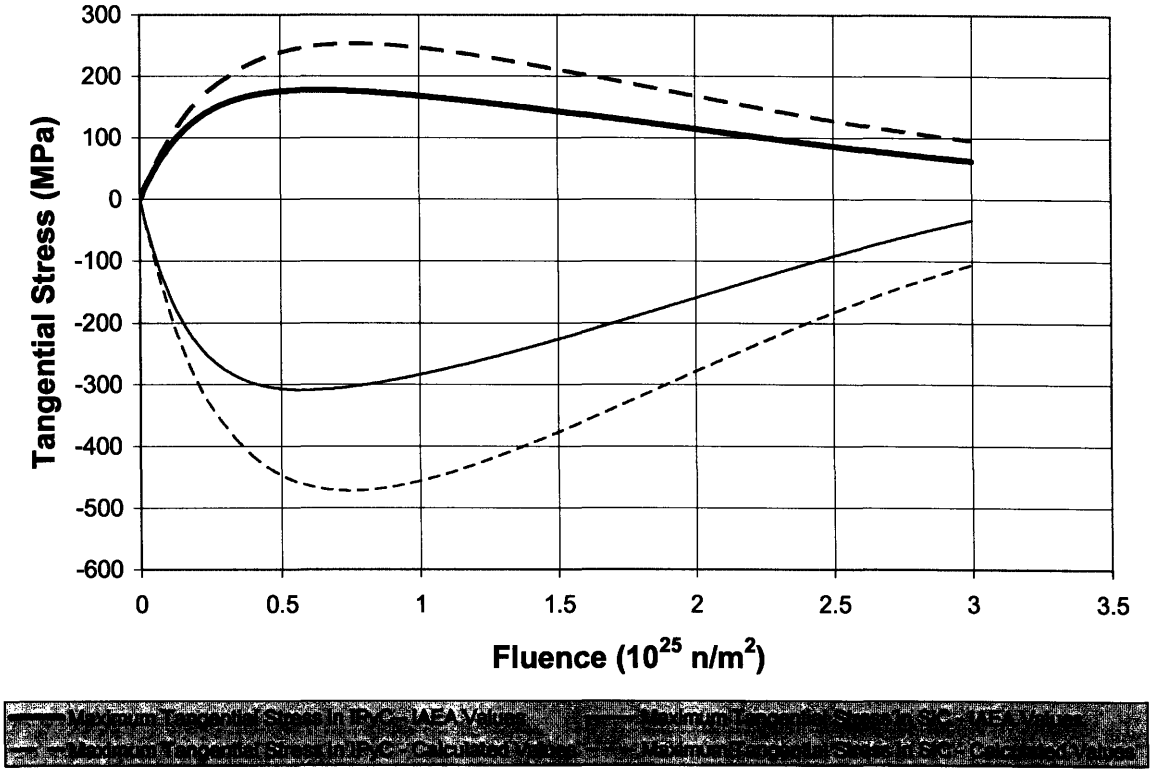

Figure 3-18: Maximum Tangential Stresses in IPyC and SiC Layers for Case 6

3.3.4 Results and Discussion Case 7

Case 7 differs from Case 6 only by the degree of anisotropy of the PyC. In Case 6 the BAF of the PyC is 1.03 and in Case 7 it is 1.06. Changing the BAF of the pyrocarbon changes the rate of irradiation induced swelling. The new correlations given in the benchmark and calculated by TIMCOAT are plotted in Figure 3-19. As before, the two correlations compare reasonably well. Comparing these swelling rates to those from Case 6, which are the same as those shown in Figure 3-11, it is seen that the effect of

higher anisotropy is to increase the rate of radial expansion and increase the rate of tangential shrinkage later in the irradiation cycle. This suggests that the increase in the anisotropy of the manufactured PyC promotes both reorientation, which increases radial swelling, and densification, which increases tangential shrinkage. It is then expected that end of cycle IPyC tangential tensile stresses would be larger due to the increased shrinkage.

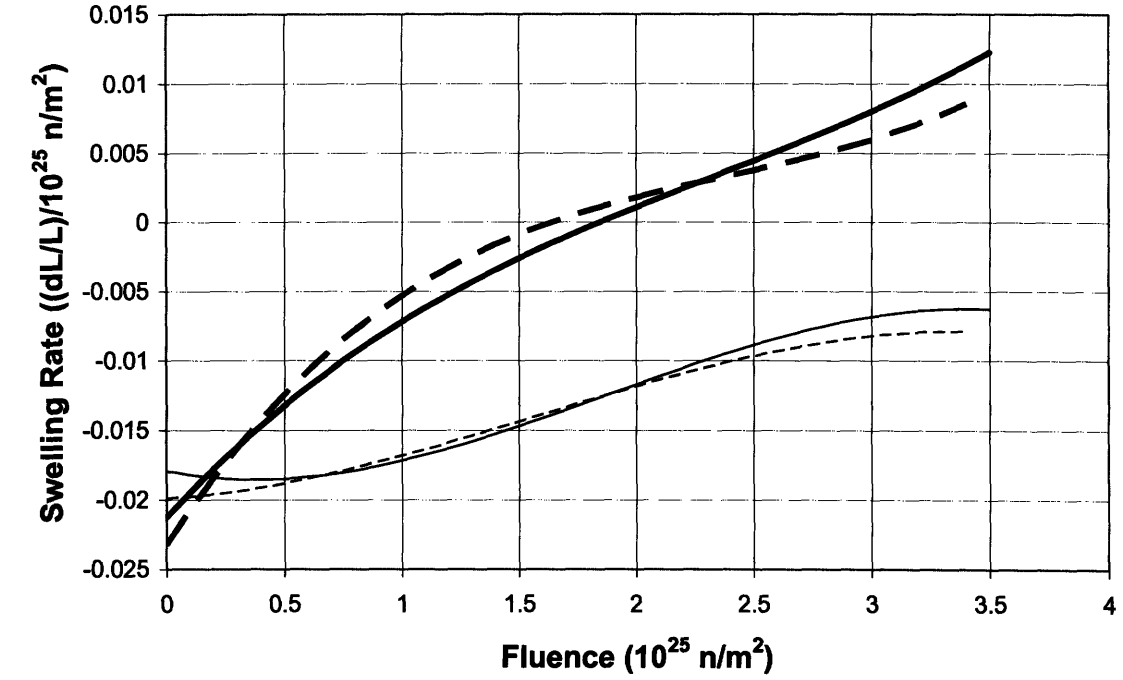

Figure 3-19: Radial and Tangential Swelling Rates for Case 7

The maximum tangential stresses occurring at the inner surfaces of the IPyC and SiC layers are displayed in Figure 3-20, and comparing them to those in Figure 3-18 shows the expected increase in tangential tensile stresses. The peak stress in the IPyC layer is approximately the same in Cases 6 and 7, differing by only about 5 Mpa, while the end of cycle stress in Case 7 is between 25 and 27 MPa larger.

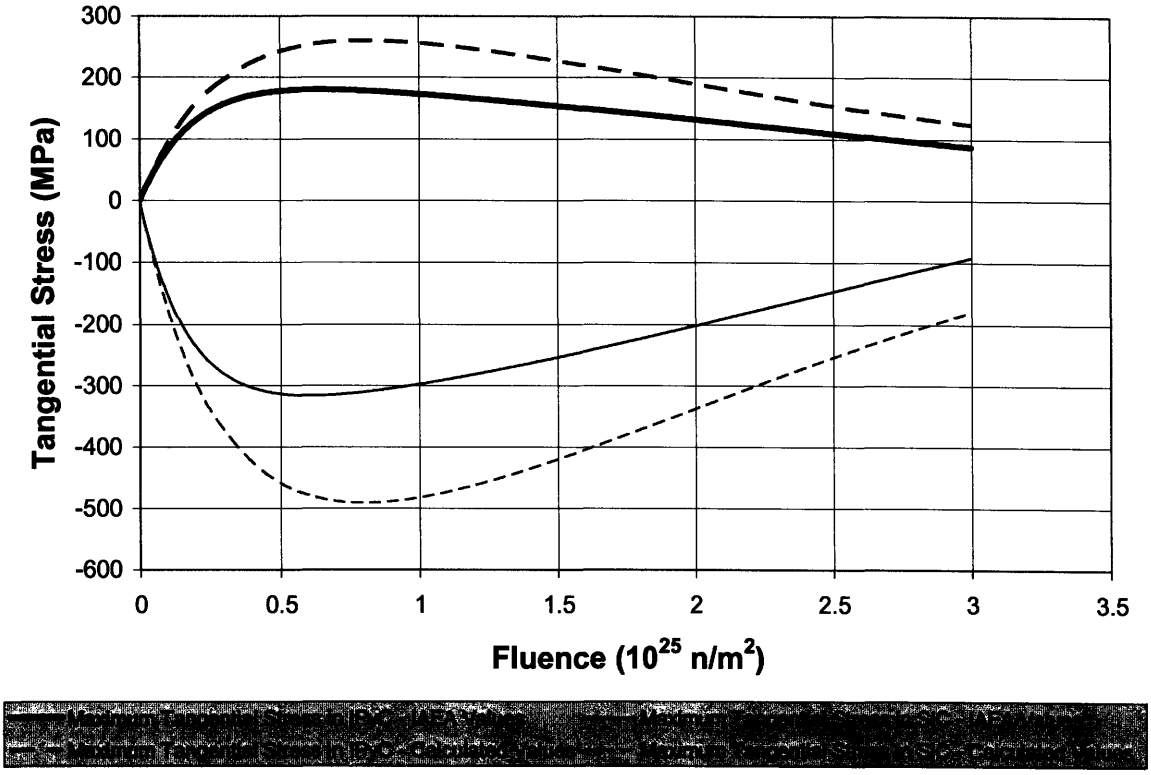

Figure 3-20: Maximum Tangential Stresses in IPyC and SiC Layers for Case 7

3.3.5 Results and Discussion Case 8

The maximum tangential stresses in the IPyC and SiC structural layers were once again found to occur at the inner surfaces of the layers. Figure 3-21 displays these results. In each of the cycles, the sudden drop in temperature and pressure led to a spike in the absolute stresses in the two layers. As temperatures rose during each cycle, these stresses relaxed. This behavior is best understood by considering Figure 3-22. The temperature and pressure drops lead to sudden contractions of the particle. The contraction places additional tensile stresses on the IPyC, and the corresponding reduction of radial force on the SiC places additional compressive stress on it. Over the 10 cycles, however, the inner surface of the IPyC does continue to displace radially outward due to irradiation induced creep. This accounts for the reduction in absolute stresses in later cycles. Further analysis indicated that if this case were run with no fluence accumulating during the cooling phases, results would not change significantly.

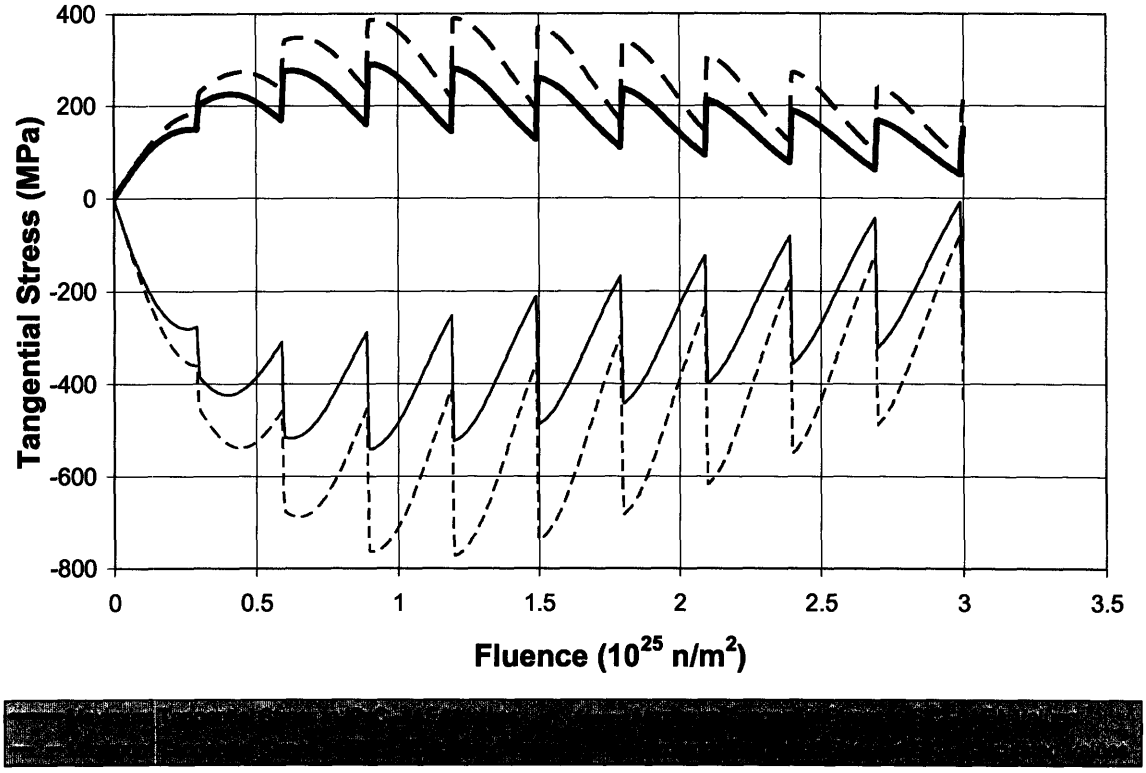

Figure 3-21: Maximum Tangential Stresses in IPyC and SiC Layers for Case 8

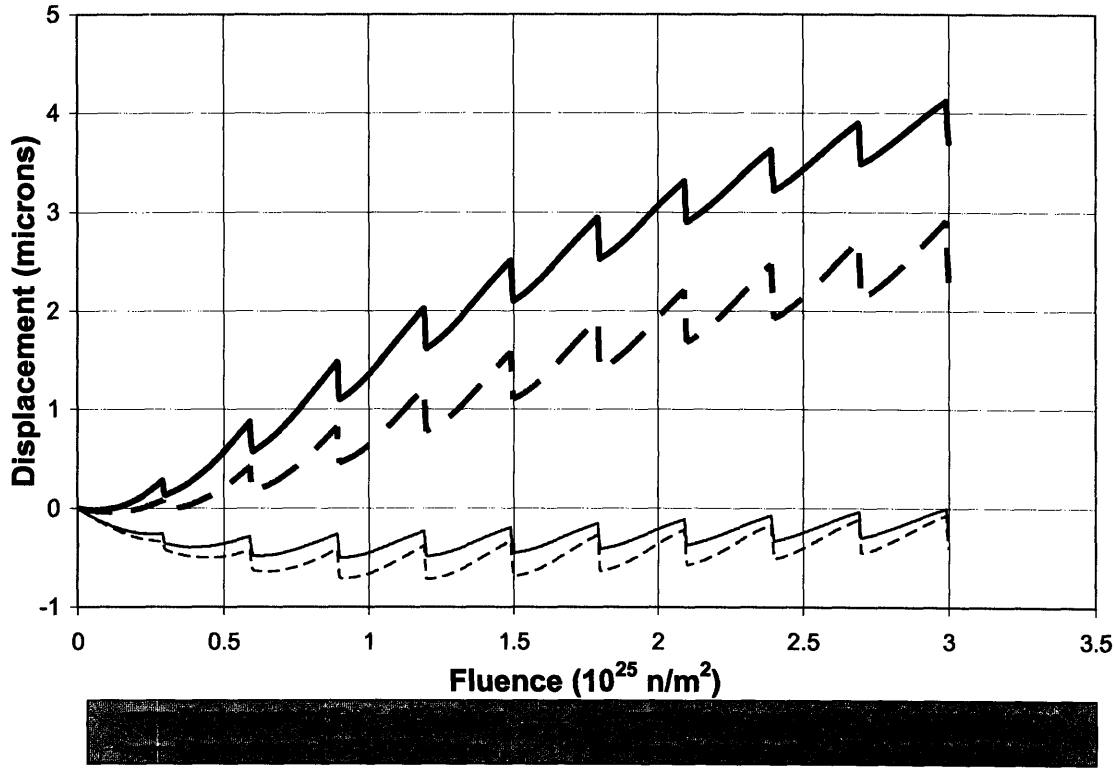

Figure 3-22: Displacement of Inner Surface IPyC and SiC Layers for Case 8

4 IAEA-CRP Sampled Coated Particle Benchmarks

Parts four and five of this benchmark consider populations of TRISO particles and the failure probabilities of each structural layer. The fourth part is designed to model particles and irradiation histories from previously conducted experiments. The fifth part is intended to model particles and irradiation histories from planned experiments. Each of the cases considers constant power, constant temperature, and irradiation.

These parts are fundamentally unlike the first three. The stresses in a normalized particle are not of primary concern here, but rather, a collection of particles are evaluated whose parameters are sampled in a Monte Carlo fashion from input standard deviations. Table 4-1 indicates which parameters are sampled by the code and the type of distribution from which they are sampled.

Table 4-1: TIMCOAT Sampled Parameters

Parameter	Distribution Type
U235 Enrichment (%)	Triangular
Kernel Diameter (μm)	Triangular
Buffer Thickness (μm)	Triangular
IPyC Thickness (μm)	Triangular
SiC Thickness (μm)	Triangular
OPyC Thickness (μm)	Triangular
Kernel Density (g/cm^3)	Triangular
Buffer Density (g/cm^3)	Triangular
IPyC BAF_0	Triangular
OPyC BAF_0	Triangular
IPyC Characteristic Strength (MPa.m$^{3/\beta}$)	Weibull
OPyC Characteristic Strength (MPa.m$^{3/\beta}$)	Weibull
SiC Characteristic Strength (MPa.m$^{3/\beta}$)	Weibull
SiC Fracture Toughness (MPa. μm$^{0.5}$)	Triangular

In addition, for these cases unlike in the previous ones, the internal pressure in the particle is not specified in the benchmark document but must be computed by TIMCOAT.

4.1 Part 4: Previous Experiment TRISO Benchmark Cases

This part contains cases 9 through 12, which model TRISO particles that were irradiated during the HRB, HFR and NPR irradiation programs. Unlike with previous parts, these cases do not build on one another, so they will be described and discussed separately below. As before, input parameters and irradiation histories can be found in Appendices I and II, respectively. Parameters that are listed in light colored text in the appendices are those that were not provided by the benchmark document and were supplied by the author. As will be discussed in Case 14, the choice of uncertainty values not provided in the benchmark can have a significant impact on failure results.

When each of these cases were run using solely the specified IAEA properties, very peculiar results were obtained, so each case was also run with a combination of TIMCOAT calculated swelling, creep and strength parameters. As with the cases in Part 3, results are presented both for the supplied IAEA parameters and TIMCOAT calculated parameters. The metrics of comparison for these four cases are the total particle failure fraction as a function of burnup and the total internal gas pressure and SiC maximum tangential stress on a normalized particle.

4.1.1 Case 9: HRB – 22 Parameters

This case considers TRISO particles irradiated in a Japanese experiment [1]. The irradiation duration is short, only 89 days with corresponding low end of life fluence and burnup. The case is notable in that the benchmark document specifics that the PyC is isotropic. Two sets of input parameters were used to model this case. Table 4-2 shows the properties that were varied between the IAEA value and TIMCOAT value runs. Any parameter not specified in this table is assumed to be the same between the two runs and has the value reported in Appendix I.

Table 4-2: Properties for Case 9

Parameter	Units	IAEA Value	Calculated Value
PyC Properties			
Radial Swelling Correlation	$(\Delta L/L)$ /10^{25} n/m^2	1.36334E-03x^3 -7.77024 E-03x^2 +2.00861E-02x -2.22642E-02	+7.67972E-05x^3 -1.56738E-03x^2 +1.07478E-02x -2.43444E-02
Tangential Swelling Correlation	$(\Delta L/L)$ /10^{25} n/m^3	-3.53804E-04x^3 +1.69251E-03x^2 +2.63307E-03x -1.91253E-02	+7.67972E-05x^3 -1.56738E-03x^2 +1.07478E-02x -2.43444E-02
Creep Coefficient	(MPa 10^{25} n/m^2)$^{-1}$	4.93E-04	1.53E-04
Poisson's Ratio In Creep		0.4	x < 0.3: 0.5 – x/3 x > 0.3: 0.4
Weibull Modulus		5	9.5
Characteristic Strength	MPa m^3/Weibull Modulus	IPyC: 2.0857 OPyC: 2.3054	14.2
Mean Strength	MPa	200	IPyC: 157 OPyC: 149
SiC Properties			
Weibull Modulus		8.02	6.0
Characteristic Strength	MPa m^3/Weibull Modulus	52.015	9.64
Mean Strength	MPa	873	420

The data in this table deserves some analysis. First consider the swelling correlations that have been plotted in Figure 4-1. As mentioned, the IPyC and OPyC are listed as having a BAF of 1.0 indicating isotropic PyC layers. This requires that the swelling rates in the tangential and radial direction be equivalent. The figure indicates that this is the case for the TIMCOAT calculated correlation, and that these TIMCOAT determined rates are close to the tangential rate specified in the benchmark document. It is curious, however, that the benchmark document specifies a different rate for radial swelling that is quite different from the tangential rate. No explanation for this deviation is given, and it is clearly nonphysical.

Next consider the creep coefficient. The IAEA value is 3.2 times larger than the calculated value. This is similar to the deviations seen in Part 3 except that in Part 3, the IAEA value was almost exactly twice that calculated by TIMCOAT, and the benchmark document indicated that this factor of two was to be expected. Here however, the document still claims a factor of two should be expected. There is not enough information to determine the cause of the additional deviation.

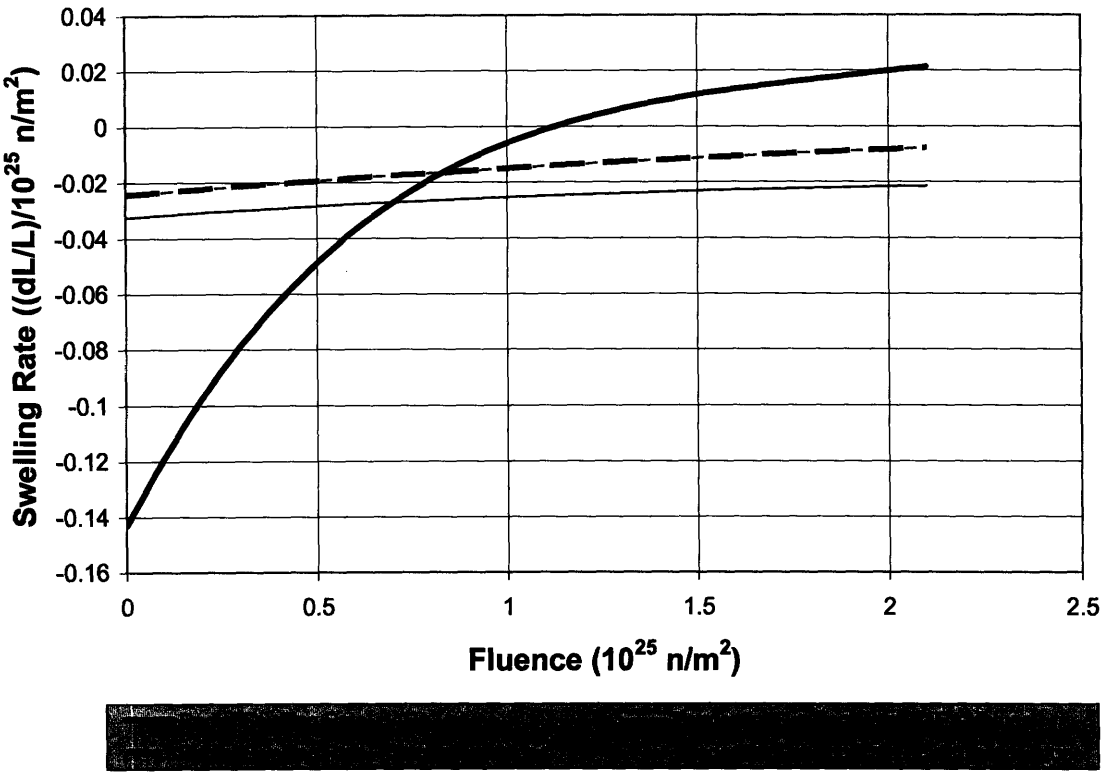

Figure 4-1: Radial and Tangential Swelling Rates for Case 9

Lastly, consider the Weibull modulus and strength data for the PyC and SiC layers. The Weibull Modulus reported for the IAEA and TIMCOAT, calculated values differ, but both are within the expected range described in CEGA-002820. Notice that the table lists both characteristic and mean strengths for the PyC and SiC layers. The benchmark document specifies a mean strength for the PyC and one for the SiC, while TIMCOAT uses a characteristic strength for each PyC layer and one for the SiC. The mean strength, S_o, can be related to the characteristic strength σ_o by the following formula:

$$S_o = \frac{\sigma_o}{(2V)^{\frac{1}{m}}}$$

where V is the volume of the layer and m its the Weibull modulus. We see then that if a characteristic strength of the PyC is specified, there will be a different mean strength for the IPyC and the OPyC as these layers have different volumes. The same is true if a single mean strength is specified. As TIMCOAT requires the user to input a characteristic strength for each layer, when appropriate, the single mean strength given by

the benchmark document is converted to two characteristic strengths. The reverse conversion is provided in the table to help the reader compare IAEA and TIMCOAT values. The formula above illustrates an interesting property of Weibull strength theory that as the volume of a layer increases, its mean strength decreases. The idea is that as the volume of a layer is increased, the probability of it incorporating a large flaw is increased. This flaw decreases the layer's strength. The theory holds the characteristic strength as an innate property of the material, while the mean strength depends on the volume of material present. A layer is assumed to fail when the mean strength of the layer is less than the mean tangential stress in that layer. Thus it is curious that the benchmark document specifies the mean strength and that it reports the same strength for all PyC layers regardless of volume.

Other than this difference in the parameter used to denote layer strength, the table shows that the TIMCOAT parameters predict PyC strengths about 25% less and SiC strength about 52% less then IAEA values. The IAEA values are not inconsistent with the ranges reported in CEGA-002820 but do not appear consistent with the volumes of the layers in this case.

4.1.2 Case 9: HRB – 22 Results and Discussion

Results from a normalized Case 9 type particle are now presented beginning with total internal gas pressure as displayed in Figure 4-2. The pressure is a monotonically increasing function of fast neutron fluence consistent with the continued buildup and release of fission product gasses from the fuel kernel. Figure 4-3 shows the maximum tangential stresses in the IPyC and SiC layers. The behavior of these stresses and the differences between the results obtained for IAEA and TIMCOAT calculated values are identical to the behavior and differences found in Part 3 of this study.

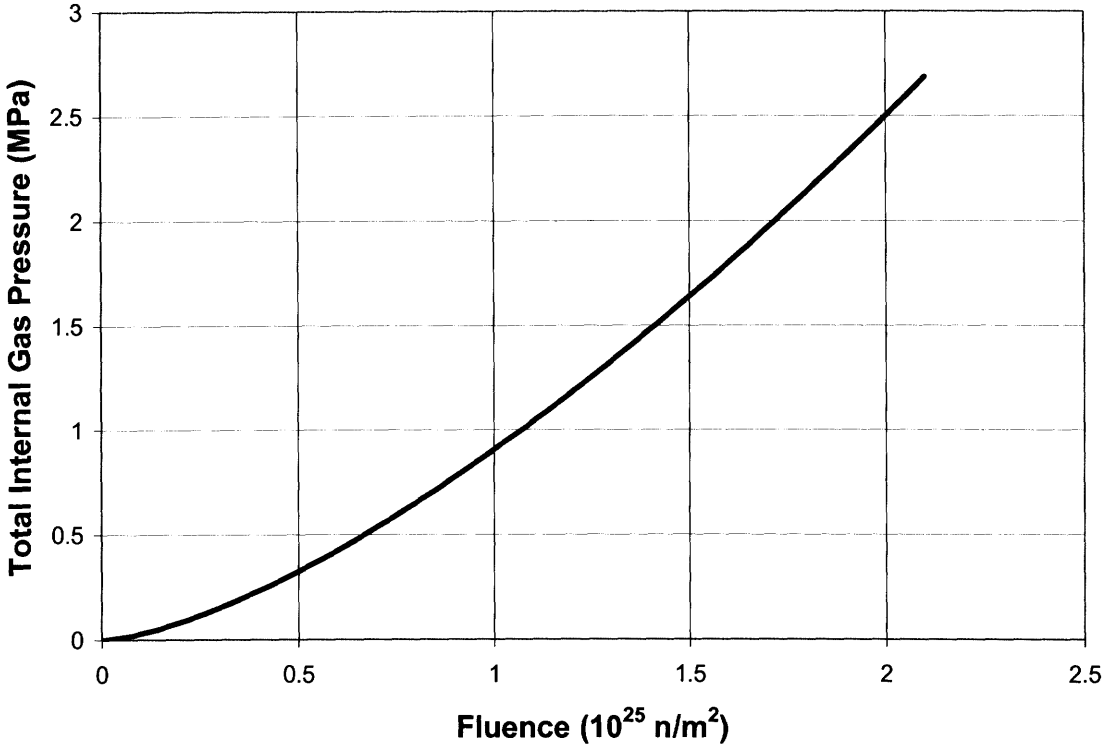

Figure 4-2: Total Internal Gas Pressure for a Nominal Particle Case 9

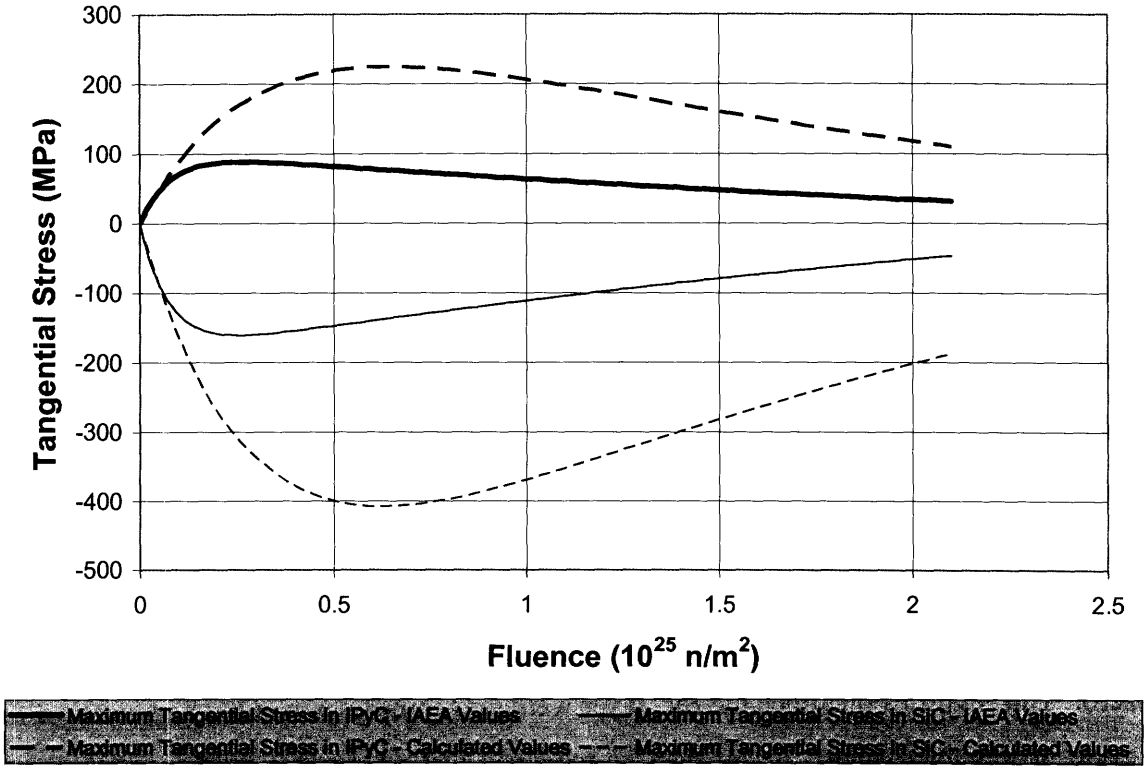

Figure 4-3: Maximum Tangential Stresses in IPyC and SiC Layers for a Nominal Particle Case 9

Now consider results from populations of one million of these particles. The first two groups of data in Table 4-3 give results from the populations described in Table 4-2. Notice that for the IAEA value particles no failures were observed in any of the three layers, while for the TIMCOAT value particles, failures were observed. This dramatic difference is only partly due to the difference in layer strengths and is a clear illustration of the effects of changing the PyC creep coefficient on the failure probability. In the case of the IPyC layer, doubling the PyC creep coefficient has reduced the maximum stress in the layer by a factor of three, and the failure probability falls accordingly. This phenomenon is easily understood. As was found in Part 2, creep acts to limit the maximum stress in the PyC. As the rate of creep is increased, the maximum stress decreases. In this case, with IAEA values, the peak stress in the IPyC layer for a normalized particle was about 90 Mpa, while its strength was about 200 Mpa. This neglects strength loss due to irradiation. The probability of sampling a particle whose maximum IPyC stress is more than twice the sample average is vanishingly small when the observed deviation is only 1.5 Mpa, so the probability of IPyC failure is correspondingly small. For the TIMCOAT values, however, the peak stress was about 225 MPa in a nominal particle with strength of 157 Mpa, so a substantial failure rate in the IPyC is obtained.

Table 4-3: Sampling Results for Case 9

	IAEA Values			TIMCOAT Values			TIMCOAT Values with fixed BAF = 1.0		
	IPyC	SiC	OPyC	IPyC	SiC	OPyC	IPyC	SiC	OPyC
Maximum Tangential Stress (MPa)	88.5 ± 1.46	~ 0	65.4 ± 0.61	240 ± 12.4	~ 0	178 ± 9.02	173 ± 19.5	12.3 ± 6.90	162 ± 11.7
Minimum Tangential Stress (MPa)	~ 0	-161 ± 13.1	~ 0	~ 0	-430 ± 48.1	~ 0	~ 0	-316 ± 41.2	~ 0
End of Life Tangential Stress (MPa)	30.4 ± 1.16	-44.3 ± 1.13	23.5 ± 1.19	180 ± 18.4	-230 ± 92.5	126 ± 18.7	166 ± 19.4	-2.92 ± 37.3	138 ± 31
Failure Probability (%)	> 1E-4	> 1E-4	> 1E-4	18.6 ± 1.3	0.70 ± 0.26	22.5 ± 1.3	100 ± 0.0063	2.62 ± 0.51	82 ± 1.18

In addition, note that for both cases the average maximum stress in the SiC was about zero. This signifies that once the SiC layer went into compression at the beginning of the cycle, it remained such. It can then be expected that no particle failures were due to

overpressure failure. This is was what was observed; all SiC failures were due to stress intensity cracking from PyC cracks.

The third group of data in Table 4-3 is meant to explore the effects of using isotropic PyC. This data was obtained using a population of particles having all of the TIMCOAT parameters except that it was assumed that the standard deviation on the BAF, as shown in Appendix I, was zero. That is, the PyC layers in all sampled particles were perfectly isotropic. When this was done, the probability of IPyC failure became essentially 100%, and the probability of SiC failure increased by a factor of 3.7 ± 0.6. At the same time the peak stress in the IPyC layer dropped about 70 MPa. At first this might seem unexpected. The maximum stress in the IPyC layer has decreased, but the failure rate of that layer and the SiC layer has increased dramatically. Understanding this behavior requires a more thorough examination of the properties of PyC (see reference [4]). It suffices here to say that as anisotropy of PyC increases, tangential stresses increase as swelling rates are more negative at the beginning of the irradiation cycle. This is countered by an increase in strength, as anisotropy increases, which reduces overall failure probability. It is noted that dominance of the increase in stress or the increase in strength will vary depending on the specifications of the particle.

Other than the overall probability of layer failure, it is possible to examine the probability of failure as a function of fast neutron fluence. Figure 4-4 and Figure 4-5 demonstrate that increasing the anisotropy of the PyC causes failures to occur later in the irradiation cycle. When the PyC is isotropic, the IPyC layers crack and fail first, followed by the OPyC layers. These cracked PyC layers then induce cracking and failure in the SiC layer a short time later. For more anisotropic PyC, IPyC and OPyC failures occur at the same fluence and are then followed by SiC failures. Recall that a TRISO particle is assumed to fail when the SiC layer fails. All particle failures were the result of SiC fracture due to IPyC cracking; there were no direct overpressure failures of SiC observed. For both anisotropies, in about half of the failures the IPyC failed first, followed by the OPyC and then the SiC. In the other half the OPyC failed first, followed by the IPyC and finally the SiC.

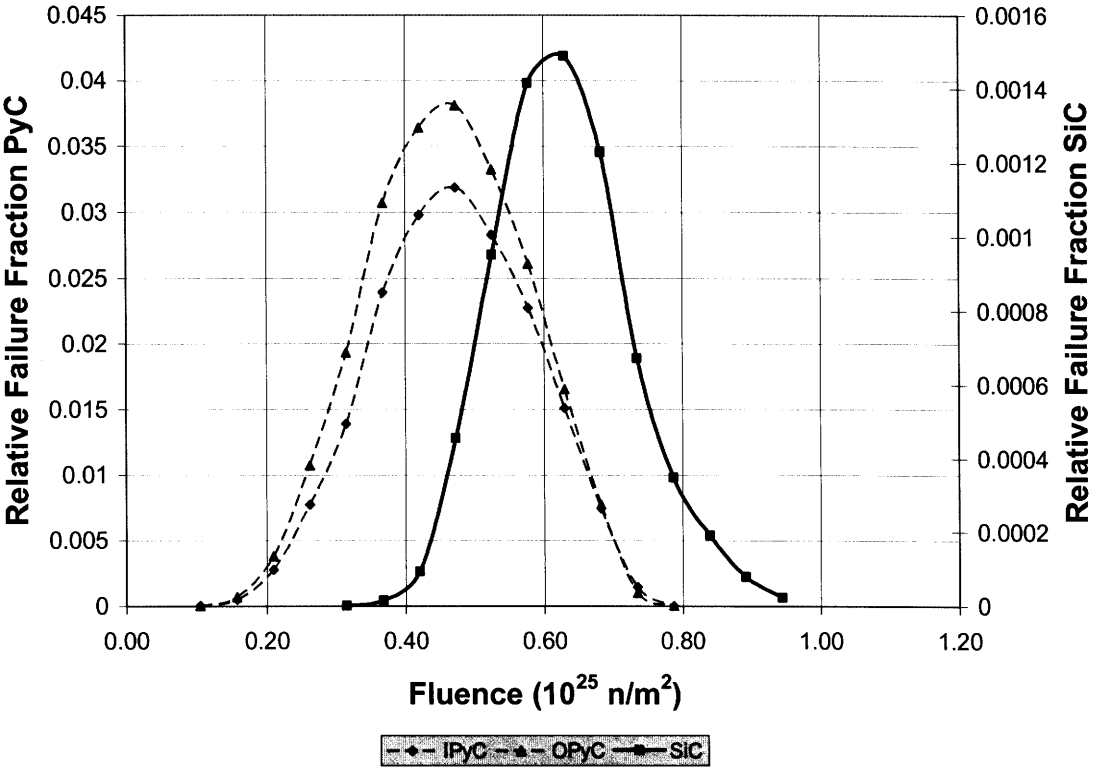

Figure 4-4: Failure Fraction for TIMCOAT Value Particles Case 9

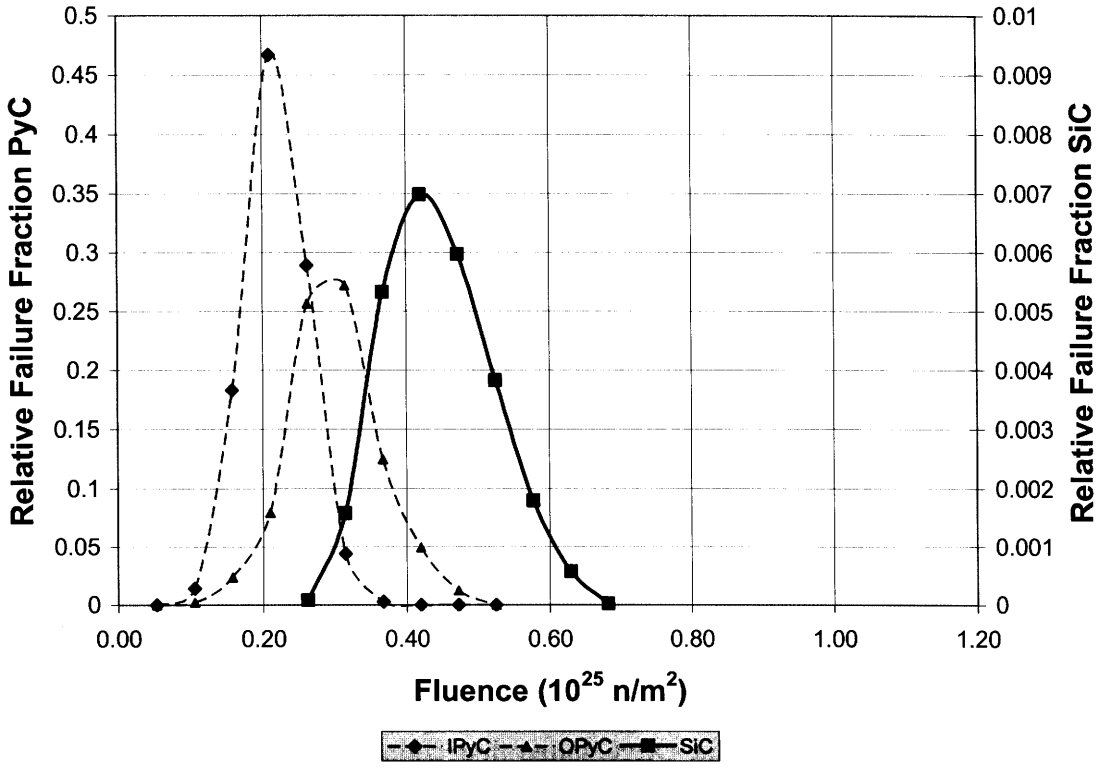

Figure 4-5: Failure Fraction for TIMCOAT Value Particles with fixed BAF = 1.0 Case 9

4.1.3 Case 10: HFR – K3 B/2 Parameters

This case considers TRISO particles irradiated in a German experiment [1]. These particles are different from the Case 9 particles in that the kernel volume is 24% less, but the fuel enrichment is 2.4 times larger. Also, the irradiation cycle is about 4 times longer. As with the Case 9 particles, two sets of parameters were simulated, as shown in Table 4-4.

Table 4-4: Properties for Case 10

Parameter	Units	IAEA Value	Calculated Value
PyC Properties			
Radial Swelling Correlation	$(\Delta L/L)/10^{25}$ n/m^2	$+1.36334E\text{-}03x^3$ $-7.77024\ E\text{-}03x^2$ $+2.00861E\text{-}02x$ $-2.22642E\text{-}02$	IPyC: $+7.69133E\text{-}04x^3$ $-5.34687E\text{-}03x^2$ $+1.643804E\text{-}02x$ $-2.00942E\text{-}02$ OPyC: $+7.3323E\text{-}04x^3$ $-4.834256E\text{-}03x^2$ $+1.438665E\text{-}02x$ $-2.10816E\text{-}02$
Tangential Swelling Correlation	$(\Delta L/L)/10^{25}$ n/m^3	$-3.53804E\text{-}04x^3$ $+1.69251E\text{-}03x^2$ $+2.63307E\text{-}03x$ $-1.91253E\text{-}02$	IPyC: $-3.19118E\text{-}05x^3$ $+9.43162E\text{-}04x^2$ $+4.71556E\text{-}03x$ $-2.11003E\text{-}02$ OPyC: $-2.92101E\text{-}04x^3$ $+6.39702E\text{-}04x^2$ $+5.82342E\text{-}03x$ $-2.06305E\text{-}02$
Creep Coefficient	(MPa 10^{25} n/m^2)$^{-1}$	4.93E-04	9.24E-05
Poisson's Ratio In Creep		0.4	$x < 0.3$: $0.5 - x/3$ $x > 0.3$: 0.4
Weibull Modulus		5	9.5
Characteristic Strength	MPa m^3/Weibull Modulus	IPyC: 2.1348 OPyC: 2.2894	24
Mean Strength	MPa	200	IPyC: 262 OPyC: 252
SiC Properties			
Weibull Modulus		8.02	6.0
Characteristic Strength	MPa m^3/Weibull Modulus	51.7469	9.64
Mean Strength	MPa	873	421

Appendix I indicates that the BAF of the two PyC layers is slightly different, 1.053 for the IPyC and 1.019 for the OPyC. Accordingly, TIMCOAT calculates a different

swelling correlation for each layer. The benchmark provides only a single correlation, and it is the same as for the Case 9 particles. These correlations are plotted in Figure 4-6. As in Case 9, the IAEA radial swelling correlation differs significantly from the TIMCOAT correlation with no apparent explanation. The figure shows that TIMCOAT predicts slightly smaller variations in the radial and tangential swelling rates over the irradiation cycle for the more isotropic OPyC than for the more anisotropic IPyC. As the rates must be the same for perfectly isotropic material, this is expected.

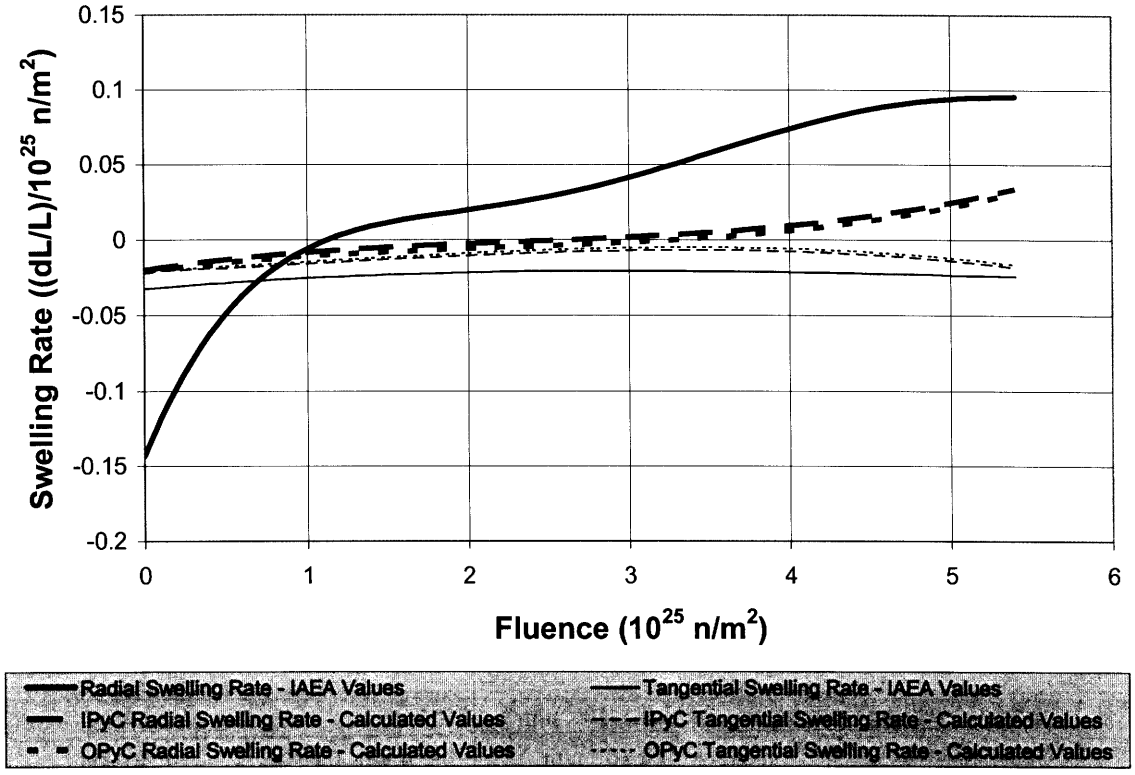

Figure 4-6: Radial and Tangential Swelling Rates for Case 10

The swelling rates toward the end of the irradiation cycle are cause for concern, however. Recall the mechanisms for swelling discussed in section 3.2: densification, which leads to shrinkage in both the radial and tangential directions and reorientation, which causes a swelling in the radial direction. Densification dominates early in the cycle and is then replaced by reorientation. This behavior is correctly captured up to a fluence of about 3 x 10^{25} n/m^2, however, the figures show that for both the TIMCOAT and IAEA correlations, the tangential rate begins to show an increased rate of shrinkage at higher fluences. This would suggest an increase in densification that is nonphysical. In the vicinity of 3 x 10^{25}

n/m^2 the swelling rate becomes almost constant, and it is much more physically reasonable to assume that it would stay constant at higher fluences. The error here is due to the curve fitting methods used to obtain both correlations. Swelling data was fit to a simple three degree polynomial that does not have enough degrees of freedom to exhibit a constant swelling rate at high fluences. In the future, refinements to the modeling approach should address this issue.

4.1.4 Case 10: HFR – K3 B/2 Results and Discussion

Beginning with results from a normalized particle, Figure 4-7 gives the total internal gas pressure as a function of fast neutron fluence, and Figure 4-8 provides the tangential stresses in the IPyC and SiC layers.

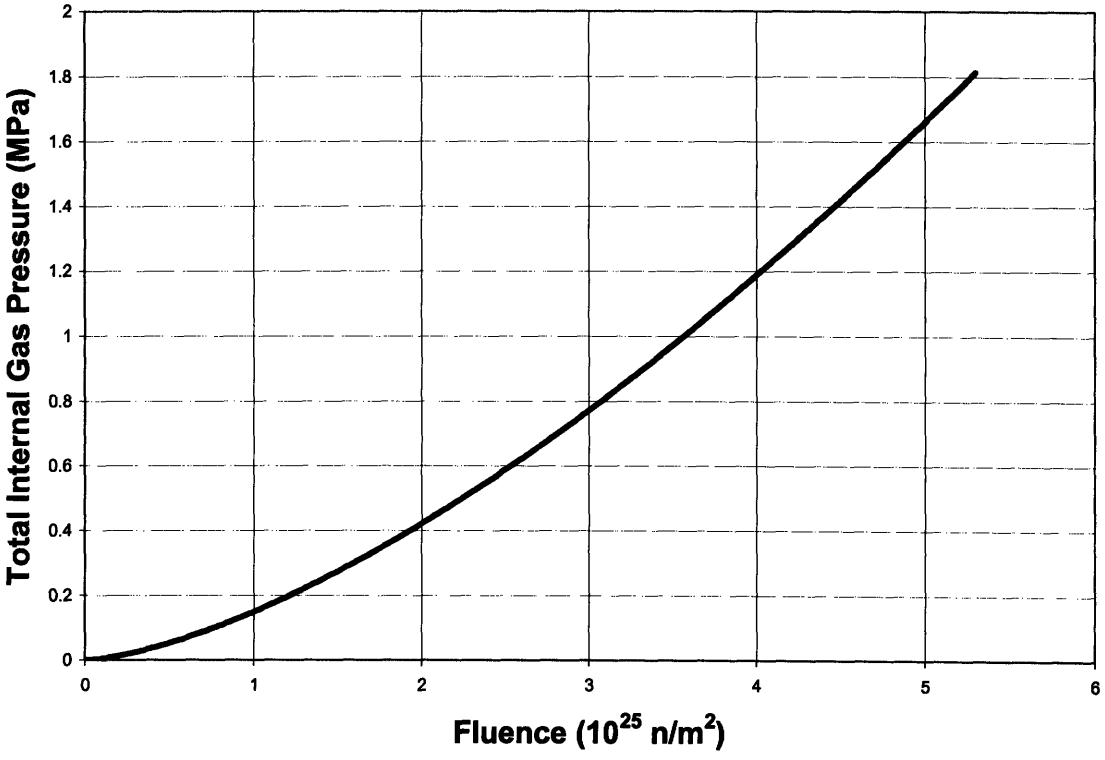

Figure 4-7: Total Internal Gas Pressure for a Nominal Particle Case 10

The observed behavior of the tangential stresses for the IAEA values is extremely disturbing. The behavior of the stresses is not physically meaningful, and it was not possible to simulate the entire irradiation cycle as the code was unable to converge at

high fluences. For the TIMCOAT calculated values, however, the behavior appears normal. The cause of the atypical stresses for the IAEA values appears to be due to the very large creep coefficient. The coefficient is such that during the irradiation cycle, the tangential stress at the inner surface of the IPyC is completely relaxed by a fluence of 2.4 x 10^{25} n/m^2. After this point, it might be expected that any loads on the IPyC are relaxed more quickly than they are applied, and so the average stress in the IPyC should asymptotically approach zero. To observe this behavior using the code's current algorithms, however, the time step for the simulation must also approach zero. The time step in TIMCOAT is not designed to adapt in this fashion, and so after the point where asymptotical behavior might result, errors begin to accumulate rapidly. In its current form, TIMCOAT cannot be used to simulate particles where the creep coefficient is sufficiently large to completely relax the stresses in the PyC layers.

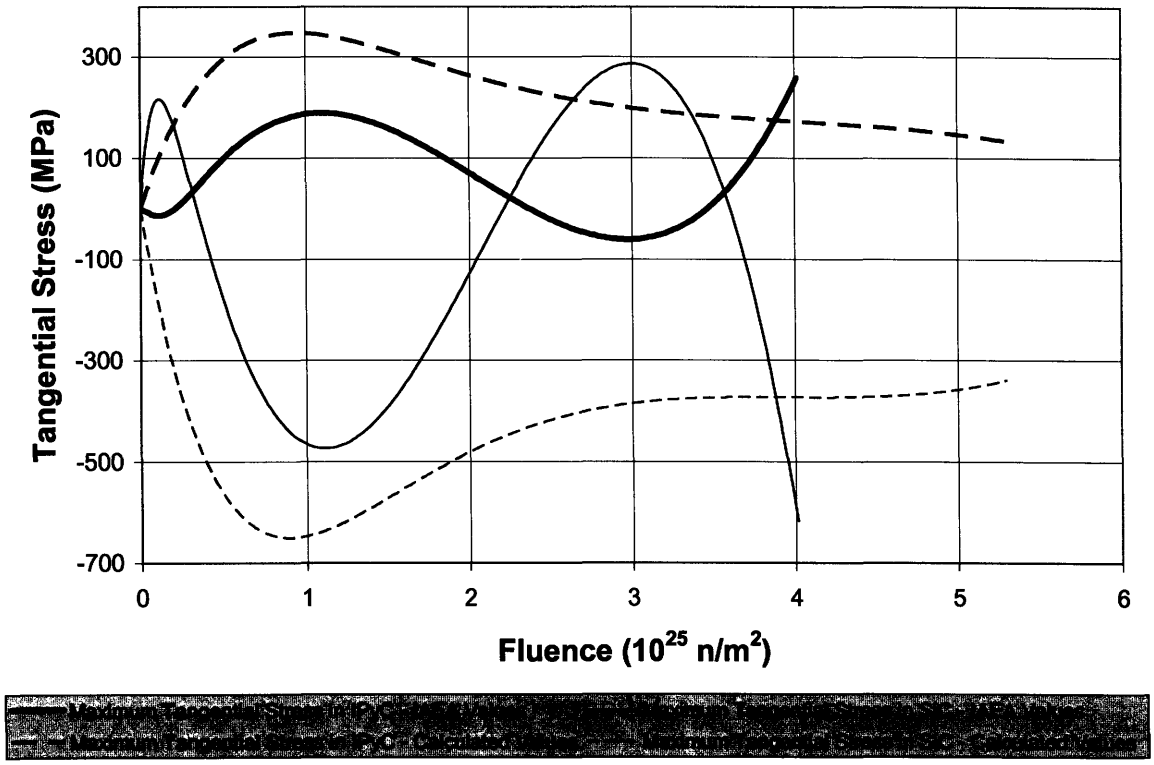

Figure 4-8: Maximum Tangential Stresses in IPyC and SiC Layers for a Nominal Particle Case 10

It is then necessary to proceed by presenting sampling results from only the TIMCOAT calculated parameters. Table 4-5 presents stress and failure probability data for the three structural layers for a population of a half million particles. If compared to the results

from Case 9, the maximum stress in the IPyC has not changed substantially. The maximum stress in the OPyC is significantly larger, however. In Case 9, the failure rates of the two PyC layers were almost identical while here, the failure rate of the OPyC is about one tenth of the IPyC despite the larger stress. This is due to the greater strength the code assigns the layer due to its slightly larger density. It is somewhat suspicious that such a small change in density (1.85 vs. 1.88 g/cc) could have such a large effect on the strength. TIMCOAT uses a piecewise discontinuous function to determine layer strength as a function of density that overlaps several sets of experimental results in CEGA-002820. This approach allows the larger changes in strength to occur. Clearly an interpolative approach would be more desirable, and it is recommended in the future. It is also seen that the SiC failure probability is almost an order of magnitude larger. As Figure 4-9 indicates this is not due to the fact that this case has a longer irradiation cycle. The peak failure rate in both Cases 9 and 10 is between 0.6 and 0.8 x 10^{25} n/m^2.

Table 4-5: Sampling Results for Case 10

	IPyC	SiC	OPyC
Maximum Tangential Stress (MPa)	292 ± 37.8	~ 0	242 ± 8.50
Minimum Tangential Stress (MPa)	~ 0	-552 ± 79.2	~ 0
End of Life Tangential Stress (MPa)	262 ± 51.8	-149 ± 69.4	142 ± 26.6
Failure Probability (%)	90.6 ± 0.32	7.08 ± 0.29	11.6 ± 0.36

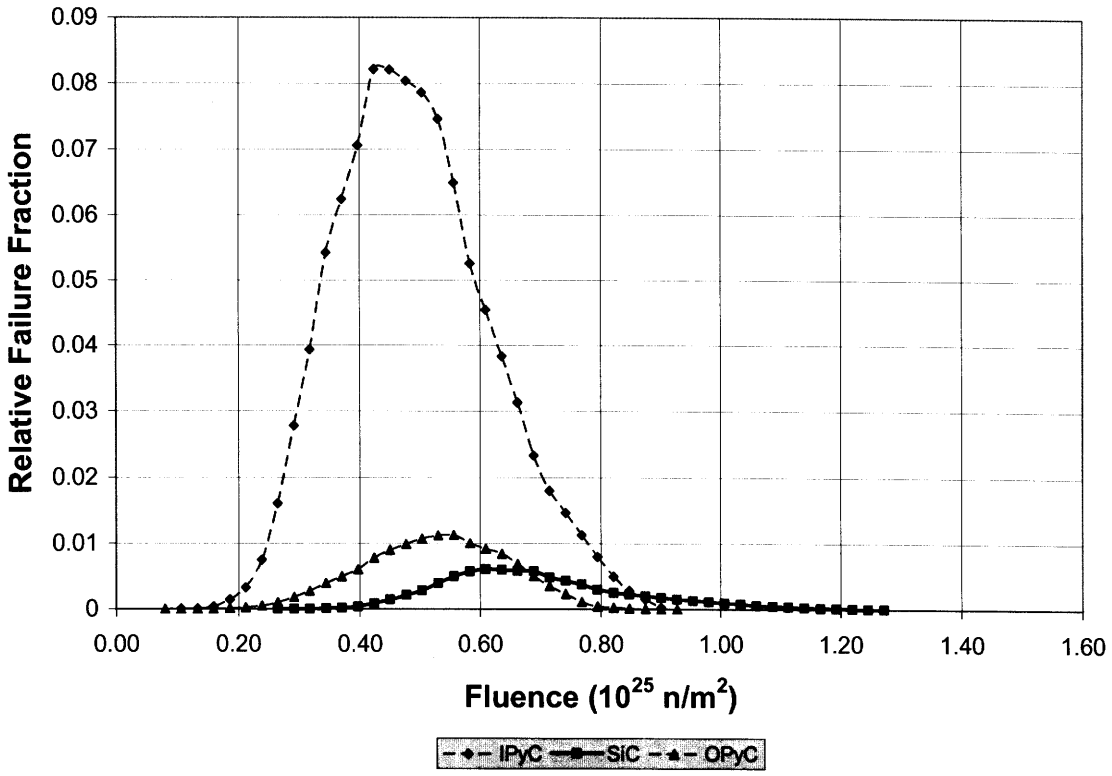

Figure 4-9: Failure Fraction Case 10

4.1.5 Case 11: HFR – P4

This case also considers particles irradiated in a German experiment [1]. Unfortunately, not much can be said here. The convergence problem that was described for the IAEA values in case 10 also occurred for the TIMCOAT values here. This case is almost identical to Case 10 except that the end of cycle fluence and cycle average temperature are larger. The higher temperatures cause TIMCOAT to increase the creep rate, and the larger fluence allowed more opportunity for creep. Figure 4-10 shows the resulting stress distribution where the tension in the IPyC is completely relaxed before the end of the cycle, but the code fails to capture this as an asymptotic trend toward equilibrium.

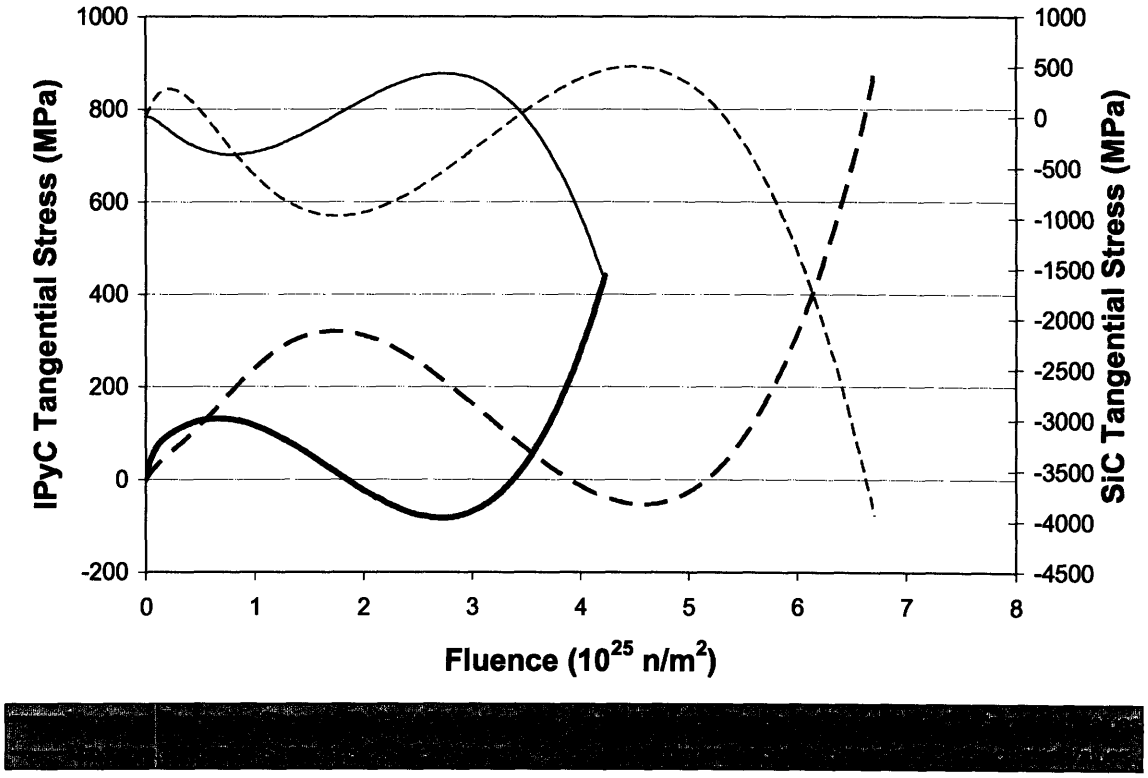

Figure 4-10: Maximum Tangential Stresses in IPyC and SiC Layers for a Nominal Particle Case 11

4.1.6 Case 12: NPR – 1A 5 Parameters

The TRISO particles simulated in this case are from an American experiment [1]. The experimental results from these particles have been used to benchmark TIMCOAT in the past. Complete details can be found in references [4] and [8]. TIMCOAT results show very good agreement with NPR data, and Figure 4-11 has been included to demonstrate this agreement. The Figure shows the ratio of Kr-85m release to background, which was detected during the experiment, and the corresponding ratios generated from TIMCOAT failure data. The version of TIMCOAT being used for this benchmark corresponds to the line A1 – A9 simulation in the figure. These results were obtained with detailed power and temperature histories from the experiment, which are not provided for this benchmark.

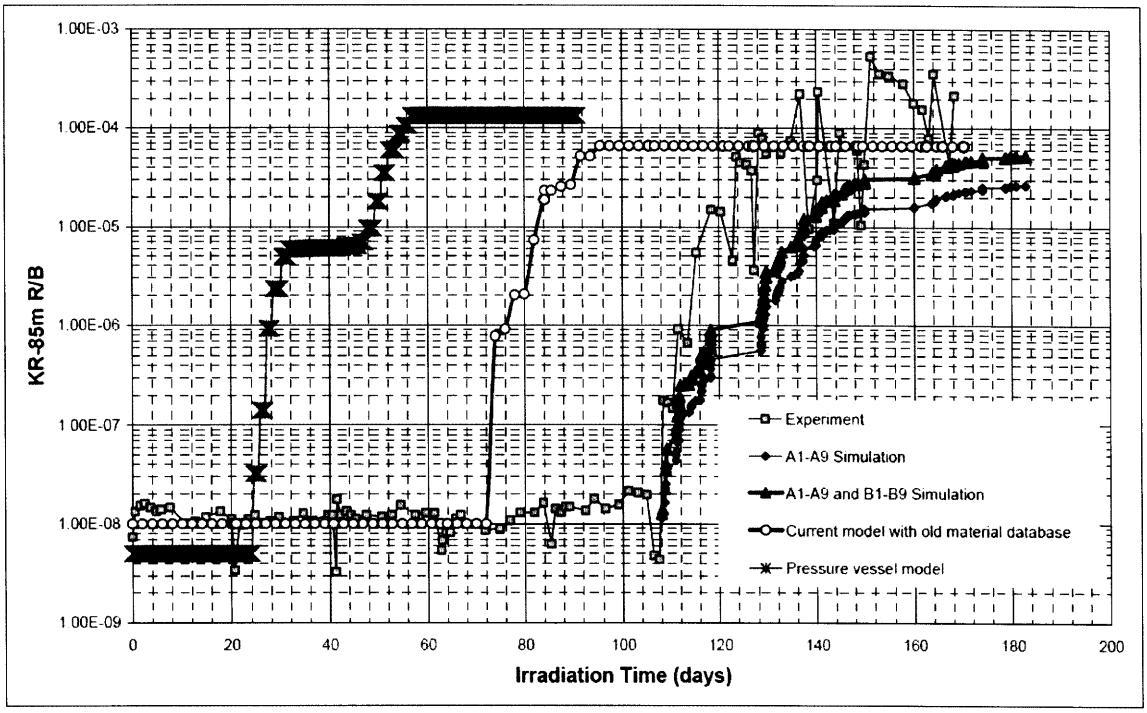

Figure 4-11: Comparison between TIMCOAT and Experimental Data for simulation of NPR1 capsules [8]

For the benchmark simulation, constant power and temperatures are assumed as shown in Appendix II. As with the previous cases, two sets of parameters were simulated, and the differences are shown in Table 4-6.

Table 4-6: Properties for Case 12

Parameter	Units	IAEA Value	Calculated Value
PyC Properties			
Radial Swelling Correlation	$(\Delta L/L)/10^{25}$ n/m^2	+4.73756E-04x^3 -3.80252E-03x^2 +1.64999E-02x -2.13483E-02	IPyC: +1.45646E-03x^3 -1.0086E-02x^2 +2.7251E-02x -2.21696E-02 OPyC: +1.37093E-03x^3 -9.85475E-03x^2 +2.891129E-02x -2.61414E-02
Tangential Swelling Correlation	$(\Delta L/L)/10^{25}$ n/m^3	-1.03249E-03x^3 +5.47396E-03x^2 -3.29740E-03x -1.83549E-02	IPyC: -6.45143E-04x^3 +3.20334E-03x^2 -7.38705E-04x -1.82424E-02 OPyC: -5.8186E-04x^3 +2.71209E-03x^2 +9.8522E-04x -2.20026E-02
Creep Coefficient	(MPa 10^{25} n/m^2)$^{-1}$	2.70E-04	IPyC: 1.25E-04 OPyC: 1.44E-04
Poisson's Ratio In Creep		0.5	x < 0.3: 0.5 – x/3 x > 0.3: 0.4
Weibull Modulus		9.5	9.5
Characteristic Strength	MPa m^3/Weibull Modulus	IPyC: 18.596 OPyC: 19.187	IPyC: 23.61 OPyC: 22.50
Mean Strength	MPa	218	IPyC: 277 OPyC: 256
SiC Properties			
Weibull Modulus		6.0	6.0
Characteristic Strength	MPa m^3/Weibull Modulus	11.482	9.64
Mean Strength	MPa	572	481

Unlike with the previous sampling cases, the swelling correlations for the IAEA and TIMCOAT values match well as shown in Figure 4-12. The TIMCOAT correlations do exhibit the curve fitting error discussed in Section 4.1.3, but the deviation appears small. The assumed strengths of the structural layers and their Weibull Modules are also in much closer agreement than in Cases 9 and 10. The IAEA creep coefficient, however, is still twice that of the TIMCOAT calculated coefficient and does not acknowledge the variation between the IPyC and OPyC due to varying densities.

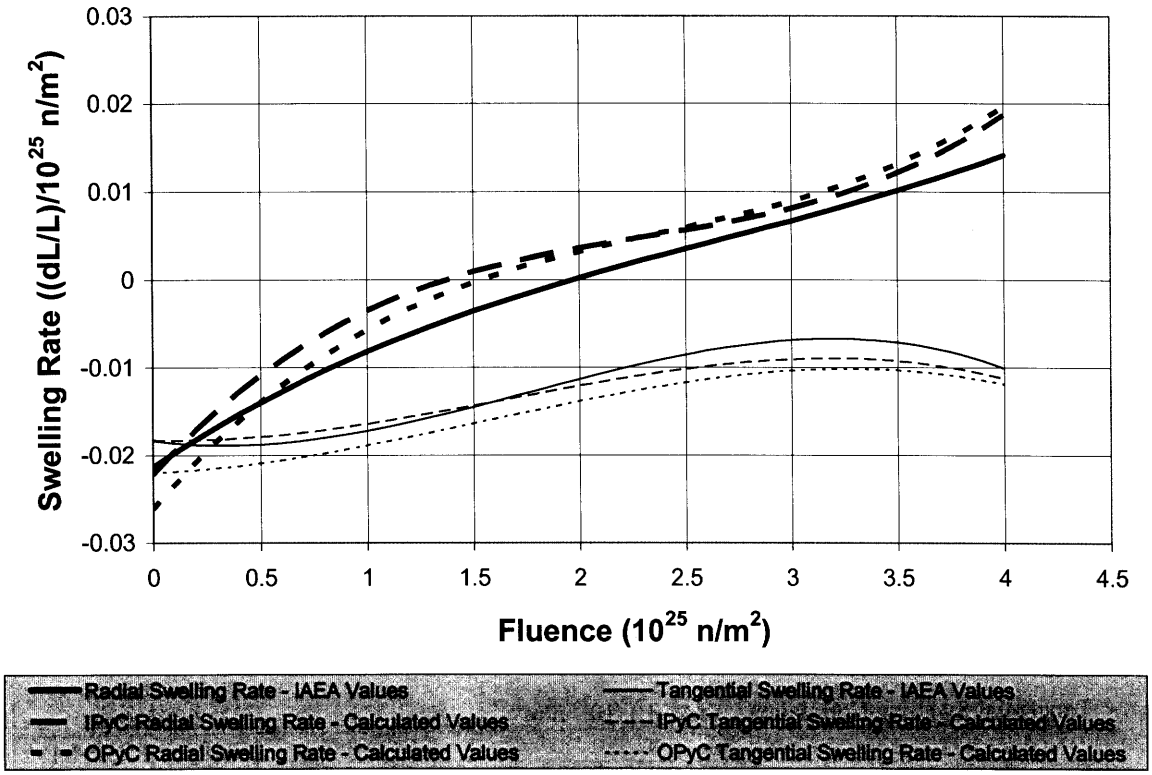

Figure 4-12: Radial and Tangential Swelling Rates for Case 12

4.1.7 Case 12: NPR – 1A 5 Results and Discussion

Moving directly to results from normalized particles, Figure 4-13 displays the buildup of fission gas pressure in the buffer as a function of fast neutron fluence, and Figure 4-14 shows the tangential stresses at the inner surfaces of the IPyC and SiC layers. Toward the end of the irradiation cycle, it is noted that the tangential stress in the IPyC for the calculated parameters relaxes below the stress predicted when using the IAEA parameters. This is unique among all the other cases considered and is a result of the larger radial swelling indicated by the TIMCOAT swelling correlation. Also of interest is the trend in the stresses shown in the figure at the end of the irradiation cycle. The two IPyC stresses reach a minimum and then begin to increase, and the two SiC stresses reach a maximum and then begin to decrease. This behavior is not physically meaningful. Once the stresses reach their extremes they can be expected to stay constant at these values, which represent a balance between creep, swelling, and internal pressure. This constant trend is not observed due to error accumulation in the code algorithm, which

makes it very difficult to capture asymptotic behavior. The error can be eliminated by applying a high precision floating point number version of TIMCOAT, but this increases computation time significantly. As the error observed here is only of order 10 MPa, it was assumed there would be very little effect on the predicted failure probabilities, and so steps were not taken to correct it.

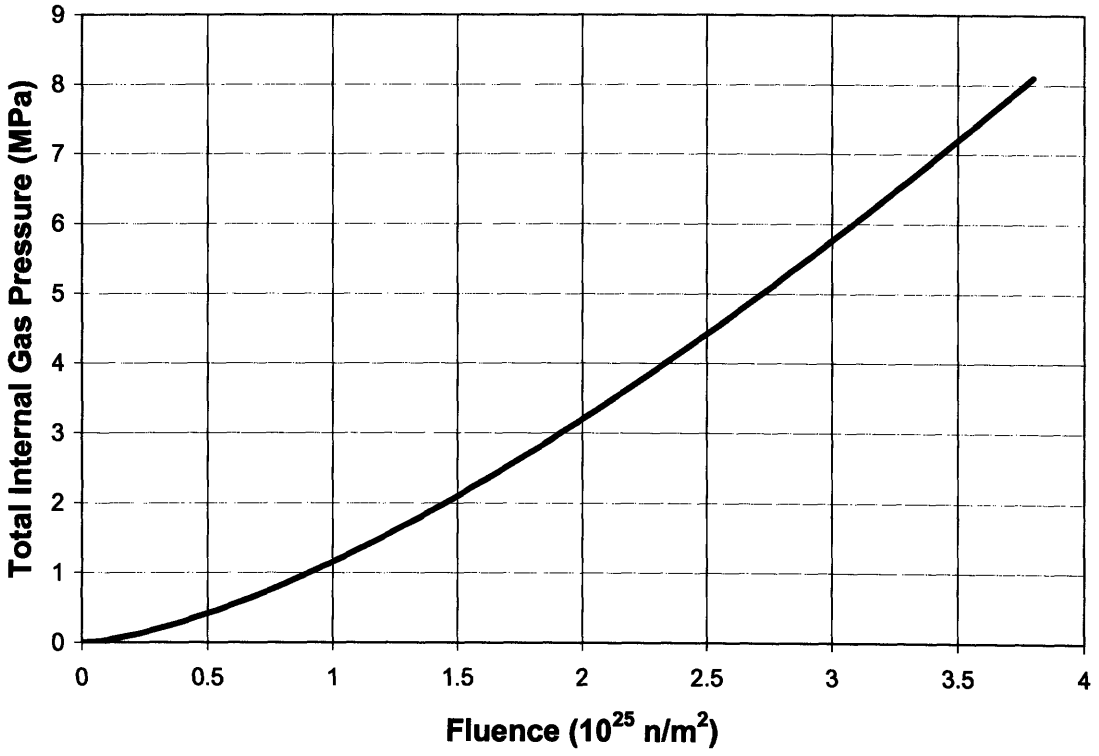

Figure 4-13: Total Internal Gas Pressure for a Nominal Particle Case 12

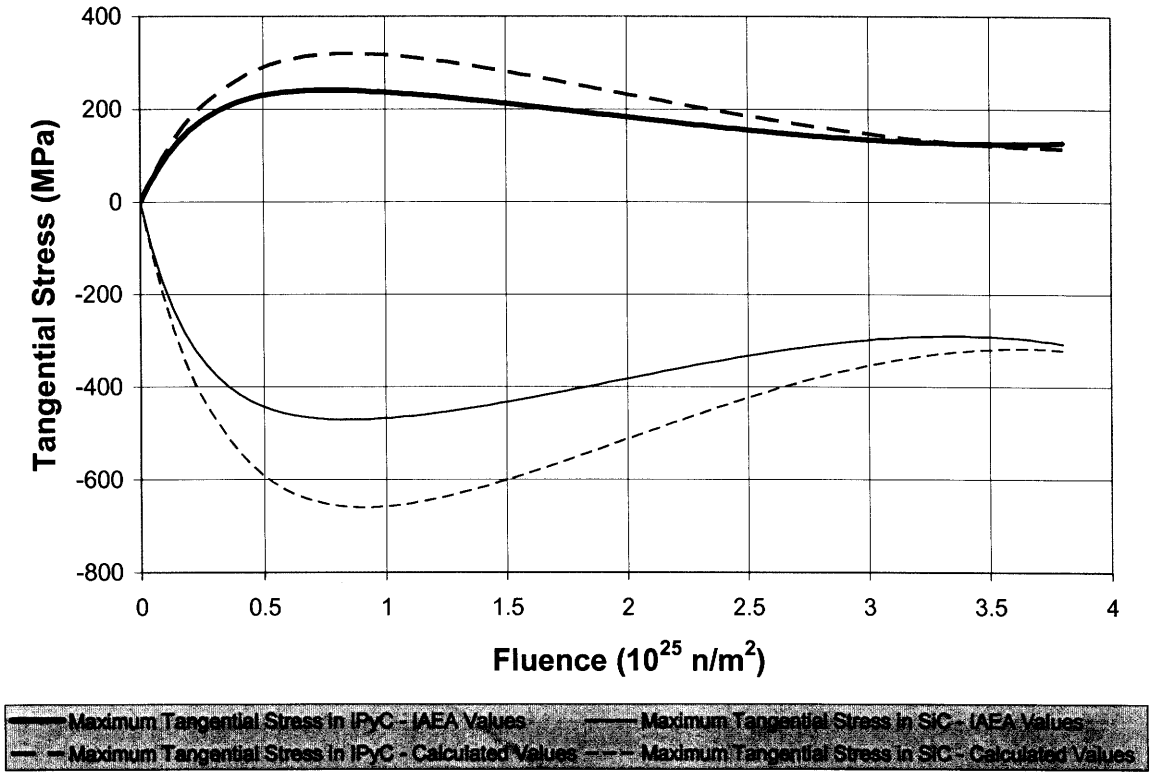

Figure 4-14: Maximum Tangential Stresses in IPyC and SiC Layers for a Nominal Particle Case 12

From a sample of one million particles, the stresses and failure probabilities shown in Table 4-6 were obtained. Note that the failure probabilities determined by the IAEA and TIMCOAT parameters are very similar, and as the maximum stresses calculated for a normalized particle in Figure 4-14 were comparable as well, this is not unexpected. Notice also the very low probability of SiC layer failure and the comparatively large standard deviation. This is a clear indication that a larger population of particles should be simulated to obtain statistically significant results. Unfortunately, this would require increasing the population by about an order or magnitude, which would require unreasonably long computation time. To alleviate this, a method of importance sampling could be introduced, and this feature is recommended in the future.

Table 4-7: Sampling Results for Case 12

	IAEA Values			TIMCOAT Values		
	IPyC	SiC	OPyC	IPyC	SiC	OPyC
Average Maximum Tangential Stress (MPa)	234 ± 17.6	-0.334 ± 0.506	121 ± 3.38	308 ± 21.2	-16.0 ± 2.45	192 ± 4.70
Average Minimum Tangential Stress (MPa)	~ 0	-457 ± 56.6	~ 0	~ 0	-638 ± 76.2	~ 0
Average End of Life Tangential Stress (MPa)	170 ± 28.7	-215 ± 101	84.3 ± 2.01	189 ± 68.5	-219 ± 96.4	108 ± 6.98
Failure Probability (%)	33.9 ± 0.48	> 1E-4	0.075 ± 0.025	39.3 ± 0.51	0.0015 ± 0.0039	1.10 ± 0.101

Figure 4-15 and Figure 4-16 show the relative failure fraction of the structural layers as a function of fluence for the two sets of parameters. Notice that the PyC failures occur at almost the exact same fluence for both sets of parameters. As in previous cases, these failures occur early in the irradiation and precede SiC failure. The data shows that all SiC failures were the result of PyC cracking. No direct overpressure failures occurred.

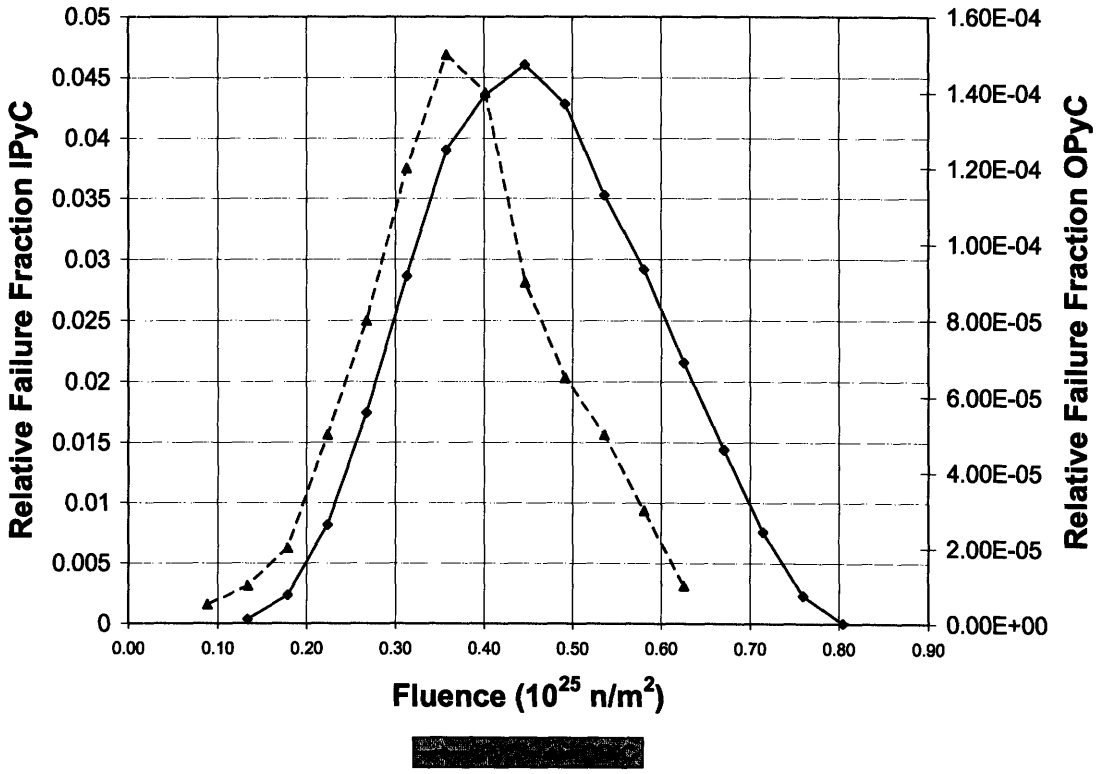

Figure 4-15: Failure Fraction for IAEA Value Particles Case 12

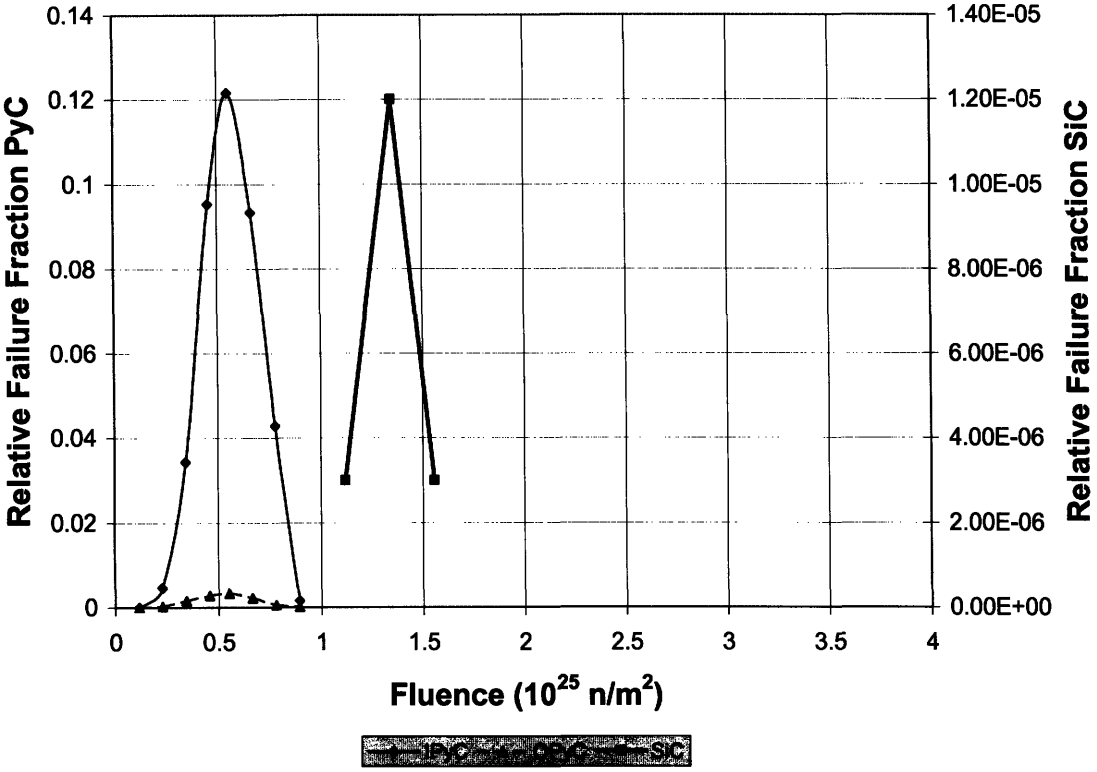

Figure 4-16: Failure Fraction for TIMCOAT Value Particles Case 12

4.2 Part 5: Future Experiment TRISO Benchmark Cases

The final part of this study considers TRISO particles from two planned experiments. These two cases, Cases 13 and 14, do not differ substantially from the UO_2 cases in Part 4. They have identical material properties and similar dimensions but slightly more highly enriched fuel kernels. The complete list of input parameters and irradiation histories are in Appendices I and II respectively, and diagrams of the particle dimensions are located in Appendix III. The metrics of comparison are the same as for Part 4.

4.2.1 Case 13: HFR EU – 1 Parameters

Following the established pattern, an IAEA set of parameters and a calculated set were simulated. The differences are shown in Table 4-8. The one notable variation for this case as compared to the previous four is that for the set of calculated parameters, IAEA strengths and modules were used. This was done as reasonable results were obtained with these IAEA parameters unlike before. The creep coefficient is still a matter of concern. Here is IAEA creep is a factor of 3.2 larger than the calculated creep.

Table 4-8: Properties for Case 13

Parameter	Units	IAEA Value	Calculated Value
PyC Properties			
Radial Swelling Correlation	$(\Delta L/L)/10^{25}$ n/m^2	+1.36334E-03x^3 -7.77024 E-03x^2 +2.00861E-02x -2.22642E-02	-7.1532E-04x^3 +4.5313E-03x^2 +1.4658E-03x -1.7564E-02
Tangential Swelling Correlation	$(\Delta L/L)/10^{25}$ n/m^3	-3.53804E-04x^3 +1.69251E-03x^2 +2.63307E-03x -1.91253E-02	+4.81209E-04x^3 -4.704724E-03x^2 +1.50758E-02x -2.60689E-02
Creep Coefficient	(MPa 10^{25} n/m^2)$^{-1}$	4.93E-04	1.54E-4
Poisson's Ratio In Creep		0.4	x < 0.3: 0.5 – x/3 x > 0.3: 0.4
Weibull Modulus		5	
Characteristic Strength	MPa m^3/Weibull Modulus	IPyC: 2.1345 OPyC: 2.2894	
Mean Strength	MPa	200	
SiC Properties			
Weibull Modulus		8.02	
Characteristic Strength	MPa m^3/Weibull Modulus	51.75	
Mean Strength	MPa	873	

Figure 4-17 displays the swelling correlations used in this case. The IAEA coefficient is the same as for Cases 9 – 11, so as before there is good agreement with the TIMCOAT correlations for tangential swelling but poor agreement for radial swelling.

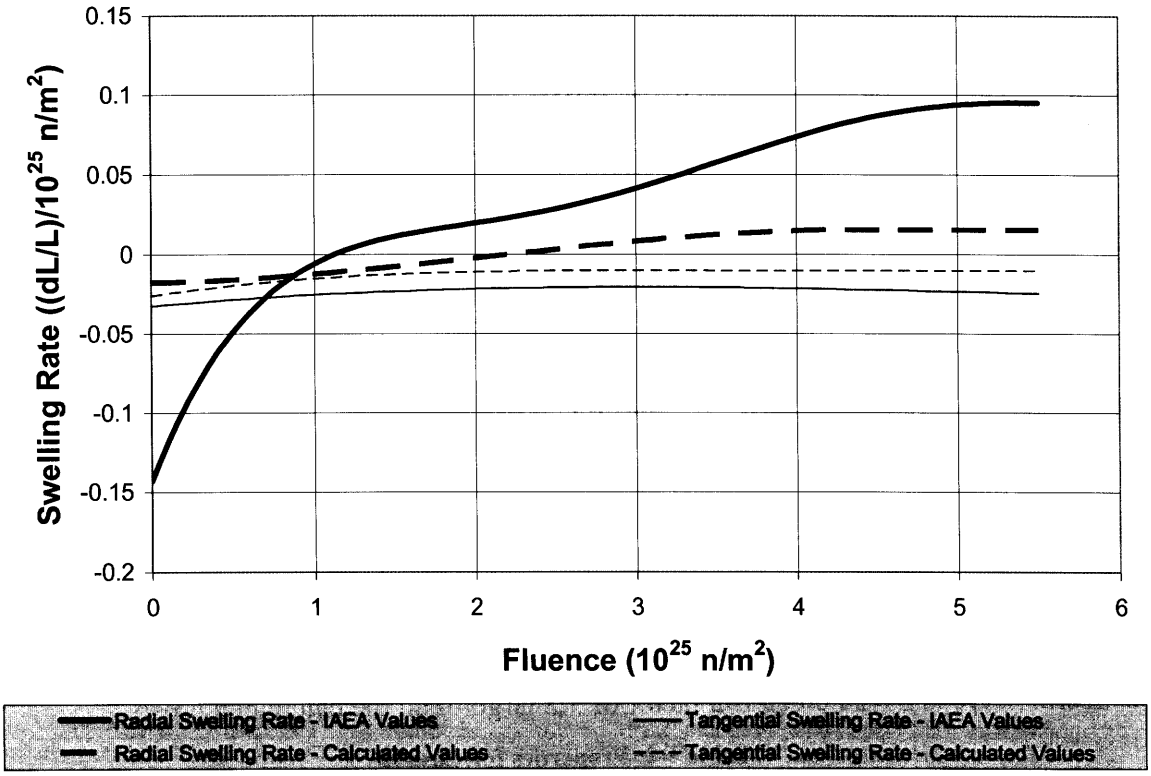

Figure 4-17: Radial and Tangential Swelling Rates for Case 13

4.2.2 Case 13: HFR EU – 1 Results and Discussion

Beginning with results from a normalized particle, the total internal pressure in the particle and tangential stresses in the IPyC and SiC are given in Figure 4-18 and Figure 4-19, respectively. Looking at the tangential stresses reveals that the IAEA parameters' large creep coefficient led to total relaxation of the tangential stresses before the end of the cycle. As in Case 10, TIMCOAT failed to simulate the particle after this point and so results from an IAEA type population of particles is not available.

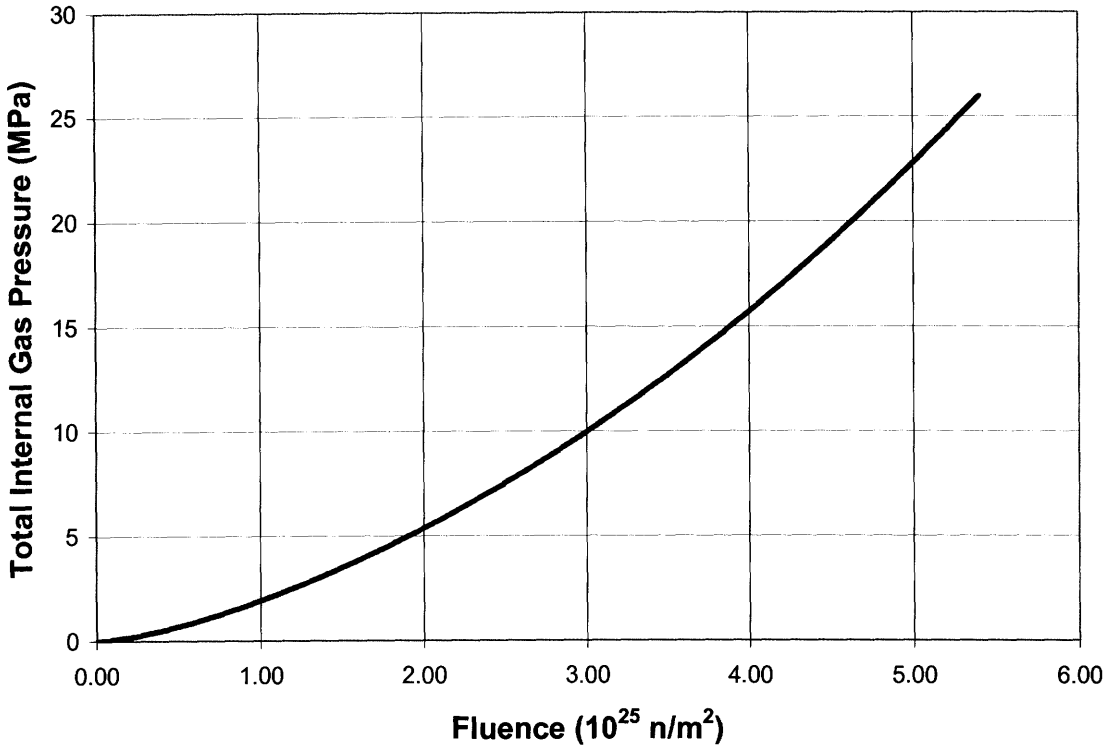

Figure 4-18: Total Internal Gas Pressure for a Nominal Particle Case 13

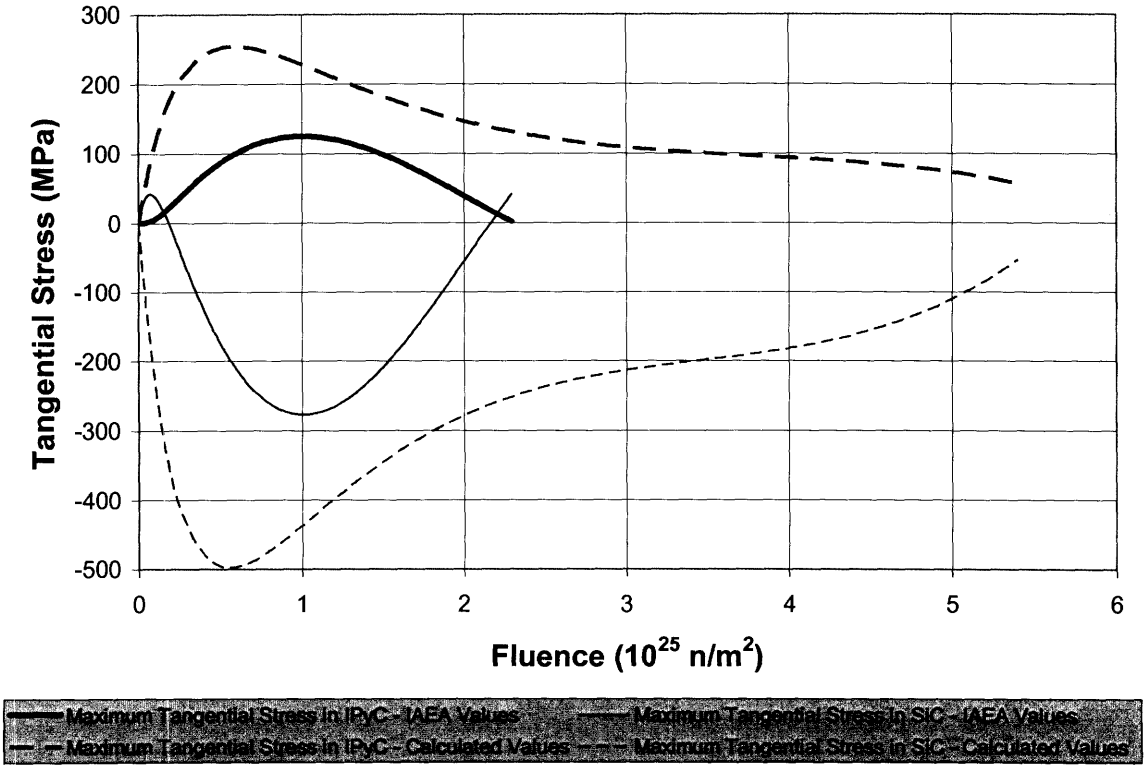

Figure 4-19: Maximum Tangential Stresses in IPyC and SiC Layers for a Nominal Particle Case 13

The remaining data was gathered from a population of one million TIMCOAT parameter type particles. Table 4-9 provides the stress and failure probability results for this population. It is noted that this is the first case where there is a significant probability that the SiC layer will be in tension by the end of the irradiation cycle, however, further examination of the data showed that all particle failures were due to IPyC and OPyC cracking, which caused fracture of the SiC. No direct SiC overpressure failures were observed and SiC failure was always preceded by cracking of both the IPyC and OPyC layers.

Table 4-9: Sampling Results for Case 13

	IPyC	SiC	OPyC
Maximum Tangential Stress (MPa)	219 ± 32.3	26.9 ± 38.1	178 ± 11.7
Minimum Tangential Stress (MPa)	~ 0	-424 ± 69.7	~ 0
End of Life Tangential Stress (MPa)	161 ± 66.2	6.87 ± 57.5	90.0 ± 38.9
Failure Probability (%)	72.7 ± 0.44	1.07 ± 0.01	24.2 ± 0.46

Recall that in the cases in Part 4, PyC failures were observed beginning at the start of the cycle, and then SiC failures followed and peaked between fluences of 0.5 and 1.5 x 10^{25} n/m^2. The rate of SiC failure then diminished, and the irradiation cycle ended. This case runs to a much larger fluence than any that were able to be simulated in Part 4, however, and interesting behavior is observed. Consider Figure 4-20, which presents a histogram of the relative number of failures of each structural layer as a function of fluence. The same early life PyC failure is observed as well as the peak in SiC failure, but then in the absence of any additional PyC failure, another set of SiC failure is observed at much higher fluences. Physically then, this implies that there is a subset of particles in which both PyC layers fail, but the stress intensity that developed at the crack tip is not immediately sufficient to crack the SiC and substantial irradiation must occur to build up additional pressure in the buffer and corresponding tension in the SiC to cause a failure. This phenomenon is more thoroughly described in reference [8].

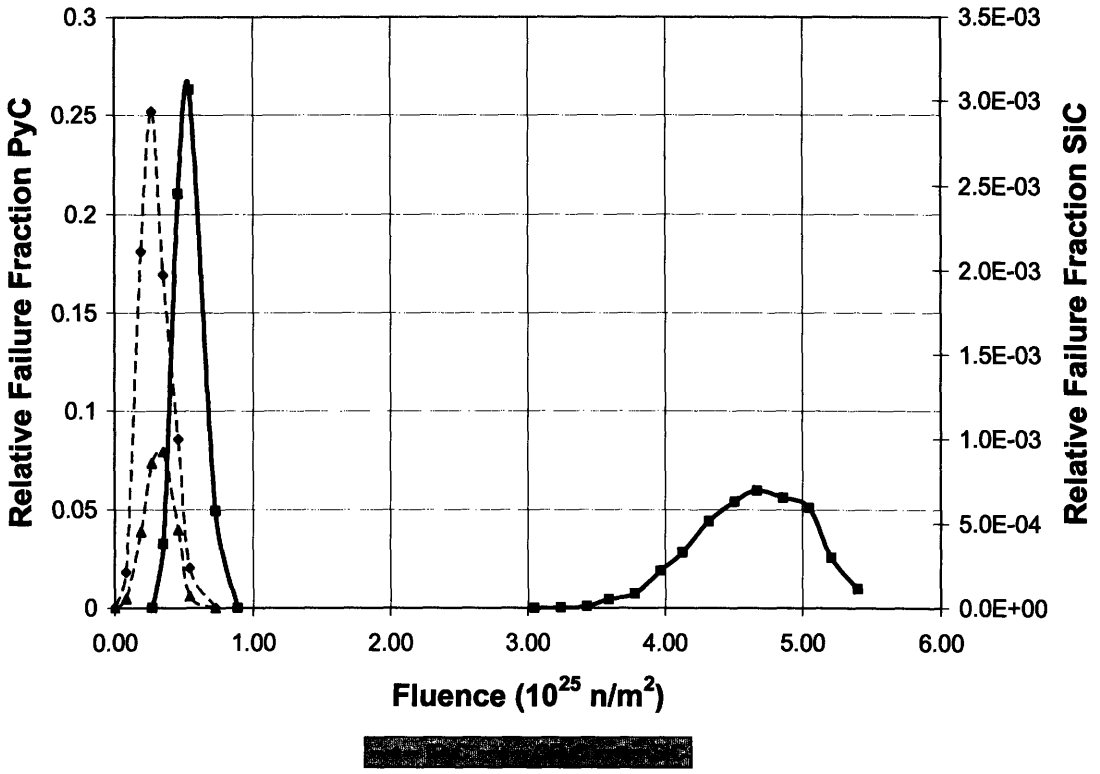

Figure 4-20: Failure Fraction for Case 13

4.2.3 Case 14: HFR EU – 2 Parameters

For this final case, the same procedure was applied. Table 4-10 describes the two sets of parameters, and Figure 4-21 plots the swelling correlations. In the interests of gathering additional interesting data, an additional parameter was varied. It was noticed in all of the other cases that particle failures were due to PyC crack induced fracture of the SiC, not direct SiC overpressure failure. So in this case a second set of calculated values was simulated, which varied the standard deviation of the SiC fracture toughness as shown in the table.

Between the calculated and IAEA values, the creep coefficient differed by a factor of 3.4, and the swelling correlations showed good agreement for tangential swelling but poor agreement for radial swelling.

Table 4-10: Properties for Case 14

Parameter	Units	IAEA Value	Calculated Value
PyC Properties			
Radial Swelling Correlation	$(\Delta L/L)/10^{25}$ n/m^2	+1.36334E-03x^3 -7.77024 E-03x^2 +2.00861E-02x -2.22642E-02	IPyC: -2.4181E-05x^3 -1.4733E-03x^2 +1.4431E-02x -1.8925E-02 OPyC: +1.8597E-04x^3 -1.8147E-03x^2 +1.2245E-02x -1.8556E-02
Tangential Swelling Correlation	$(\Delta L/L)/10^{25}$ n/m^3	-3.53804E-04x^3 +1.69251E-03x^2 +2.63307E-03x -1.91253E-02	IPyC: +1.3676E-04x^3 -1.38453E-03x^2 +6.37144E-03x -2.058E-02 OPyC: +2.3471E-05x^3 -1.1598E-03x^2 +7.4011E-03x -2.0746E-02
Creep Coefficient	(MPa 10^{25} n/m^2)$^{-1}$	4.93E-04	1.45E-4
Poisson's Ratio In Creep		0.4	x < 0.3: 0.5 – x/3 x > 0.3: 0.4
Weibull Modulus		5	
Characteristic Strength	MPa m^3/Weibull Modulus	IPyC: 2.1341 OPyC: 2.2823	
Mean Strength	MPa	200	
SiC Properties			
Weibull Modulus		8.02	
Characteristic Strength	MPa m^3/Weibull Modulus	52.20	
Mean Strength	MPa	873	
Fracture Toughness	MPa μm$^{1/2}$	3300	1.) 3300 ± 530 2.) 3300 ± 1060

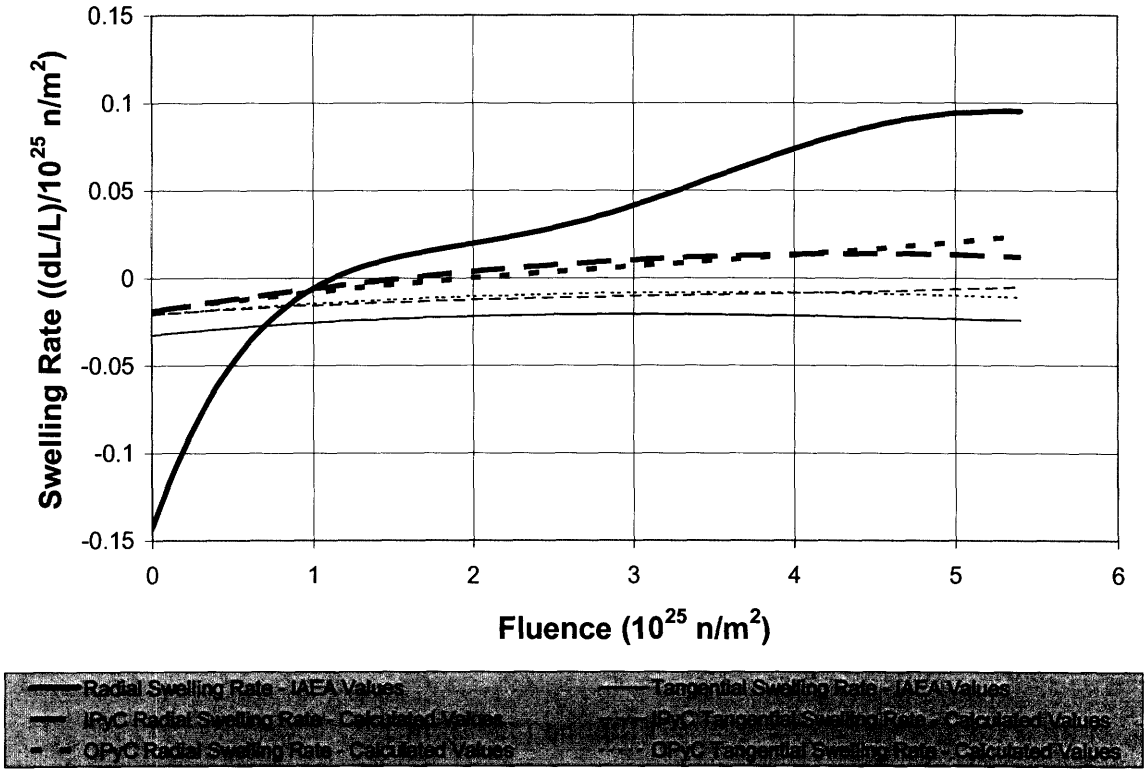

Figure 4-21: Radial and Tangential Swelling Rates for Case 14

4.2.4 Case 14: HFR EU – 2 Results and Discussion

Figure 4-22 and Figure 4-23 show the total internal pressure and tangential stresses in a normalized particle. As in previous cases, the IAEA parameters appear to lead to an asymptotic equilibration of the tangential stresses before the end of the irradiation cycle. TIMCOAT, however, is unable to capture this behavior, and error begins to accumulate in the algorithm invalidating the results obtained using the IAEA parameters. Otherwise, the pressure and stress curves are unremarkable.

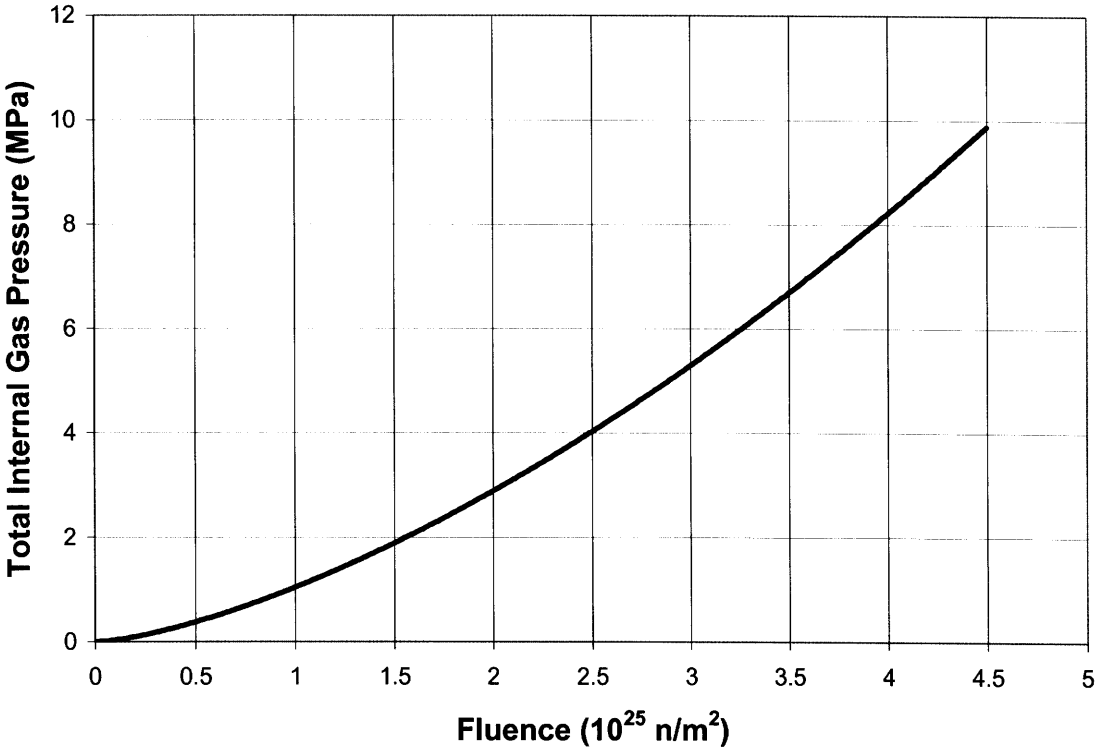

Figure 4-22: Total Internal Gas Pressure for a Nominal Particle Case 14

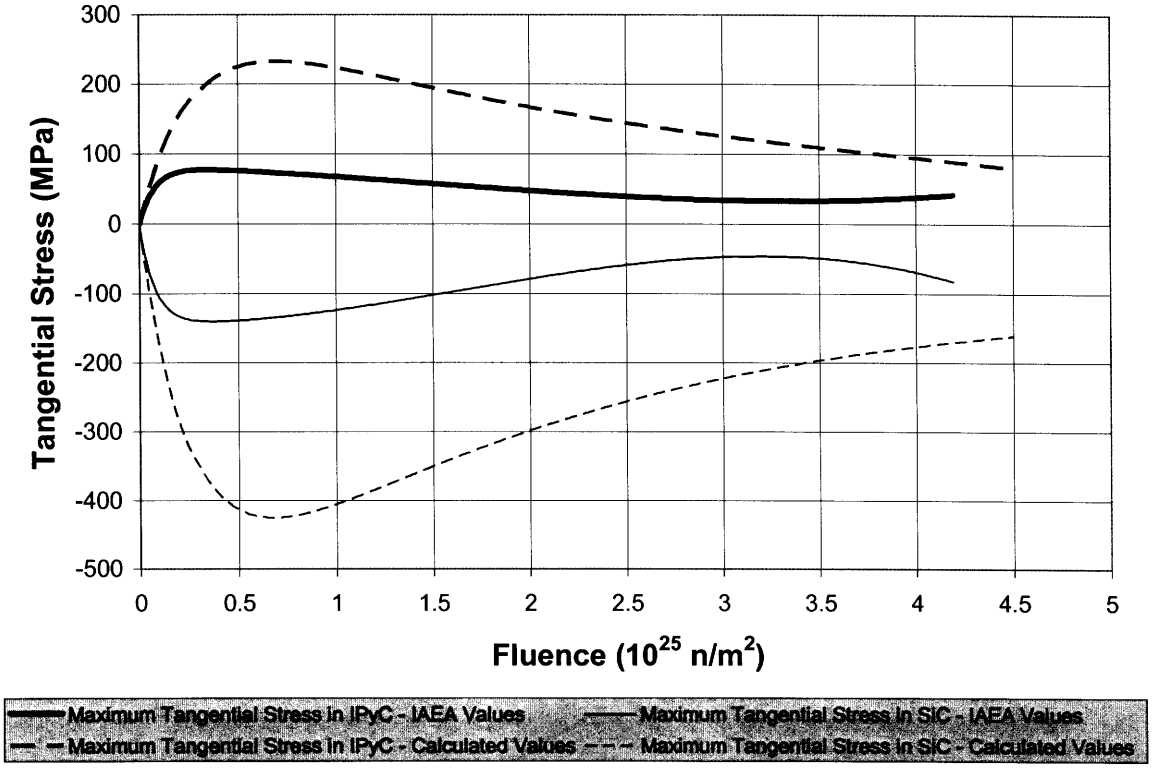

Figure 4-23: Maximum Tangential Stresses in IPyC and SiC Layers for a Nominal Particle Case 14

Table 4-11 shows the results of the two remaining simulations. Both used TIMCOAT parameters but varied the SiC fracture toughness. The one listed as having large variable fracture toughness used 3300 ± 1060 MPa $\mu m^{1/2}$, and the other used the standard 3300 ± 530 MPa $\mu m^{1/2}$. The intention of this change was to produce some particles with a SiC layer particularly resistant to PyC crack induced fracture. This would allow stresses in the layer to continue to build even after both PyC layers failed and allow for the possibility of direct SiC overpressure failure. The table shows, however, that this change had little effect on the average end of life and maximum stresses in the SiC layer and further analysis of the data indicated that all observed failures were still due to PyC crack induced fracture. The table also shows that doubling the variation of the fracture toughness increased the particle failure probability by about an order of magnitude.

Table 4-11: Sampling Results for Case 14

	TIMCOAT Values Large variable Fracture Toughness			TIMCOAT Values Small variable Fracture Toughness		
	IPyC	SiC	OPyC	IPyC	SiC	OPyC
Average Maximum Tangential Stress (MPa)	213 ± 27.3	4.48 ± 15.9	167 ± 9.36	213 ± 27.3	5.40 ± 17.2	167 ± 9.34
Average Minimum Tangential Stress (MPa)	~ 0	-384 ± 59.8	~ 0	~ 0	-384 ± 59.8	~ 0
Average End of Life Tangential Stress (MPa)	147 ± 56.3	-67.1 ± 60.5	94.2 ± 26.0	147 ± 56.3	-66.1 ± 61.9	94.2 ± 26.0
Failure Probability (%)	58.8 ± 0.49	2.02 ± 0.14	17.0 ± 0.41	58.8 ± 0.48	0.247 ± 0.046	17.0 ± 0.43

Now consider Table 4-12, which shows data for a histogram of the number of failures in each layer as a function of fast neutron fluence. In the previous cases this information was presented in a graph, but here it spans too many orders of magnitude to be effectively represented in graphical form. First, notice that there is a distribution of PyC failures from 0 to 1 x 10^{25} n/m^2 with a peak at about 0.37 x 10^{25} n/m^2 with an almost identical number of failures for both runs. This is expected as varying the SiC fracture toughness should not affect the failure behavior of the PyC layers. Next, notice that there is a distribution of SiC failures between 0.37 and 1 x 10^{25} n/m^2 for both runs, but for the run with a larger variation in the SiC fracture toughness, there are more SiC failures. After this fluence, the behavior of the two runs diverges substantially. No additional failures in any of the structural layers are observed in the small variation run, but in the large

variation run, another distribution of SiC and OPyC failures is observed between 1.6 and 4.3 x 10^{25} n/m^2 with the number of failures in the two layers being the same. Further examination of the data shows that this behavior is very different from that observed in any of the other cases. Previously both the IPyC and OPyC layers failed, and these failures induced SiC failure some time later. Here however, the IPyC failed, and the failure of this single PyC layer was sufficient to fracture the SiC layer sometime later in the irradiation. TIMCOAT assumes that if the SiC layer fails, all other layers fail.

Table 4-12: Number of Failures Case 14

Small variable Fracture Toughness				Large variable Fracture Toughness			
Fluence 10^{25} n/m^2	IPyC	SiC	OPyC	Fluence 10^{25} n/m^2	IPyC	SiC	OPyC
0	0	0	0	0	0		0
0.129	49693	0	12607	0.129	49693		12739
0.2365	312445	0	67330	0.2365	312451	0	67332
0.3655	316612	3	100176	0.3655	316809	1012	99981
0.4945	167137	702	65638	0.4945	166921	11812	65658
0.6235	35655	1857	8460	0.6235	35707	13567	8455
0.731	1	967	6	0.731	1	3330	7
0.86	0	175	0	0.86	0	298	3
				1.0965		3	3
				1.419		0	0
				1.591		11	11
				1.849		18	18
				2.0855		28	28
				2.3435		49	49
				2.58		46	46
				2.8165		43	43
				3.0745		41	41
				3.311		12	12
				3.569		9	9
				3.8055		7	7
				4.0635		1	1
				4.3		1	1

5 Conclusions, Comments and Future Work

As this was a blind benchmark, no independent studies are currently available to compare TIMCOAT results. Thus, little can be said concerning the accuracy or precision of TIMCOAT beyond the conclusions of Wang [4] and Soontrapa [8], which were briefly referred to in Case 12. These authors found that TIMCOAT is capable of reproducing experimental results quite accurately, at least for the NRP 1 irradiation test. In addition, it was demonstrated here that for the analytically solvable Case 1, TIMCOAT matched the stress calculations perfectly. Apart from these observations, it is necessary to restrict this discussion to the parameters used in the benchmark, the general behavior of the stress results and insights from the few parametric studies.

5.1 IAEA Parameters and TIMCOAT Calculations

The IAEA benchmark document, which was used to guide this study, specified all of the material properties of PyC and SiC layers that were to be used in each simulation. As was shown, not all of these parameters necessarily need to be input into the MIT code. In particular, the code is capable of generating creep and swelling properties for PyC from its own material database drawn from information in CEGA-002820 [11]. For most of the cases, the IAEA supplied properties were compared to the code calculated properties, and some general trends were observed.

In all cases, the PyC creep coefficient provided was found to be at least twice the calculated value. This led to large reductions in the maximum tangential IPyC stresses. A doubling of the creep coefficient was found to almost halve the stress and reduce the failure probability of the IPyC by as much as several orders of magnitude. This clearly indicates that highly accurate information about the PyC creep coefficient must be available to correctly simulate TRISO performance. Simply knowing the coefficient to within a factor of 2 is not unacceptable. When the larger creep coefficient was used in TIMCOAT, the failure behavior was quite pathologic with most cases showing no particle failures. It is assumed that when the benchmark was designed at INL, it was not done so to test cases with vanishingly low failure probabilities. This would suggest either a fundamental difference between the treatment of creep by TIMCOAT and the INL

code, which was used in the development of the benchmark [1], or an additional source of stress in the INL code not found in TIMCOAT.

The latter appears to be true. According to Petti [15], the INL code includes the buildup of carbon monoxide in its internal pressure model. TIMCOAT accounts only for the release of gaseous fission products and oxygen. Petti reports that accounting for carbon monoxide results in a large increase in internal pressure which increases stresses and leads to reasonable failure fractions with the larger creep rate. Furthermore, Petti indicated that this larger creep coefficient was arbitrarily selected by INL to bring the ratio of PyC to SiC failures calculated in their model into agreement with available experimental data. Recall, however, the results in Case 12 where TIMCOAT accurately matched the particle failure rates shown by the NPR 1 experiment without a carbon monoxide model and with the smaller creep rate. This will need to be explored further once TIMCOAT is adapted to model the buildup of carbon monoxide and once results from other benchmark participants are available for comparison.

The swelling correlations governing irradiation induced dimensional changes in PyC also deserve some attention. For the simple single and double structural layer simulations in Cases 1 – 3, the IAEA swelling correlations and the calculated correlations compared very well. For the more complex cases, the benchmark dealt cursorily with these correlations, using the same ones for PyC layers with very different anisotropies and densities. These correlations did not agree with the TIMCOAT calculated ones, and this is not surprising as the TIMCOAT treatment appears much more detailed, attempting to account for small changes in density and isotropy. Even though the correlations differed, however, they did not seem to affect either the stress calculations or the failure probabilities to an appreciable extent except at high fluences. At high fluences, greater than 4×10^{25} n/m^2, when the PyC is swelling rapidly in the radial direction, there must physically come a point when the material's strength declines significantly as it begins to decompose. This is not captured by TIMCOAT, and so the swelling correlations obtained in this range must be subject to some scrutiny. In addition, the curve fitting

methods used to determine these correlations from experimental data accumulate error near the upper limit of available data. This should be corrected.

Lastly, the strength of the PyC layers should be examined. The MIT code uses characteristic strengths to specify the strength of the PyC. As was discussed, this method is consistent with Weibull strength theory and shows a decline in strength as the volume of the layer increase. The benchmark specified uniform mean strengths for the PyC layers regardless of their volume and density. This would seem to indicate a fundamental difference between the TIMCOAT approach to PyC failure and the INL approach. When attempting to equate these two approaches, it was seen that the benchmark assumed significantly stronger PyC than TIMCOAT, and this led to correspondingly lower failure probabilities. The strength of the PyC must be well known in order to obtain physically meaningful results.

5.2 Stress Calculations and Results

The stress calculations found in Cases 11 and 12 uncovered limitations of the MIT code's ability to capture asymptotic behavior. In Case 11, the creep coefficient is sufficiently large to relax all tension in the IPyC during the irradiation cycle. As the tangential stress relaxes, it should asymptotically approach zero. TIMCOAT, however, uses a central difference approach with fixed time steps to approximate derivatives and compute stresses, and so as the stress nears zero, the code overshoots this equilibrium and a nonphysical negative stress is obtained. After this point, additional errors accumulate rapidly, and the code fails. In Case 12, equilibrium is reached between the accumulation of internal pressure, swelling, and creep, and again stresses in the structural layers should asymptotically approach an equilibrium value. As in Case 11, however, TIMCOAT misses this behavior and begins to show non physical results.

These two cases are not particularly unusual and describe TRISO particles that were studied in previous experiments. TIMCOAT should have the ability to model them correctly. In order to so, the algorithms in the code that simultaneously calculate stress,

strain, and displacement of the structural layers will need to be modified to use a more advanced numerical technique for approximating derivatives. This is a well developed field in numerical analysis, and there are a number of predictor-corrector algorithms that would be appropriate [13]. Implementing these new algorithms would require a significant rewrite of the existing code, however, and other less invasive options should be considered. These might include a first derivative test which could identify asymptotic behavior and assign parameters their projected asymptotic values automatically.

5.3 Parametric Insights

Two parametric studies were conducted in the course of this benchmark, one in Case 9 where the effects of varying PyC anisotropy were investigated and one Case 14 where variations in the SiC fracture toughness were considered. In each of these cases, the mean value of the parameter of interest was not changed, only the degree of variation about that mean. In both cases the data revealed that the failure probabilities of the resulting populations of particles were significantly affected. In Case 9, fixing the BAF of the PyC at 1.0 increased the failure probability by a factor of 3.7 ± 0.6 as compared to the run where it was allowed to vary. In Case 14, doubling the standard deviation of the SiC fracture toughness increased the particle failure by a factor of 8.2 ± 0.2. While it is hardly surprising that the code and the physical environment being modeled are particularly sensitive to certain parameters, what is more interesting is the large sensitivity to relatively small changes in the distributions from which these parameters are drawn even when the mean value is maintained.

In the benchmarking document very few of the standard deviations on the parameters necessary to run TIMCOAT were provided, and the author supplemented with data from Wang [4]. These two examples from Cases 9 and 14 indicate that the results reported here can reasonably be expected to be highly sensitive to these deviation selections. This then makes it very difficult to compare results between codes that might have assumed different distributions, even though they selected the same mean values. In the future it is

recommended that any benchmarking program specify the distributions to be simulated, not just the mean values of the parameters.

References

[1] J.T. Maki, G.K. Miller, "TRSIO-Coated Particle Fuel Performance Benchmark Cases", INL-EDF 3981 Rev. 2, March 23rd, 2005.

[2] F.A. Silady, L.L. Parme, "The Safety Approach of the Modular High Temperature Gas Cooled Reactor (MHTGR)", 11th International Conference on the HTGR, Dimitrovgrad, June 13-16, 1989

[3] K. Sawa, K. Minato, "An Investigation of Irradiation Performance of High Burnup HTGR Fuel", Journal of Nuclear Science & Technology, 36, No. 9, 781-791 (1999)

[4] J. Wang. "An Integrated Performance Model for High Temperature Gas Cooled Reactor Coated Particle Fuel." PhD Thesis. Massachusetts Institute of Technology. February 2004.

[5] J. Drowart, et al., "Thermodynamic Study of SiC Using a Mass Spectrometer", Journal of Chemical Physics, 29, 1015 (1958)

[6] K. Minato, T. Ogawa, K. Fukuda, et al. "Fission product behavior in Triso-coated UO2 fuel particles." Journal of Nuclear Materials. Vol. 208, p. 266-281. (1994)

[7] O.M. Stansfield, C.B. Scott, and J. Chin. "Kernel Migration in Coated Carbide Fuel Particles." Nuclear Technology. Vol. 25, p. 517-530, (1975).

[8] C. Soontrapa, "Design Optimization and Analysis of Coated Particle Fuel Using Advanced Fuel Performance Modeling Techniques", M.S. Thesis, Massachusetts Institute of Technology, February 2005.

[9] J. Case, L. Chilver, C. Ross. "Strength of Materials and Structures (4th Edition)". Elsevier. (1999).

[10] T. D. Burchell. "Carbon Materials for Advanced Technologies". Pergamom. (1999).

[11] F. Ho, "Material Models of Pyrocarbon and Pyrolytic Silicon Carbide", CEGA-002820, Rev. 1, July 1993

[12] J.L. Kaae, "On Irradiation-Induced Creep of Pyrolytic Carbon in a General State of Stress", Journal of Nuclear Materials, 34, 208 (1970)

[13] S. C. Chapra and R. Canale, "Numerical Methods for Engineers", McGraw-Hill Science/Engineering/Math; 4 edition, July 16, 2001.

[14] G. K. Miller, D. A. Petti, and J. T. Maki, "Statistical Approach and Benchmarking for Modeling of Multi-dimensional Behavior in TRISO-coated Fuel Particles", J. Nucl. Materials, 317 (2003) p. 69.

[15] D. Petti, personal communications, April 26, 2006.

Appendix I – Input Parameters

I.1 Sample TIMCOAT Input File

```
FUELTYPE    = Fuel kernel type
OURAT       = Oxygen to Uranium ratio
CURAT       = Carbon to Uranium ratio
U235ENR     = U235 enrichment (%)
U235VAR     = Standard deviation on U235 enrichment (%)
KERNT       = Kernel theoretical density (g/cm3)
KERND       = Kernel density (g/cm3)
KERNDVAR    = Standard deviation on kernel density (g/cm3)
KERNDIA     = Kernel diameter (µm)
KERNVAR     = Standard deviation on kernel diameter (µm)
BUFFT       = Buffer theoretical density (g/cm3)
BUFFD       = Buffer density (g/cm3)
BUFFDVAR    = Standard deviation on buffer density (g/cm3)
BUFFTHK     = Buffer thickness (µm)
BUFFVAR     = Standard deviation on buffer thickness (µm)
IPYCBAF0I   = IPyC as-fabricated BAF
IPYCBAFVAR  = Standard deviation on IPyC as-fabricated BAF
IPYCCRATE   = IPyC coating rate (µm/min)
IPYCLC      = IPyC crystallite length (µm)
IPYCMIN     = IPyC Weibull modulus
IPYCFIN     = IPyC characteristic strength (MPa.m3/modulus)
IPYCD       = IPyC density (g/cm3)
IPYCTHK     = IPyC thickness (µm)
IPYCVAR     = Standard deviation on IPyC thickness (µm)
SICMIN      = SiC Weibull modulus
SICFIN      = SiC characteristic strength (MPa.m3/modulus)
SICKIC0     = SiC fracture toughness (MPa.µm1/2)
SICKVAR     = Standard deviation on SiC fracture toughness
SICTHK      = SiC thickness (µm)
SICVAR      = Standard deviation on SiC thickness (µm)
OPYCBAF0I   = OPyC as-fabricated BAF
OPYCBAFVAR  = Standard deviation on OPyC as-fabricated BAF
OPYCCRATE   = OPyC coating rate (µm/min)
OPYCLC      = OPyC crystallite length (µm)
OPYCMIN     = OPyC Weibull modulus
OPYCFIN     = OPyC characteristic strength (MPa.m3/modulus)
OPYCD       = OPyC density (g/cm3)
OPYCTHK     = OPyC thickness (µm)
OPYCVAR     = Standard deviation on OPyC thickness (µm)
YOUNGPYC    = Young's modulus for PYC
NUPYC       = Elastic Poisson's ratio in PyC
NUPYCCREEP  = PyC Poisson's ratio in creep
ALPHAPYC    = Coefficient of thermal expansion in PyC (1/K)
PYCCC       = PyC creep coefficient ((MPa 10^21 n/cm2)^-1)
YOUNGSIC    = Young's modulus for SiC
NUSIC       = Elastic Poisson's ratio in SiC
ALPHASIC    = Coefficient of thermal expansion in SiC (1/K)
IRRTIME     = Irradiation time(Day)
EOLBUP      = EOL burnup (FIMA)
EOLFLU      = EOL fluence (10E21n/cm2)
T_IRR       = Irradiation temperature (°C)
PINT        = Internal Pressure
PAMB        = Ambient pressure (MPa)
DT          = Time step size (s)
TITLE       = Name of the Case being run
OSPEC       = Output File Name
DEBUG       = Flag for debugging
ISEED       = Initial seed for random number generator
NBURP       = Send intermediate outputs for every NBURP sampled particles
NCASES      = Number of particles to be sampled
NOMINAL     = Flag turning on/off Monte Carlo sampling
DIFFUSION   = Flag turning on/off diffusion model for gas release
HISTOGRAM   = Flag turning on/off histogram outputs
RUNIRR      = Flag turning on/off fuel failure evaluation
USERSEED    = Flag determining whether ISEED from users is used
CHEMISTRY   = Flag turning on/off chemistry model
```

I.2 Input Parameters for Cases 1, 2 and 3:

Parameter	Units	Case 1	Case 2	Case 3
Fuel Characteristics				
Fuel Type		UO_2	UO_2	UO_2
Oxygen to Uranium Ratio	Atom Ratio	2	2	2
Carbon to Uranium Ratio	Atom Ratio	0	0	0
U-235 Enrichment	Weight %	10	10	10
Kernel Density	g/cc	10.8	10.8	10.8
Kernel Diameter	μm	500	500	500
Buffer Density	g/cc	0.95	0.95	0.95
Buffer Thickness	μm	100	100	100
IPyC BAF		none	1.00	1.03
IPyC Density	g/cc	none	1.9	1.9
IPyC Thickness	μm	none	90	40
SiC Thickness	μm	35	none	35
Material Properties				
PyC Modulus of Elasticity	MPa	none	3.94E+04	3.94E+04
PyC Poisson's Ratio		none	0.33	0.33
SiC Modulus of Elasticity	MPa	3.70E+05	none	3.70E+05
SiC Poisson's Ratio		0.13	none	0.13
Irradiation Conditions				
Irradiation Duration	Effective Full Power Days	0	0	0
End of Life Burnup	% FIMA	0	0	0
End of Life Fluence	10^{25} n/m^2	0	0	0
Irradiation Temperature	C	1000	1000	1000
Internal Pressure	MPa	25	25	25
Ambient Pressure	MPa	0.1	0.1	0.1
Modeling Parameters				
Elapsed Time	Days	1	1	1
Time Step	Days	1	1	1

I.2 Input Parameters for Cases 4a – 4d:

Parameter	Units	Case 4a	Case 4b	Case 4c	Case 4d
Fuel Characteristics					
Fuel Type		UO_2	UO_2	UO_2	UO_2
Oxygen to Uranium Ratio	Atom Ratio	2	2	2	2
Carbon to Uranium Ratio	Atom Ratio	0	0	0	0
U-235 Enrichment	Weight %	10	10	10	10
Kernel Density	g/cc	10.8	10.8	10.8	10.8
Kernel Diameter	μm	500	500	500	500
Buffer Density	g/cc	0.95	0.95	0.95	0.95
Buffer Thickness	μm	100	100	100	100
IPyC BAF		1.03	1.03	1.03	1.03
IPyC Density	g/cc	1.9	1.9	1.9	1.9
IPyC Thickness	μm	40	40	40	40
SiC Thickness	μm	35	35	35	35
Material Properties					
PyC Modulus of Elasticity	MPa	3.94E+04	3.94E+04	3.94E+04	3.94E+04
PyC Poisson's Ratio		0.33	0.33	0.33	0.33
PyC Poisson's Ratio In Creep		none	0.5	0.5	0.5
PyC Creep Coefficient	$(MPa\ 10^{25}\ n/m^2)^{-1}$	none	2.71E-04	2.71E-04	2.71E-04
PyC Swelling Strain Rate	$(\Delta L/L)\ 10^{25}\ n/m^2$	-0.005x isotropic	0	-0.005x isotropic	See Table 3-6
SiC Modulus of Elasticity	MPa	3.70E+05	3.70E+05	3.70E+05	3.70E+05
SiC Poisson's Ratio		0.13	0.13	0.13	0.13
Irradiation Conditions					
Irradiation Duration	Effective Full Power Days	0	0	0	0
End of Life Burnup	% FIMA	0	0	0	0
End of Life Fluence	$10^{25}\ n/m^2$	3	3	3	3
Irradiation Temperature	C	1000	1000	1000	1000
Internal Pressure	MPa	25	25	25	25
Ambient Pressure	MPa	0.1	0.1	0.1	0.1
Modeling Parameters					
Elapsed Time	Days	1000	1000	1000	1000
Time Step	Days	1	1	1	1

I.3 Input Parameters for Cases 5 – 8:

Parameter	Units	Case 5	Case 6	Case 7	Case 8
Fuel Characteristics					
Fuel Type		UO_2	UO_2	UO_2	UO_2
Oxygen to Uranium Ratio	Atom Ratio	2	2	2	2
Carbon to Uranium Ratio	Atom Ratio	0	0	0	0
U-235 Enrichment	Weight %	10	10	10	10
Kernel Density	g/cc	10.8	10.8	10.8	10.8
Kernel Diameter	μm	350	500	500	500
Buffer Density	g/cc	0.95	0.95	0.95	0.95
Buffer Thickness	μm	100	100	100	100
IPyC BAF		1.03	1.03	1.06	1.03
IPyC Density	g/cc	1.9	1.9	1.9	1.9
IPyC Thickness	μm	40	40	40	40
SiC Density	g/cc	3.2	3.2	3.2	3.2
SiC Thickness	μm	35	35	35	35
OPyC BAF		1.03	1.03	1.06	1.03
OPyC Density	g/cc	1.9	1.9	1.9	1.9
OPyC Thickness	μm	40	40	40	40
Material Properties					
PyC Modulus of Elasticity	MPa	3.94E+04	3.94E+04	3.94E+04	3.94E+04
PyC Poisson's Ratio		0.33	0.33	0.33	0.33
PyC Poisson's Ratio In Creep		0.5	0.5	0.5	0.5
PyC Coefficient of Thermal Expansion	K^{-1}	none	none	none	5.35E-06
PyC Creep Coefficient	$(MPa\ 10^{25}\ n/m^2)^{-1}$	2.71E-04	2.71E-04	2.71E-04	See Figure 3-15
PyC Swelling Strain Rate	$(\Delta L/L)\ 10^{25}\ n/m^2$	See Table 3-7	See Table 3-8	See Table 3-9	See Table 3-10
SiC Modulus of Elasticity	MPa	3.70E+05	3.70E+05	3.70E+05	3.70E+05
SiC Poisson's Ratio		0.13	0.13	0.13	0.13
SiC Coefficient of Thermal Expansion	K^{-1}	none	none	none	4.90E-06
Irradiation Conditions					
Irradiation Duration	Effective Full Power Days	1000	1000	1000	1000
End of Life Burnup	% FIMA	10	10	10	10
End of Life Fluence	$10^{25}\ n/m^2$	3	3	3	3
Irradiation Temperature	C	1000	1000	1000	See Figure 3-14
Internal Pressure	MPa	15.54/3*x	26.20/3*x	26.20/3*x	See Figure 3-14
Ambient Pressure	MPa	0.1	0.1	0.1	0.1

I.4 Input Parameters for Cases 9 – 12:

Parameter	Units	Case 9	Case 10	Case 11	Case 12
Fuel Characteristics					
Fuel Type		UO_2	UO_2	UO_2	UCO
Oxygen to Uranium Ratio	Atom Ratio	2	2	2	1.51
Carbon to Uranium Ratio	Atom Ratio	0	0	0	0.36
U-235 Enrichment	Weight %	4.07 ± 0.1	9.82 ± 0.1	9.82 ± 0.1	93.15 ± 0.01
Kernel Theoretical Density	g/cc	10.95	10.95	10.95	11.03
Kernel Density	g/cc	10.84 ± 0.05	10.81 ± 0.05	10.81 ± 0.05	10.52 ± 0.01
Kernel Diameter	μm	544 ± 9	497 ± 14	497 ± 14	200 ± 5
Buffer Theoretical Density	g/cc	2.25	2.25	2.25	2.25
Buffer Density	g/cc	1.1 ± 0.05	1 ± 0.05	1 ± 0.05	0.96 ± 0.05
Buffer Thickness	μm	97 ± 13	94 ± 10	94 ± 10	102 ± 10
IPyC BAF		1.00 ± 0.0	1.053 ± 0.005	1.053 ± 0.005	1.058 ± 0.005
IPyC Coating Rate	μm/min	1	1	1	1.5
IPyC Crystallite Length	μm	29.98	29.98	29.98	29.98
IPyC Weibull Modulus		5	5	5	9.5
IPyC Characteristic Strength	MPa m^3/Weibull Modulus	2.0857	2.1266	2.1266	18.596
IPyC Density	g/cc	1.85	1.88	1.88	1.92
IPyC Thickness	μm	33 ± 3	41 ± 4	41 ± 4	53 ± 4
SiC Weibull Modulus		8.02	8.02	8.02	6
SiC Characteristic Strength	MPa m^3/Weibull Modulus	52.015	51.833	51.833	11.482
SiC Fracture Toughness	MPa $\mu m^{1/2}$	3300 ± 530	3300 ± 530	3300 ± 530	3500 ± 530
SiC Density	g/cc				
SiC Thickness	μm	34 ± 2	36 ± 2	36 ± 2	35 ± 3
OPyC BAF		1.00 ± 0.0	1.019 ± 0.005	1.019 ± 0.005	1.052 ± 0.006
OPyC Coating Rate	μm/min	1	1	1	3
OPyC Crystallite Length	μm	29.98	29.98	29.98	29.98
OPyC Weibull Modulus		5	5	5	9.5
OPyC Characteristic Strength	MPa m^3/Weibull Modulus	2.3054	2.2842	2.2842	19.226
OPyC Density	g/cc	1.85	1.88	1.88	1.86
OPyC Thickness	μm	39 ± 3	40 ± 2	40 ± 2	39 ± 4

Material Properties					
PyC Modulus of Elasticity	MPa	3.96E+04	3.96E+04	3.96E+04	3.96E+04
PyC Poisson's Ratio		0.33	0.33	0.33	0.33
PyC Poisson's Ratio In Creep		0.4	0.4	0.4	0.5
PyC Coefficient of Thermal Expansion	K^{-1}	5.50E-06	5.50E-06	5.50E-06	5.50E-06
PyC Creep Coefficient	$(MPa\ 10^{25}\ n/m^2)^{-1}$	4.93E-04	4.93E-04	4.93E-04	2.70E-04
PyC Swelling Strain Rate	$(\Delta L/L)\ 10^{25}\ n/m^2$	Table 4-2	Table 4-4	Table 4-4	Table 4-7
SiC Modulus of Elasticity	MPa	3.70E+05	3.70E+05	3.70E+05	3.70E+05
SiC Poisson's Ratio		0.13	0.13	0.13	0.13
SiC Coefficient of Thermal Expansion	K^{-1}	4.90E-06	4.90E-06	4.90E-06	4.90E-06
Irradiation Conditions					
Irradiation Duration	Effective Full Power Days	89	359	351	170
End of Life Burnup	% FIMA	4.79	10	14	79
End of Life Fluence	$10^{25}\ n/m^2$	2.1	5.3	7.2	3.8
Irradiation Temperature	C	1030	800	1062	987
Internal Pressure	MPa	auto	auto	auto	auto
Ambient Pressure	MPa	0.1	0.1	0.1	0.1

I.5 Input Parameters for Cases 13 and 14:

Parameter	Units	Case 13	Case 14
Fuel Characteristics			
Fuel Type		UO_2	UO_2
Oxygen to Uranium Ratio	Atom Ratio	2	2
Carbon to Uranium Ratio	Atom Ratio	0	0
U-235 Enrichment	Weight %	16.7 ± 0.1	10.6 ± 0.1
Kernel Theoretical Density	g/cc	10.95	10.95
Kernel Density	g/cc	10.81 ± 0.05	10.72 ± 0.05
Kernel Diameter	μm	502 ± 11	508 ± 10
Buffer Theoretical Density	g/cc	2.25	2.25
Buffer Density	g/cc	1.01± 0.05	1.02± 0.05
Buffer Thickness	μm	95 ± 14	102 ± 12
IPyC BAF		1.02 ± 0.005	1.04 ± 0.005
IPyC Coating Rate	μm/min	1	1
IPyC Crystallite Length	μm	29.98	29.98
IPyC Weibull Modulus		5	5
IPyC Characteristic Strength	MPa m^3/Weibull Modulus	2.1345	2.1341
IPyC Density	g/cc	1.87	1.92
IPyC Thickness	μm	41 ± 3	39 ± 4
SiC Weibull Modulus		8.02	8.02
SiC Characteristic Strength	MPa m^3/Weibull Modulus	51.75	52.2
SiC Fracture Toughness	MPa $\mu m^{1/2}$	3300 ± 530	3300 ± 530
SiC Thickness	μm	35 ± 2	36 ± 2
OPyC BAF		1.02 ± 0.005	1.02 ± 0.005
OPyC Coating Rate	μm/min	1	1
OPyC Crystallite Length	μm	29.98	29.98
OPyC Weibull Modulus		5	5
OPyC Characteristic Strength	MPa m^3/Weibull Modulus	2.2894	2.2823
OPyC Density	g/cc	1.87	1.92
OPyC Thickness	μm	40 ± 4	38 ± 4
Material Properties			
PyC Modulus of Elasticity	MPa	3.96E+04	3.96E+04
PyC Poisson's Ratio		0.33	0.33
PyC Poisson's Ratio In Creep		0.4	0.4
PyC Coefficient of Thermal Expansion	K^{-1}	5.50E-06	5.50E-06
PyC Creep Coefficient	(MPa 10^{25} n/m^2)$^{-1}$	4.93E-04	4.93E-04
PyC Swelling Strain Rate	(ΔL/L) 10^{25} n/m^2	Table 4-8	Table 4-10
SiC Modulus of Elasticity	MPa	3.70E+05	3.70E+05
SiC Poisson's Ratio		0.13	0.13
SiC Coefficient of Thermal Expansion	K^{-1}	4.90E-06	4.90E-06
Irradiation Conditions			
Irradiation Duration	Effective Full Power Days	600	350
End of Life Burnup	% FIMA	20	10
End of Life Fluence	10^{25} n/m^2	5.4	4.5
Irradiation Temperature	C	1025	1050
Internal Pressure	MPa	auto	auto
Ambient Pressure	MPa	0.1	0.1

Appendix II – Irradiation Histories

II.1 Irradiation History for Cases 1, 2 and 3:

Elapsed time (days)	Full power days	Irradiation Temp. (°C)	Fast Fluence (10^21nvt)	Burnup (% FIMA)
0	0	1000	0	0
0	0	1000	0	0

II.2 Irradiation History for Cases 4a – 4d:

Ellapsed time (days)	Full power days	Irradiation Temp. (°C)	Fast Fluence (10^21nvt)	Burnup (% FIMA)
0	0	1000	0	0
1	0	1000	0.003	0
2	0	1000	0.006	0
3	0	1000	0.009	0
4	0	1000	0.012	0
5	0	1000	0.015	0
6	0	1000	0.018	0
7	0	1000	0.021	0
8	0	1000	0.024	0
9	0	1000	0.027	0
10	0	1000	0.03	0
11	0	1000	0.033	0
12	0	1000	0.036	0
13	0	1000	0.039	0
14	0	1000	0.042	0
15	0	1000	0.045	0
...	...	...	...	...
985	0	1000	2.955	0
986	0	1000	2.958	0
987	0	1000	2.961	0
988	0	1000	2.964	0
989	0	1000	2.967	0
990	0	1000	2.97	0
991	0	1000	2.973	0
992	0	1000	2.976	0
993	0	1000	2.979	0
994	0	1000	2.982	0
995	0	1000	2.985	0
996	0	1000	2.988	0
997	0	1000	2.991	0
998	0	1000	2.994	0
999	0	1000	2.997	0
1000	0	1000	3	0

II.3 Irradiation History for Cases 5 – 7:

Ellapsed time (days)	Full power days	Irradiation Temp. (°C)	Fast Fluence (10^21nvt)	Burnup (% FIMA)
0	0	1000	0	0
1	1	1000	0.003	0.01
2	2	1000	0.006	0.02
3	3	1000	0.009	0.03
4	4	1000	0.012	0.04
5	5	1000	0.015	0.05
6	6	1000	0.018	0.06
7	7	1000	0.021	0.07
8	8	1000	0.024	0.08
9	9	1000	0.027	0.09
10	10	1000	0.03	0.1
11	11	1000	0.033	0.11
12	12	1000	0.036	0.12
13	13	1000	0.039	0.13
14	14	1000	0.042	0.14
15	15	1000	0.045	0.15
16	16	1000	0.048	0.16
17	17	1000	0.051	0.17
18	18	1000	0.054	0.18
19	19	1000	0.057	0.19
20	20	1000	0.06	0.2
...	...	...	...	...
980	980	1000	2.94	9.8
981	981	1000	2.943	9.81
982	982	1000	2.946	9.82
983	983	1000	2.949	9.83
984	984	1000	2.952	9.84
985	985	1000	2.955	9.85
986	986	1000	2.958	9.86
987	987	1000	2.961	9.87
988	988	1000	2.964	9.88
989	989	1000	2.967	9.89
990	990	1000	2.97	9.9
991	991	1000	2.973	9.91
992	992	1000	2.976	9.92
993	993	1000	2.979	9.93
994	994	1000	2.982	9.94
995	995	1000	2.985	9.95
996	996	1000	2.988	9.96
997	997	1000	2.991	9.97
998	998	1000	2.994	9.98
999	999	1000	2.997	9.99
1000	1000	1000	3	10

II.4 Irradiation History for Case 8:

Ellapsed time (days)	Full Power Days	Irradiation Temp. (°C)	Fast Fluence (10^21nvt)	Burnup (% FIMA)	Internal Pressure
0	0	600.00	0.000	0.000	0.000
1	1	604.12	0.003	0.010	0.001
2	2	608.25	0.006	0.020	0.003
3	3	612.37	0.009	0.030	0.004
4	4	616.49	0.012	0.040	0.006
5	5	620.62	0.015	0.050	0.007
...	...	...	...	...	...
95	95	991.75	0.285	0.950	0.137
96	96	995.88	0.288	0.960	0.139
97	97	1000.00	0.291	0.970	0.140
98	98	866.67	0.294	0.980	0.100
99	99	733.33	0.297	0.990	0.060
100	100	600.00	0.300	1.000	0.020
101	101	604.12	0.303	1.010	0.029
102	102	608.25	0.306	1.020	0.039
103	103	612.37	0.309	1.030	0.048
104	104	616.49	0.312	1.040	0.058
105	105	620.62	0.315	1.050	0.067
...	...	...	...	...	...
195	195	991.75	0.585	1.950	0.921
196	196	995.88	0.588	1.960	0.931
197	197	1000.00	0.591	1.970	0.940
198	198	866.67	0.594	1.980	0.640
199	199	733.33	0.597	1.990	0.340
200	200	600.00	0.600	2.000	0.040
201	201	604.12	0.603	2.010	0.066
202	202	608.25	0.606	2.020	0.093
203	203	612.37	0.609	2.030	0.119
204	204	616.49	0.612	2.040	0.145
205	205	620.62	0.615	2.050	0.171
...	...	...	...	...	...
295	295	991.75	0.885	2.950	2.537
296	296	995.88	0.888	2.960	2.564
297	297	1000.00	0.891	2.970	2.590
298	298	866.67	0.894	2.980	1.750
299	299	733.33	0.897	2.990	0.910
300	300	600.00	0.900	3.000	0.070
301	301	604.12	0.903	3.010	0.119
302	302	608.25	0.906	3.020	0.169
303	303	612.37	0.909	3.030	0.218
304	304	616.49	0.912	3.040	0.268
305	305	620.62	0.915	3.050	0.317
...	...	...	...	...	...
395	395	991.75	1.185	3.950	4.771
396	396	995.88	1.188	3.960	4.821

397	397	1000.00	1.191	3.970	4.870
398	398	866.67	1.194	3.980	3.280
399	399	733.33	1.197	3.990	1.690
400	400	600.00	1.200	4.000	0.100
401	401	604.12	1.203	4.010	0.178
402	402	608.25	1.206	4.020	0.255
403	403	612.37	1.209	4.030	0.333
404	404	616.49	1.212	4.040	0.411
405	405	620.62	1.215	4.050	0.489
...	...	...	...	...	...
495	495	991.75	1.485	4.950	7.485
496	496	995.88	1.488	4.960	7.562
497	497	1000.00	1.491	4.970	7.640
498	498	866.67	1.494	4.980	5.140
499	499	733.33	1.497	4.990	2.640
500	500	600.00	1.500	5.000	0.140
501	501	604.12	1.503	5.010	0.250
502	502	608.25	1.506	5.020	0.360
503	503	612.37	1.509	5.030	0.469
504	504	616.49	1.512	5.040	0.579
505	505	620.62	1.515	5.050	0.689
...	...	...	...	...	...
595	595	991.75	1.785	5.950	10.570
596	596	995.88	1.788	5.960	10.680
597	597	1000.00	1.791	5.970	10.790
598	598	866.67	1.794	5.980	7.260
599	599	733.33	1.797	5.990	3.730
600	600	600.00	1.800	6.000	0.200
601	601	604.12	1.803	6.010	0.345
602	602	608.25	1.806	6.020	0.490
603	603	612.37	1.809	6.030	0.635
604	604	616.49	1.812	6.040	0.780
605	605	620.62	1.815	6.050	0.925
...	...	...	...	...	...
695	695	991.75	2.085	6.950	13.970
696	696	995.88	2.088	6.960	14.115
697	697	1000.00	2.091	6.970	14.260
698	698	866.67	2.094	6.980	9.593
699	699	733.33	2.097	6.990	4.927
700	700	600.00	2.100	7.000	0.260
701	701	604.12	2.103	7.010	0.443
702	702	608.25	2.106	7.020	0.626
703	703	612.37	2.109	7.030	0.808
704	704	616.49	2.112	7.040	0.991
705	705	620.62	2.115	7.050	1.174
...	...	...	...	...	...
795	795	991.75	2.385	7.950	17.624
796	796	995.88	2.388	7.960	17.807

797	797	1000.00	2.391	7.970	17.990
798	798	866.67	2.394	7.980	12.103
799	799	733.33	2.397	7.990	6.217
800	800	600.00	2.400	8.000	0.330
801	801	604.12	2.403	8.010	0.553
802	802	608.25	2.406	8.020	0.776
803	803	612.37	2.409	8.030	0.999
804	804	616.49	2.412	8.040	1.222
805	805	620.62	2.415	8.050	1.445
...	...	...	...	...	...
895	895	991.75	2.685	8.950	21.514
896	896	995.88	2.688	8.960	21.737
897	897	1000.00	2.691	8.970	21.960
898	898	866.67	2.694	8.980	14.777
899	899	733.33	2.697	8.990	7.593
900	900	600.00	2.700	9.000	0.410
901	901	604.12	2.703	9.010	0.675
902	902	608.25	2.706	9.020	0.940
903	903	612.37	2.709	9.030	1.205
904	904	616.49	2.712	9.040	1.471
905	905	620.62	2.715	9.050	1.736
...	...	...	...	...	...
995	995	991.75	2.985	9.950	25.600
996	996	995.88	2.988	9.960	25.865
997	997	1000.00	2.991	9.970	26.130
998	998	866.67	2.994	9.980	17.587
999	999	733.33	2.997	9.990	9.043
1000	1000	600.00	3.000	10.000	0.500

II.5 Irradiation History for Case 9:

Ellapsed time (days)	Full Power Days	Irradiation Temp. (°C)	Fast Fluence (10^21nvt)	Burnup (% FIMA)
0	0	1030	0.000	0.000
4.45	4.45	1030	0.105	0.240
8.9	8.9	1030	0.210	0.479
13.35	13.35	1030	0.315	0.719
17.8	17.8	1030	0.420	0.958
22.25	22.25	1030	0.525	1.198
26.7	26.7	1030	0.630	1.437
31.15	31.15	1030	0.735	1.677
35.6	35.6	1030	0.840	1.916
40.05	40.05	1030	0.945	2.156
44.5	44.5	1030	1.050	2.395
48.95	48.95	1030	1.155	2.635
53.4	53.4	1030	1.260	2.874
57.85	57.85	1030	1.365	3.114
62.3	62.3	1030	1.470	3.353
66.75	66.75	1030	1.575	3.593
71.2	71.2	1030	1.680	3.832
75.65	75.65	1030	1.785	4.072
80.1	80.1	1030	1.890	4.311
84.55	84.55	1030	1.995	4.551
89	89	1030	2.100	4.790

II.6 Irradiation History for Case 10:

Ellapsed time (days)	Full Power Days	Irradiation Temp. (°C)	Fast Fluence (10^21nvt)	Burnup (% FIMA)
0	0	1030	0.000	0.000
4.45	4.45	1030	0.105	0.240
8.9	8.9	1030	0.210	0.479
13.35	13.35	1030	0.315	0.719
17.8	17.8	1030	0.420	0.958
22.25	22.25	1030	0.525	1.198
26.7	26.7	1030	0.630	1.437
31.15	31.15	1030	0.735	1.677
35.6	35.6	1030	0.840	1.916
40.05	40.05	1030	0.945	2.156
44.5	44.5	1030	1.050	2.395
48.95	48.95	1030	1.155	2.635
53.4	53.4	1030	1.260	2.874
57.85	57.85	1030	1.365	3.114
62.3	62.3	1030	1.470	3.353
66.75	66.75	1030	1.575	3.593
71.2	71.2	1030	1.680	3.832
75.65	75.65	1030	1.785	4.072
80.1	80.1	1030	1.890	4.311
84.55	84.55	1030	1.995	4.551
89	89	1030	2.100	4.790

II.7 Irradiation History for Case 12:

Ellapsed time (days)	Full Power Days	Irradiation Temp. (°C)	Fast Fluence (10^21nvt)	Burnup (% FIMA)
0	0	987	0.000	0.000
2	2	987	0.045	0.929
4	4	987	0.089	1.859
6	6	987	0.134	2.788
8	8	987	0.179	3.718
10	10	987	0.224	4.647
12	12	987	0.268	5.576
14	14	987	0.313	6.506
16	16	987	0.358	7.435
18	18	987	0.402	8.365
20	20	987	0.447	9.294
22	22	987	0.492	10.224
24	24	987	0.536	11.153
26	26	987	0.581	12.082
28	28	987	0.626	13.012
30	30	987	0.671	13.941
32	32	987	0.715	14.871
34	34	987	0.760	15.800
36	36	987	0.805	16.729
38	38	987	0.849	17.659
40	40	987	0.894	18.588
...	...	...	...	...
130	130	987	2.906	60.412
132	132	987	2.951	61.341
134	134	987	2.995	62.271
136	136	987	3.04	63.2
138	138	987	3.085	64.129
140	140	987	3.129	65.059
142	142	987	3.174	65.988
144	144	987	3.219	66.918
146	146	987	3.264	67.847
148	148	987	3.308	68.776
150	150	987	3.353	69.706
152	152	987	3.398	70.635
154	154	987	3.442	71.565
156	156	987	3.487	72.494
158	158	987	3.532	73.424
160	160	987	3.576	74.353
162	162	987	3.621	75.282
164	164	987	3.666	76.212
166	166	987	3.711	77.141
168	168	987	3.755	78.071
170	170	987	3.8	79

II.8 Irradiation History for Case 13:

Ellapsed time (days)	Full Power Days	Irradiation Temp. (°C)	Fast Fluence (10^21nvt)	Burnup (% FIMA)
0	0	1025	0.000	0.000
10	10	1025	0.090	0.333
20	20	1025	0.180	0.667
30	30	1025	0.270	1.000
40	40	1025	0.360	1.333
50	50	1025	0.450	1.667
60	60	1025	0.540	2.000
70	80	1025	0.720	2.667
80	100	1025	0.900	3.333
90	120	1025	1.080	4.000
100	140	1025	1.260	4.667
110	160	1025	1.440	5.333
120	180	1025	1.620	6.000
130	200	1025	1.800	6.667
140	220	1025	1.980	7.333
150	240	1025	2.160	8.000
160	260	1025	2.340	8.667
170	280	1025	2.520	9.333
180	300	1025	2.700	10.000
190	320	1025	2.880	10.667
200	340	1025	3.060	11.333
210	360	1025	3.240	12.000
220	380	1025	3.420	12.667
230	400	1025	3.600	13.333
240	420	1025	3.780	14.000
250	440	1025	3.960	14.667
260	460	1025	4.140	15.333
270	480	1025	4.320	16.000
280	500	1025	4.500	16.667
290	520	1025	4.680	17.333
300	540	1025	4.860	18.000
310	560	1025	5.040	18.667
320	580	1025	5.220	19.333
330	600	1025	5.400	20.000

II.9 Irradiation History for Case 14:

Ellapsed time (days)	Full Power Days	Irradiation Temp. (°C)	Fast Fluence (10^21nvt)	Burnup (% FIMA)
0	0	1050	0.000	0.000
10	10	1050	0.129	0.286
20	20	1050	0.257	0.571
30	30	1050	0.386	0.857
40	40	1050	0.514	1.143
50	50	1050	0.643	1.429
60	60	1050	0.771	1.714
70	70	1050	0.900	2.000
90	90	1050	1.157	2.571
110	110	1050	1.414	3.143
130	130	1050	1.671	3.714
150	150	1050	1.929	4.286
170	170	1050	2.186	4.857
190	190	1050	2.443	5.429
210	210	1050	2.700	6.000
230	230	1050	2.957	6.571
250	250	1050	3.214	7.143
270	270	1050	3.471	7.714
290	290	1050	3.729	8.286
310	310	1050	3.986	8.857
330	330	1050	4.243	9.429
350	350	1050	4.500	10.000

Appendix III – Particle Dimensions

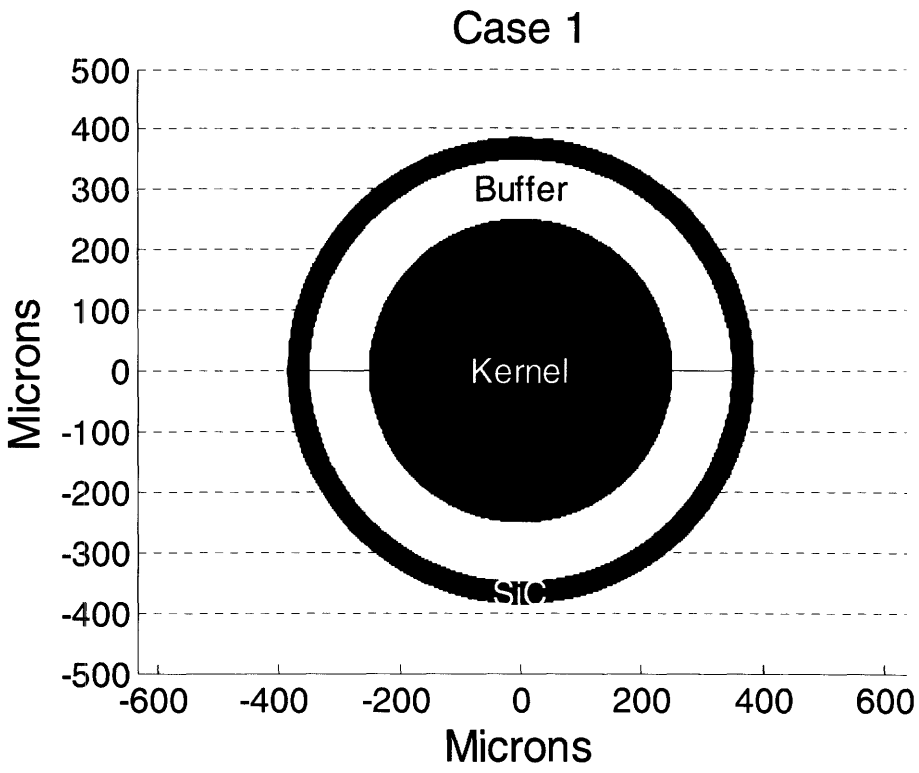

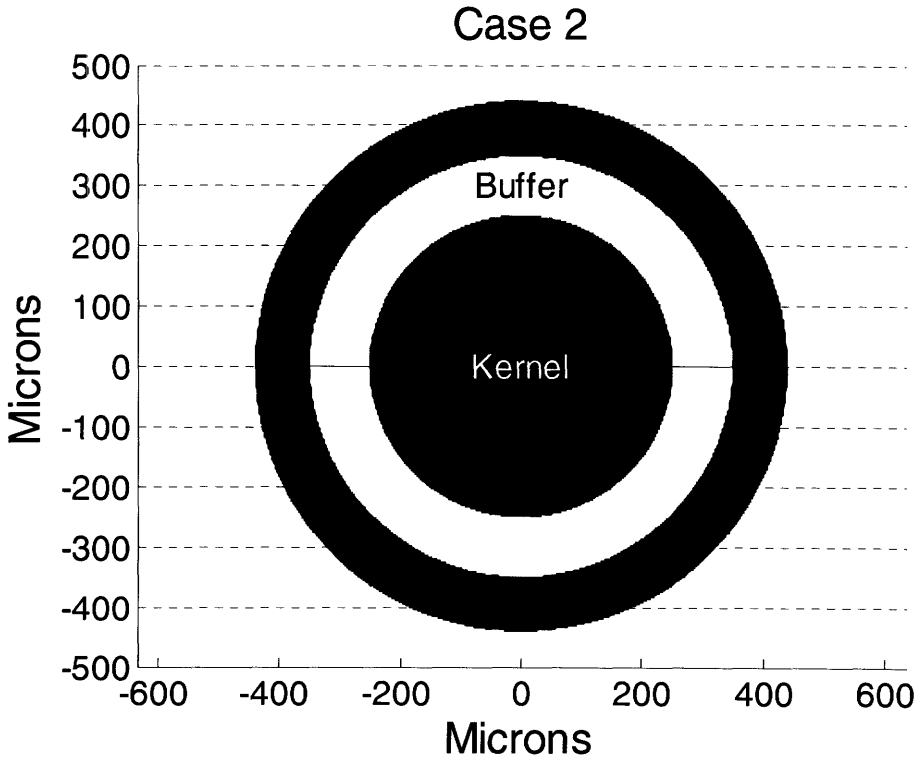

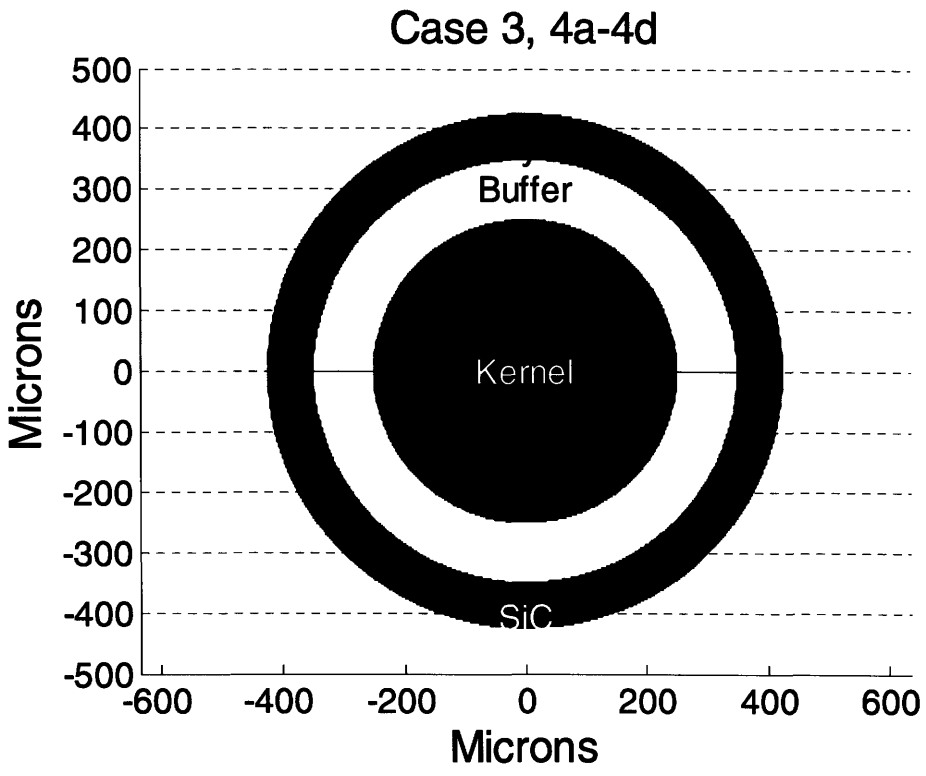
Case 3, 4a-4d
Buffer
Kernel
SiC
Microns
Microns
500
400
300
200
100
0
-100
-200
-300
-400
-500
-600
-400
-200
0
200
400
600

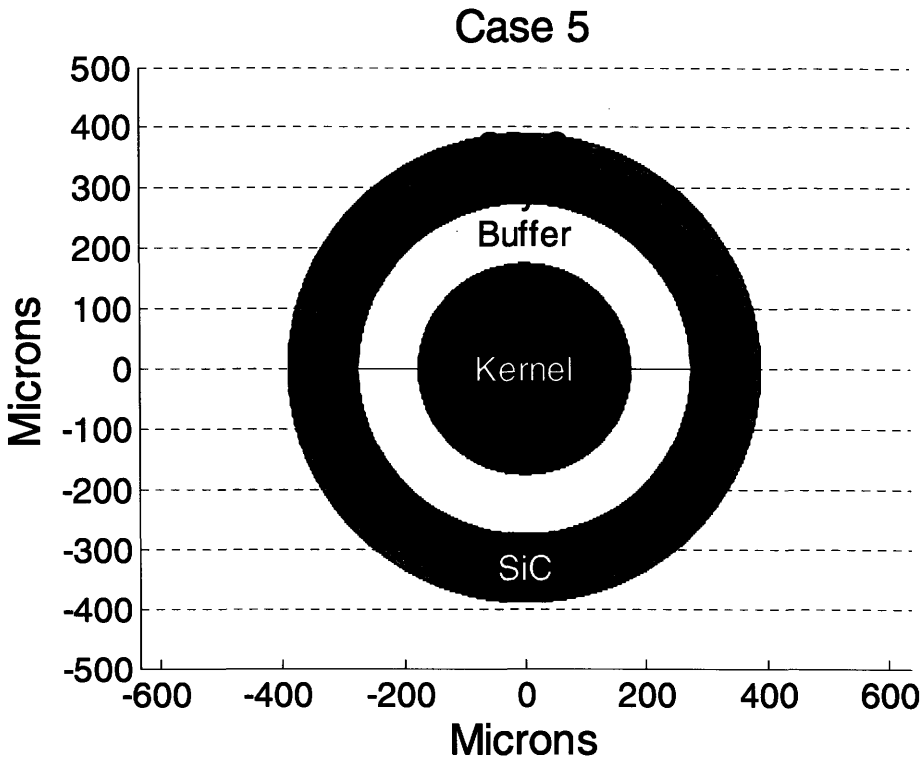
Case 5
Buffer
Kernel
SiC
Microns
Microns
500
400
300
200
100
0
-100
-200
-300
-400
-500
-600
-400
-200
0
200
400
600

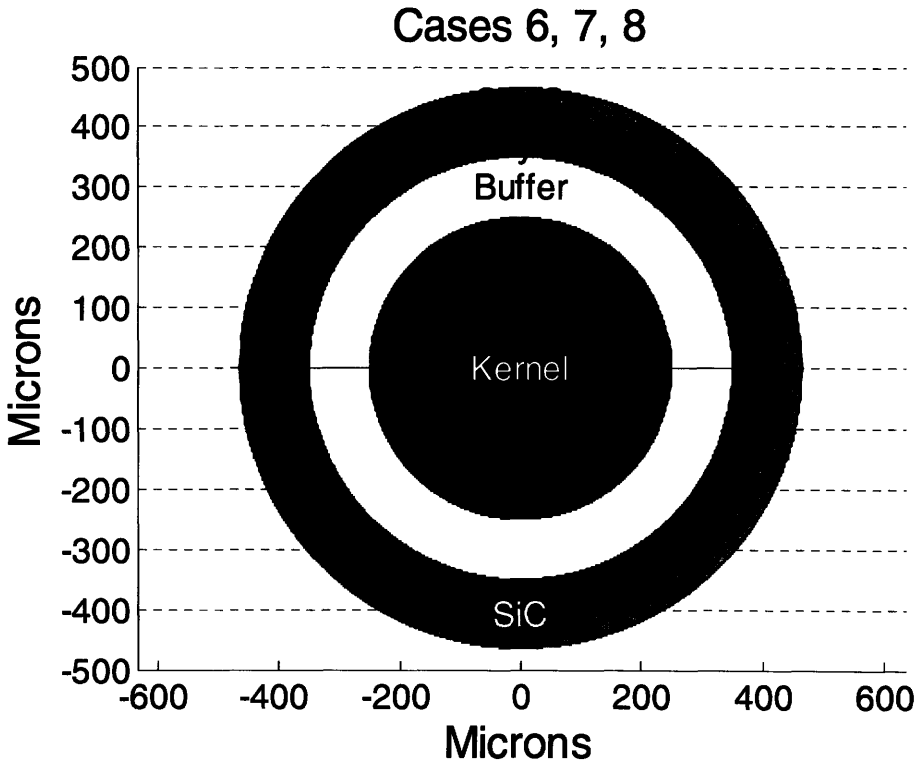
Cases 6, 7, 8
500
400
300
200
100
0
-100
-200
-300
-400
-500
Microns
Buffer
Kernel
SiC
-600
-400
-200
0
200
400
600
Microns

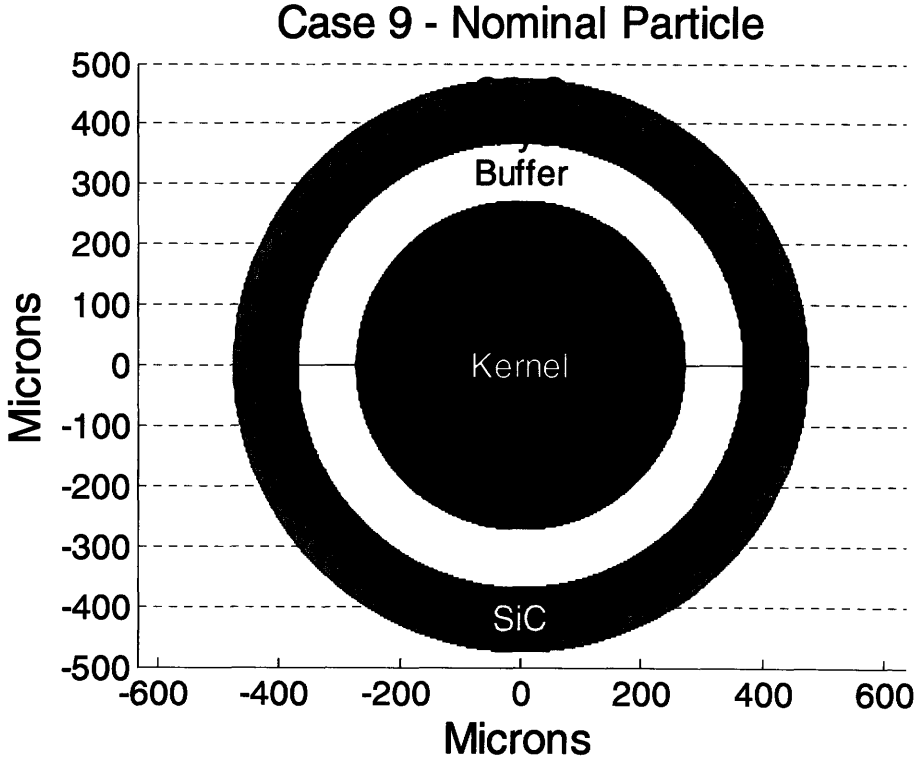
Case 9 - Nominal Particle
500
400
300
200
100
0
-100
-200
-300
-400
-500
Microns
Buffer
Kernel
SiC
-600
-400
-200
0
200
400
600
Microns

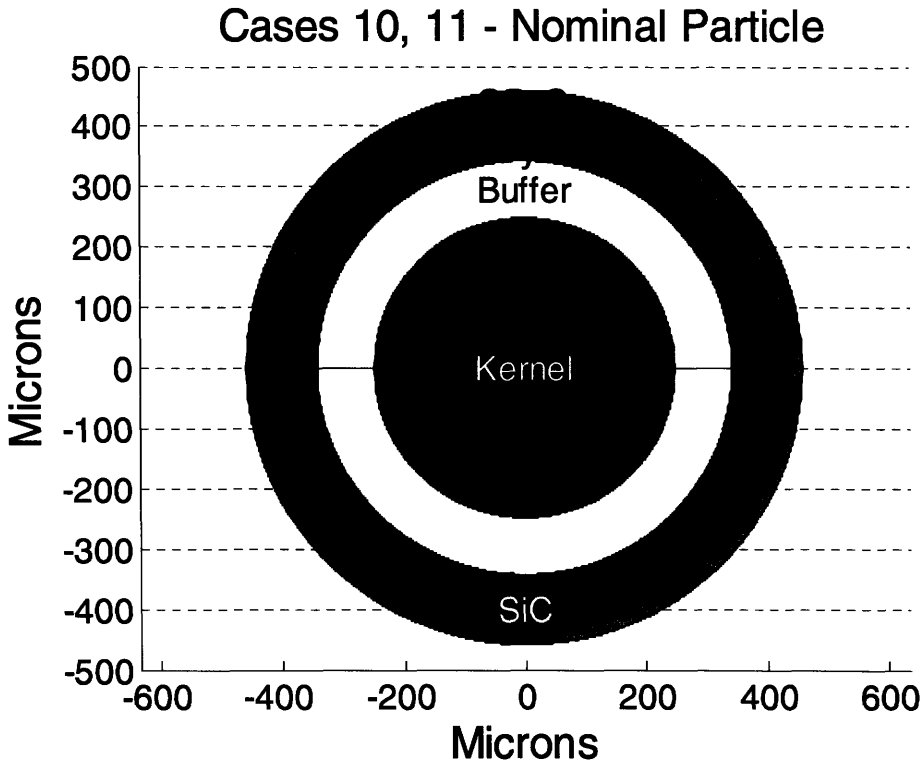
Cases 10, 11 - Nominal Particle
Buffer
Kernel
SiC
Microns
Microns
500
400
300
200
100
0
-100
-200
-300
-400
-500
-600
-400
-200
0
200
400
600

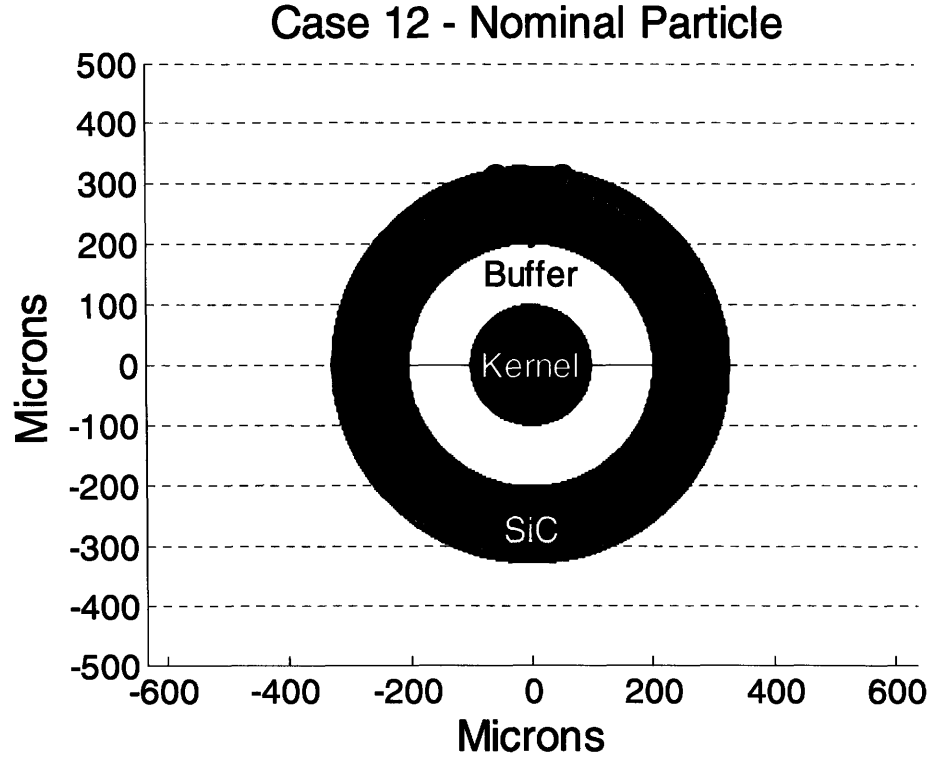
Case 12 - Nominal Particle
Buffer
Kernel
SiC
Microns
Microns
500
400
300
200
100
0
-100
-200
-300
-400
-500
-600
-400
-200
0
200
400
600

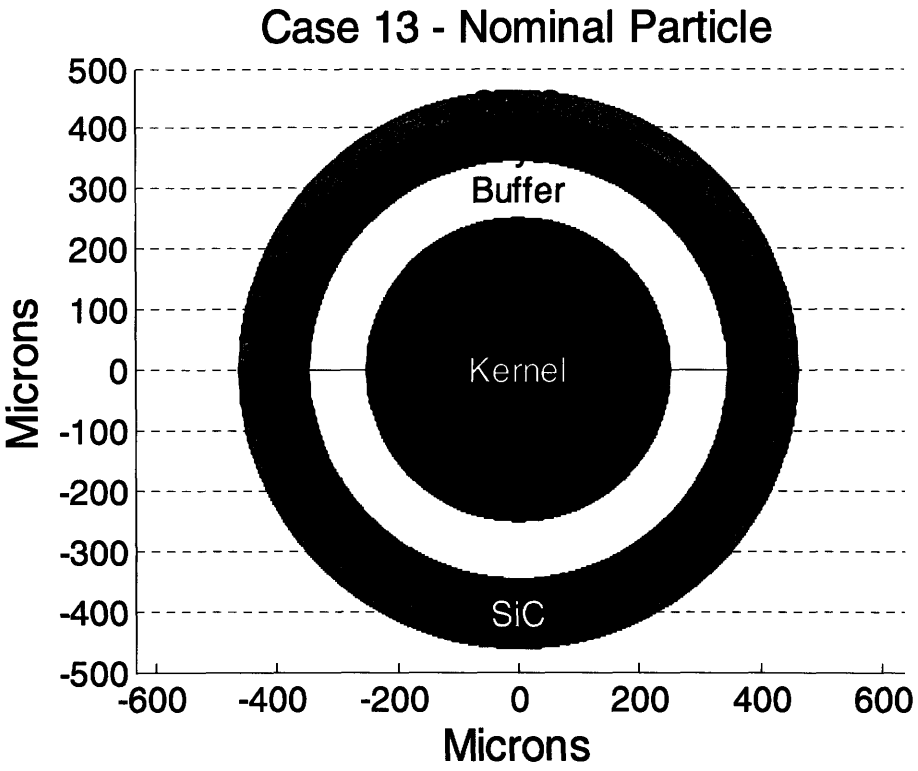
Case 13 - Nominal Particle
Buffer
Kernel
SiC
Microns
Microns
500
400
300
200
100
0
-100
-200
-300
-400
-500
-600
-400
-200
0
200
400
600

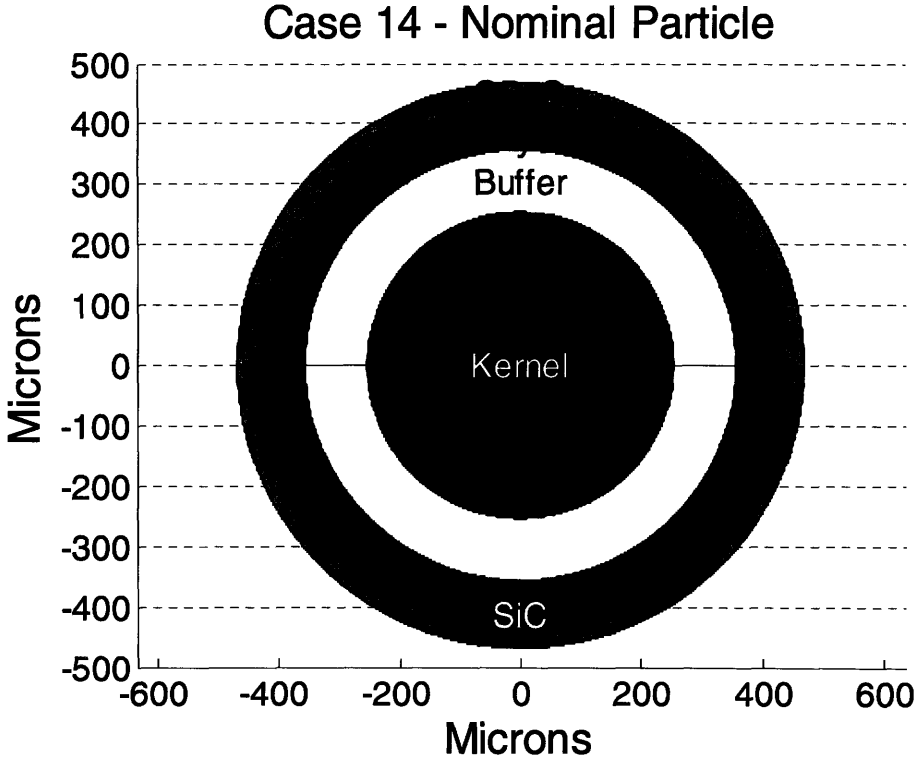
Case 14 - Nominal Particle
Buffer
Kernel
SiC
Microns
Microns
500
400
300
200
100
0
-100
-200
-300
-400
-500
-600
-400
-200
0
200
400
600

Appendix IV – EDF 3981 Rev. 2

431.02
01/30/2003
Rev. 11

ENGINEERING DESIGN FILE

EDF No.: 3981 EDF Rev. No.: 2 Project File No.: 23841

1. Title: TRISO-Coated Particle Fuel Performance Benchmark Cases

2. Index Codes:
   Building/Type N/A SSC ID N/A Site Area N/A

3. NPH Performance Category: _____ or ☒ N/A

4. EDF Safety Category: _____ or ☒ N/A SCC Safety Category: _____ or ☒ N/A

5. Summary:
   This EDF presents a benchmark plan for the comparison of particle fuel performance codes. The benchmark is set up in five parts. The first two parts consist of simple analytical cases, the third represents a fuel particle with more complexity added with each subsequent case, the fourth part consists of past irradiation experiments, and the fifth consists of planned experiments. This document incorporates a consistent set of input marterial properties resulting from comments received concerning Revision 1 of this EDF.

6. Review (R) and Approval (A) and Acceptance (Ac) Signatures:
   (See instructions for definitions of terms and significance of signatures.)

	R/A	Typed Name/Organization	Signature	Date
Performer/ Author	N/A	John T. Maki Gregory K. Miller	John T. Maki GK Miller	3/14/05 3-14-05
Technical Checker	R			
Independent Peer Reviewer (if applicable)	R	Darrell L. Knudson	DKnudson	3-14-05
Approver	A	David A. Petti	David Petti	3-14-05
Requestor (if applicable)	Ac			
Doc. Control		Kathryn Jensen	Kathryn Jensen	3-23.05

7. Distribution: (Name and Mail Stop) John R. Cox, MS 3750; Darrell L. Knudson, MS 3840; Robert E. Korenke, MS 3750; John T. Maki, MS 3870; Gregory K. Miller, MS 3765; David A. Petti, MS 3860; W.L. Stoneberg, MS 3750

8. Does document contain sensitive unclassified information? ☐ Yes ☒ No
   If Yes, what category:

9. Can document be externally distributed? ☒ Yes ☐ No

10. Uniform File Code: Disposition Authority:
    Record Retention Period:

11. For QA Records Classification Only: ☐ Lifetime ☐ Nonpermanent ☐ Permanent
    Item and activity to which the QA Record apply:

12. NRC related? ☐ Yes ☒ No

ENGINEERING DESIGN FILE

EDF No.: 3981 EDF Rev. No.: 2 Project File No.: 23841

1. Title: TRISO-Coated Particle Fuel Performance Benchmark Cases
2. Index Codes: Building/Type N/A SSC ID N/A Site Area N/A
13. Registered Professional Engineer's Stamp (if required)

ENGINEERING DESIGN FILE

TRISO-Coated Particle Fuel Performance Benchmark Cases

John T. Maki
Gregory K. Miller

March 14, 2005

Foreword

This document describes a set of code benchmarking activities that will be used to compare normal operation, coated fuel particle performance codes around the world. These activities are part of an International Atomic Energy Agency (IAEA) Coordinated Research Program (CRP) on coated particle fuel technology. Expected participants in the code benchmark are the United States (Idaho National Laboratory (INL) and Massachusetts Institute of Technology (MIT)), United Kingdom (UK), Russia, France and Germany. Each participant is funded separately for this activity. Only the INL work is funded by the Department of Energy (DOE) Advanced Gas Reactor (AGR) Fuel Development and Qualification Program. This document also serves as the starting point for verification and validation of the PARFUME code for the AGR Fuel Development and Qualification Program. Revision 1 of this document incorporates comments made by AGR participants on formal comment resolution forms based on the original issuance of the document. It also incorporates informal comments made by international benchmark participants at the last IAEA CRP meeting in December 2003. Revision 2 incorporates a consistent set of input material properties to be used for the benchmark cases. This allows a more direct comparison of code results by eliminating a potential source of variability.

TRISO-Coated Particle Fuel Performance Benchmark Cases

March 14, 2005

Introduction

This benchmark is set up in five parts. In the first part, we begin with simple analytical cases to test simple thermo-mechanical behavior. Pyrocarbon layer behavior is tested in the second part. The third part represents a single particle with more complexity added with each subsequent case. These three parts should allow us to test different segments of our structural models under controlled conditions. In the fourth part, we propose more complicated benchmarks of actual experiments that have been completed while the fifth part encompasses planned experiments. Since this is part of a six year research plan, we welcome other experiments from the participating members.

Benchmark Cases 1 through 8 are for single particles while the remaining cases represent a population of particles within an experiment. Input parameters for the simple analytical cases, Cases 1 through 3, are listed in Table 1. Table 2 lists the input parameters for the analytical pyrocarbon layer cases, Cases 4a through 4d. These cases do have unrealistic input parameters such as zero burnup and a finite internal gas pressure. This is intended to reduce the model variability among the different codes. Input parameters for the single particle cases, Cases 5 through 8, are listed in Table 3, input for past irradiation experiments, Cases 9 through 12, are listed in Table 4, and input for future irradiation experiments, Cases 13 and 14 are listed in Table 5. Internal pressure for these cases (Cases 9 through 14) must be determined by each code. Note that fast neutron fluences listed in the tables are for energies greater than 0.18 MeV (29 fJ). To convert fast fluences to energies greater than 0.10 MeV (16 fJ), multiply the listed fluences by a factor of 1.10. Assume that both burnup and fast fluence accumulate linearly with time (effective full power days) for all cases. Input parameters or model correlations not specified in the tables should be supplied by the participant.

Unless noted below, material properties listed in Tables 1 through 5 are based upon values documented by CEGA (CEGA, 1993).

Based upon evaluations of the US New Production Reactor (NPR) experiments (Miller, 2003), the pyrocarbon creep coefficients for Cases 1 through 7 and Case 12 are increased by a factor of 2 over those reported by CEGA. For Case 8, the pyrocarbon creep coefficient is to vary over the temperature range of 873 to 1273 K according to Correlation (d) given below Table 3.

For Cases 1 through 7, the particle is considered to be thermally stress free. Therefore, thermal expansion coefficients are not actually needed for these cases. For Case 8, the particle is considered to be thermally stress free at the initial temperature of 873 K. Differential expansion stresses occur as the irradiation temperature changes. The PyC

thermal expansion coefficient given in Table 1 for Case 8 is representative of the average temperature of 1073 K.

The PyC swelling is assumed to be isotropic for cases 4a and 4c.

Since Cases 1 through 8 consider only a single particle, mean strengths and Weibull moduli do not apply.

It is intended that Cases 1 through 8 focus only on the behavior of the outer coating layers (IPyC, SiC, OPyC). There is no temperature variation assumed through the coating layers. Except for the internal gas pressure that is applied to the inner surface of the IPyC, the kernel and buffer are assumed not to interact with the outer layers. Internal pressures for these cases are provided in the input parameter tables.

For the irradiation experiment cases other than Case 12, material properties are based upon those used in the STRESS3 Code (Martin, 2001). The SiC mean strength and Weibull modulus for these cases (except Case 12) are based on data obtained from H. Nabielek (Nabielek, 2003). Material properties for Case 12 are based upon the values documented by CEGA (CEGA, 1993). As was done for Cases 1 through 7, the pyrocarbon creep coefficient reported by CEGA was multiplied by a factor of 2 based upon NPR experiment evaluations (Miller, 2003).

The comparison metric for Cases 1 through 8 is the maximum stress, either compressive or tensile but whichever has the greatest magnitude, occurring within the indicated layer. Only the tangential stress should be reported for Cases 1 through 3 while both the tangential and radial stress histories (as a function of fast neuron fluence) should be reported for Cases 4a through 4d. The tangential stress history (also as a function of fast neutron fluence) should be reported for Cases 5 through 8. These stress histories should be for the location within the indicated layer where the stress reaches a maximum value. For the irradiation experiment cases, past and future, the primary comparison metric is the particle failure fraction reported as a function of burnup (% FIMA). Failure is defined in this case as a through-wall SiC crack. Other results that should be also reported as a function of burnup for the irradiation experiment cases include the total internal gas pressure, internal gas pressure due to CO and due to fission product gases, and maximum SiC tangential stresses. For each case, these metrics should be for a nominal particle irradiated under the same conditions used to determine the failure fraction history.

A brief description of each benchmark case follows.

Case 1 – Elastic SiC

This particle has a kernel diameter of 500 μm and a buffer thickness of 100 μm. It has only one coating layer, a 35-μm thick SiC layer. Therefore, the coating behavior is elastic.

Case 2 - Simple BISO

This particle is the same as in Case 1, except that the single coating is a 90 μm thick IPyC layer. The BAF for the IPyC material is assumed to have a value of 1.0.

Case 3 – IPyC/SiC Composite without fluence

This particle has two coating layers, an IPyC and SiC layer. The BAF for the IPyC in this case is 1.03.

Case 4a – IPyC/SiC Composite with no creep and constant swelling

This is the same particle as in Case 3, except that it experiences a fast neutron fluence with the IPyC layer imposed to swell. The internal pressure of 25 MPa is assumed to be constant.

Case 4b – IPyC/SiC Composite with constant creep and no swelling

This is the same particle as in Case 3, except that it experiences a fast neutron fluence with the IPyC layer imposed to creep. The internal pressure of 25 MPa is assumed to be constant.

Case 4c – IPyC/SiC Composite with constant creep and constant swelling

This is the same particle as in Case 3, except that it experiences a fast neutron fluence with the IPyC layer imposed to creep and swell at constant rates. The internal pressure of 25 MPa is assumed to be constant.

Case 4d – IPyC/SiC Composite with constant creep and fluence dependent swelling

This is the same particle as in Case 3, except that it experiences a fast neutron fluence with the IPyC layer swelling at a variable rate. The internal pressure of 25 MPa is assumed to be constant.

Case 5 – TRISO, 350-μm kernel

This is a full three layer (TRISO) coated particle with a 350 μm diameter kernel under realistic service conditions.

Case 6 – TRISO, 500-μm kernel

This TRISO coated particle has a 500 μm diameter kernel with all other parameters the same as in Case 5.

Case 7 – TRISO, high BAF

This particle is the same as in Case 6 except that the pyrocarbon BAF is increased to 1.06.

Case 8 – TRISO, cyclic temperature history

This is a TRISO particle subjected to a cyclic temperature history characteristic of fuel in a pebble bed reactor. It is assumed that the particle experiences ten cycles where the temperature is initially 873 K and increases linearly to 1273 K, and then decreases immediately back to 873 K. The period for each cycle is one-tenth the total irradiation time, or 100 days.

Particles from Past Irradiation Experiments

These cases characterize fuel particles from past irradiation experiments. These include the HRB-22 (Japanese) experiment, HFR-K3 (German) experiment, HFR-P4 (German) experiment and the NPR-1 (US) experiment. Parameters for these cases (Petti, et al., 2002; Nabielek, 2003) are listed in Table 4.

Particles from Future Irradiation Experiments

These cases characterize particles from experiments to be completed in the future. Experiments would include HFR EU-1, HFR EU-2, AGR-1 (planned US experiment, details not yet available) and perhaps other experiments to be determined. Parameters for HFR EU-1 and HFR EU-2 (Verfondern and Nabielek, 2000; Conrad, et al., 2002; Nabielek, 2003) are listed in Table 5.

Table 1. Input parameters for analytical thermo-mechanical benchmark cases.

Parameter	**Units**	**Case 1: Elastic SiC**	**Case 2: Simple BISO**	**Case 3: IPyC/ SiC Comp. without fluence**
Fuel Characteristics				
Oxygen to Uranium ratio	atom ratio	2	2	2
Carbon to Uranium ratio	atom ratio	0	0	0
U-235 enrichment	weight %	10	10	10
Kernel diameter	μm	500	500	500
Buffer thickness	μm	100	100	100
IPyC thickness	μm	none	90	40
SiC thickness	μm	35	none	35
OPyC thickness	μm	none	none	none
Kernel density	Mg/m^3	10.8	10.8	10.8
Buffer density	Mg/m^3	0.95	0.95	0.95
IPyC density	Mg/m^3	none	1.9	1.9
SiC density	Mg/m^3	3.20	none	3.20
OPyC density	Mg/m^3	none	none	none
IPyC BAF		none	1.0	1.03
OPyC BAF		none	none	none
Irradiation Conditions				
Irradiation duration	effective full power days	0	0	0
End of life burnup	% FIMA	0	0	0
End of life fluence	10^{25} n/m^2 E > 0.18 Mev	0	0	0
Constant temperature	K	1273	1273	1273
Constant internal pressure	MPa	25	25	25
Ambient pressure	MPa	0.1	0.1	0.1

Table 1 continued. Input parameters for analytical thermo-mechanical benchmark cases.

Parameter	**Units**	**Case 1: Elastic SiC**	**Case 2: Simple BISO**	**Case 3: IPyC/ SiC Comp. without fluence**
Material Properties				
PyC modulus of elasticity	MPa	None	3.96×10^{4}	3.96×10^{4}
PyC Poisson's ratio		None	0.33	0.33
PyC Poisson's ratio in creep		None	None	None
PyC coefficient of thermal expansion	K^{-1}	None	5.50×10^{-6}	5.50×10^{-6}
PyC creep coefficient	$(MPa - 10^{25}$ $n/m^2)^{-1}$, E>0.18 MeV	None	None	None
PyC swelling strain rate	$(\Delta L/L)/10^{25}$ n/m^2, E>0.18 MeV	None	None	None
SiC modulus of elasticity	MPa	3.70×10^{5}	None	3.70×10^{5}
SiC Poisson's ratio		0.13	None	0.13
SiC coefficient of thermal expansion	K^{-1}	4.90×10^{-6}	None	4.90×10^{-6}
Comparison Metrics				
Comparison metric(1)	MPa	maximum SiC tangential stress	maximum IPyC tangential stress	maximum tangential stresses for SiC and IPyC

Note (1): The maximum stress can be either compressive or tensile but whichever has the greatest magnitude occurring within the indicated layer. The location within the indicated layer is where the stress reaches its maximum absolute value.

Table 2. Input parameters for analytical pyrocarbon layer benchmark cases.

Parameter	**Units**	**Case 4a: No creep / constant swelling**	**Case 4b: Constant creep / no swelling**	**Case 4c: Constant creep / constant swelling**	**Case 4d: Constant creep and fluence dependent swelling**
Fuel Characteristics					
Oxygen to Uranium ratio	atom ratio	2	2	2	2
Carbon to Uranium ratio	atom ratio	0	0	0	0
U-235 enrichment	weight %	10	10	10	10
Kernel diameter	μm	500	500	500	500
Buffer thickness	μm	100	100	100	100
IPyC thickness	μm	40	40	40	40
SiC thickness	μm	35	35	35	35
OPyC thickness	μm	none	none	none	none
Kernel density	Mg/m^3	10.8	10.8	10.8	10.8
Buffer density	Mg/m^3	0.95	0.95	0.95	0.95
IPyC density	Mg/m^3	1.9	1.9	1.9	1.9
SiC density	Mg/m^3	3.20	3.20	3.20	3.20
OPyC density	Mg/m^3	none	none	none	none
IPyC BAF		1.03	1.03	1.03	1.03
OPyC BAF		none	none	none	none
Irradiation Conditions					
Irradiation duration	effective full power days	0	0	0	0
End of life burnup	% FIMA	0	0	0	0
End of life fluence	10^{25} n/m^2 $E > 0.18$ Mev	3	3	3	3
Constant temperature	K	1273	1273	1273	1273
Constant internal pressure	MPa	25	25	25	25
Ambient pressure	MPa	0.1	0.1	0.1	0.1

Table 2 continued. Input parameters for analytical pyrocarbon layer benchmark cases.

Parameter	Units	Case 4a: No creep / constant swelling	Case 4b: Constant creep / no swelling	Case 4c: Constant creep / constant swelling	Case 4d: Constant creep and fluence dependent swelling
Material Properties					
PyC modulus of elasticity	MPa	3.96×10^4	3.96×10^4	3.96×10^4	3.96×10^4
PyC Poisson's ratio		0.33	0.33	0.33	0.33
PyC Poisson's ratio in creep		None	0.50	0.50	0.50
PyC coefficient of thermal expansion	K^{-1}	5.50×10^{-6}	5.50×10^{-6}	5.50×10^{-6}	5.50×10^{-6}
PyC creep coefficient	$(MPa - 10^{25}$ $n/m^2)^{-1}$, E>0.18 MeV	None	2.71×10^{-4}	2.71×10^{-4}	2.71×10^{-4}
PyC swelling strain rate	$(\Delta L/L)/10^{25}$ n/m^2, E>0.18 MeV	-0.005 (isotropic)	None	-0.005 (isotropic)	Correlation (a)
SiC modulus of elasticity	MPa	3.70×10^5	3.70×10^5	3.70×10^5	3.70×10^5
SiC Poisson's ratio		0.13	0.13	0.13	0.13
SiC coefficient of thermal expansion	K^{-1}	4.90×10^{-6}	4.90×10^{-6}	4.90×10^{-6}	4.90×10^{-6}
Comparison Metrics					
Comparison metric	MPa	maximum radial stress between IPyC and SiC, maximum tangential IPyC stress (inner surface), and maximum tangential SiC stress (inner surface) as a function of fast neutron fluence			

Correlation (a):

PyC radial swelling/shrinkage rate $[(\Delta L/L)/10^{25}\ n/m^2] =$

$$1.36334 \times 10^{-3}\ x^3 - 7.77024 \times 10^{-3}\ x^2 + 2.00861 \times 10^{-2}\ x - 2.22642 \times 10^{-2}$$

PyC tangential swelling/shrinkage rate $[(\Delta L/L)/10^{25}\ n/m^2] =$

$$-3.53804 \times 10^{-4}\ x^3 + 1.69251 \times 10^{-3}\ x^2 + 2.63307 \times 10^{-3}\ x - 1.91253 \times 10^{-2}$$

where x = (fast neutron fluence)$/10^{25}$ n/m^2 for E>0.18 MeV

Note: divide fast neutron fluences for E>0.10 MeV by a factor of 1.10 to obtain fast neutron fluences for E>0.18 MeV.

Table 3. Input parameters for single particle benchmark cases.

Parameter	**Units**	**Case 5: TRISO 350 μm kernel**	**Case 6: TRISO 500 μm kernel**	**Case 7: TRISO High BAF**	**Case 8: TRISO Cyclic Temp.**
Fuel Characteristics					
Oxygen to Uranium ratio	atom ratio	2	2	2	2
Carbon to Uranium ratio	atom ratio	0	0	0	0
U-235 enrichment	weight %	10	10	10	10
Kernel diameter	μm	350	500	500	500
Buffer thickness	μm	100	100	100	100
IPyC thickness	μm	40	40	40	40
SiC thickness	μm	35	35	35	35
OPyC thickness	μm	40	40	40	40
Kernel density	Mg/m^3	10.8	10.8	10.8	10.8
Buffer density	Mg/m^3	0.95	0.95	0.95	0.95
IPyC density	Mg/m^3	1.9	1.9	1.9	1.9
SiC density	Mg/m^3	3.20	3.20	3.20	3.20
OPyC density	Mg/m^3	1.9	1.9	1.9	1.9
IPyC BAF		1.03	1.03	1.06	1.03
OPyC BAF		1.03	1.03	1.06	1.03
Irradiation Conditions					
Irradiation duration	effective full power days	1000	1000	1000	1000
End of life burnup	% FIMA	10	10	10	10
End of life fluence	10^{25} n/m^2 E>0.18 Mev	3	3	3	3
Constant irradiation temperature(1)	K	1273	1273	1273	873 to 1273 (10 cycles)
End of life internal pressure(2)	MPa	15.54	26.20	26.20	Table 3a
Ambient pressure	MPa	0.1	0.1	0.1	0.1

Note (1): For Cases 5 through 7, temperature is constant through time and constant throughout the particle. For Case 8, temperature increases linearly from 873 to 1273 K for each 100 day cycle and is constant throughout the particle.
Note (2): For Cases 5 through 7, the internal gas pressure increases linearly with time from zero to the listed end of life value. See Table 3a for Case 8 internal pressures.

Table 3 continued. Input parameters for single particle benchmark cases.

Parameter	**Units**	**Case 5: TRISO 350 μm kernel**	**Case 6: TRISO 500 μm kernel**	**Case 7: TRISO High BAF**	**Case 8: TRISO Cyclic Temp.**
Material Properties					
PyC modulus of elasticity	MPa	3.96×10^{4}	3.96×10^{4}	3.96×10^{4}	3.96×10^{4}
PyC Poisson's ratio		0.33	0.33	0.33	0.33
PyC Poisson's ratio in creep		0.50	0.50	0.50	0.50
PyC coefficient of thermal expansion	K^{-1}	5.50×10^{-6}	5.50×10^{-6}	5.50×10^{-6}	5.35×10^{-6}
PyC creep coefficient	$(MPa - 10^{25}$ $n/m^2)^{-1}$, E>0.18 MeV	2.71×10^{-4}	2.71×10^{-4}	2.71×10^{-4}	Correlation (d)
PyC swelling strain rate	$(\Delta L/L)/10^{25}$ n/m^2, E>0.18 MeV	Correlation (a)	Correlation (a)	Correlation (b)	Correlation (c)
SiC modulus of elasticity	MPa	3.70×10^{5}	3.70×10^{5}	3.70×10^{5}	3.70×10^{5}
SiC Poisson's ratio		0.13	0.13	0.13	0.13
SiC coefficient of thermal expansion	K^{-1}	4.90×10^{-6}	4.90×10^{-6}	4.90×10^{-6}	4.90×10^{-6}
Comparison Metrics					
Comparison metric[(1)]	MPa	maximum SiC and IPyC tangential stress as a function of fast neutron fluence			

Note (1): The maximum stress can be either compressive or tensile but whichever has the greatest magnitude occurring within the indicated layer. The location within the indicated layer is where the stress reaches its maximum absolute value.

Correlation (a):

PyC radial swelling/shrinkage rate $[(\Delta L/L)/10^{25}\ n/m^2] =$
$1.36334 \times 10^{-3}\ x^3 - 7.77024 \times 10^{-3}\ x^2 + 2.00861 \times 10^{-2}\ x - 2.22642 \times 10^{-2}$

PyC tangential swelling/shrinkage rate $[(\Delta L/L)/10^{25}\ n/m^2] =$
$-3.53804 \times 10^{-4}\ x^3 + 1.69251 \times 10^{-3}\ x^2 + 2.63307 \times 10^{-3}\ x - 1.91253 \times 10^{-2}$

where x = (fast neutron fluence)/10^{25} n/m^2 for E>0.18 MeV.

Correlation (b):

PyC radial swelling/shrinkage rate $[(\Delta L/L)/10^{25}\ n/m^2] =$
$7.27026 \times 10^{-4}\ x^3 - 5.05553 \times 10^{-3}\ x^2 + 1.83715 \times 10^{-2}\ x - 2.12522 \times 10^{-2}$

PyC tangential swelling/shrinkage rate $[(\Delta L/L)/10^{25}\ n/m^2] =$
$-8.88086 \times 10^{-4}\ x^3 + 5.03465 \times 10^{-3}\ x^2 - 3.42182 \times 10^{-3}\ x - 1.79113 \times 10^{-2}$

where x = (fast neutron fluence)/10^{25} n/m^2 for E>0.18 MeV.

Correlation (c):

PyC radial swelling/shrinkage rate $[(\Delta L/L)/10^{25}\ n/m^2] =$
$4.03266 \times 10^{-4}\ x^3 - 2.25937 \times 10^{-3}\ x^2 + 9.82884 \times 10^{-3}\ x - 1.80613 \times 10^{-2}$

PyC tangential swelling/shrinkage rate $[(\Delta L/L)/10^{25}\ n/m^2] =$
$-4.91648 \times 10^{-4}\ x^3 + 2.32979 \times 10^{-3}\ x^2 + 1.71315 \times 10^{-3}\ x - 1.78392 \times 10^{-2}$

where x = (fast neutron fluence)/10^{25} n/m^2 for E>0.18 MeV.

Note: divide fast neutron fluences for E>0.10 MeV by a factor of 1.10 to obtain fast neutron fluences for E>0.18 MeV.

Correlation (d):

PyC creep coefficient $[(MPa - 10^{25}\ n/m^2)^{-1}$, E>0.18 MeV] =
$4.386 \times 10^{-4} - 9.70 \times 10^{-7}\ T + 8.0294 \times 10^{-10}\ T^2$
where T = temperature in °C.

Table 3a. Internal pressure for Case 8.

Fast Fluence (10^{25} n/m^2, E>0.18 MeV)	**Irradiation Duration** (effective full power days)	**Internal Pressure** (MPa)
0.00	0.00	0.00
0.29	96.67	0.14
0.30	100.00	0.02
0.59	196.67	0.94
0.60	200.00	0.04
0.89	296.67	2.59
0.90	300.00	0.07
1.19	396.67	4.87
1.20	400.00	0.10
1.49	496.67	7.64
1.50	500.00	0.14
1.79	596.67	10.79
1.80	600.00	0.20
2.09	696.67	14.26
2.10	700.00	0.26
2.39	796.67	17.99
2.40	800.00	0.33
2.69	896.67	21.96
2.70	900.00	0.41
2.99	996.67	26.13
3.00	1000.00	0.50

For Case 8, the internal pressure is determined by linearly interpolating between the listed point values of pressure. This pressure history for the first two cycles of Case 8 is illustrated in Figure 1.

It is recognized that the pressure cycles listed for Case 8 are not realistic. The actual pressure is likely to drop off almost instantaneously at the end of each cycle (as well as not increasing exactly linearly). Spreading the pressure drop over a finite time interval in these calculations is intended to alleviate convergence problems that could occur when solving for an instantaneous change in pressure. Likewise, if an instantaneous change in temperature poses difficulties when solving for Case 8, it may similarly be assumed for this exercise that the temperature drop at the end of each cycle occurs over a finite time interval.

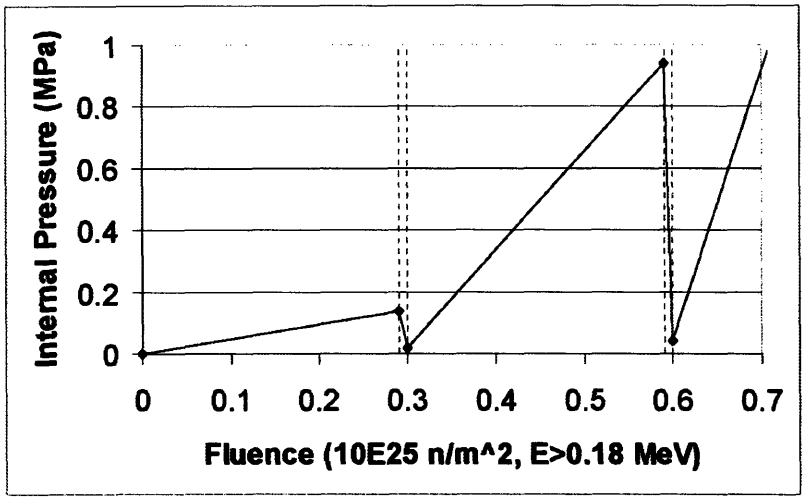

Figure 1. Internal pressure during the first two cycles of Case 8.

Table 4. Input parameters for past irradiation experiments.

Parameter	Units	Case 9: HRB-22	Case 10: HFR-K3 B/2	Case 11: HFR-P4 3	Case 12: NPR-1A 5
Fuel Characteristics					
Oxygen to Uranium ratio	atom ratio	2	2	2	1.51
Carbon to Uranium ratio	atom ratio	0	0	0	0.36
U-235 enrichment	weight %	4.07	9.82	9.82	93.15 ± 0.01
Kernel diameter	μm	544 ± 9	497 ± 14	497 ± 14	200 ± 5
Buffer thickness	μm	97 ± 13	94 ± 10	94 ± 10	102 ± 10
IPyC thickness	μm	33 ± 3	41 ± 4	41 ± 4	53 ± 4
SiC thickness	μm	34 ± 2	36 ± 2	36 ± 2	35 ± 3
OPyC thickness	μm	39 ± 3	40 ± 2	40 ± 2	39 ± 4
Kernel density	Mg/m^3	10.84	10.81	10.81	10.52 ± 0.01
Buffer density	Mg/m^3	1.10	1.00	1.00	0.96 ± 0.05
IPyC density	Mg/m^3	1.85	1.88	1.88	1.92 ± 0.01
SiC density	Mg/m^3	3.20	3.20	3.20	3.23
OPyC density	Mg/m^3	1.85	1.88	1.88	1.86 ± 0.01
IPyC BAF		1.00	1.053	1.053	1.058 ± 0.005
OPyC BAF		1.00	1.019	1.019	1.052 ± 0.006
Irradiation Conditions					
Irradiation duration	effective full power days	89	359	351	170
End of life burnup	% FIMA	4.79	10	14	79
End of life fluence	10^{25} n/m^2 E>0.18 MeV	2.1	5.3	7.2	3.8
Time-average, volume-average irradiation temperature	K	1303	1073	1335	1260
Ambient pressure	MPa	0.1	0.1	0.1	0.1

Notes: The ± values are one standard deviation.
Modeling of irradiation temperature, such as a constant temperature or a distribution of temperatures, is left to the decision of each participant.

Table 4 continued. Input parameters for past irradiation experiments.

Parameter	Units	Case 9: HRB-22	Case 10: HFR-K3 B/2	Case 11: HFR-P4 3	Case 12: NPR-1A 5
Material Properties					
PyC modulus of elasticity	MPa	$3.96x10^4$	$3.96x10^4$	$3.96x10^4$	$3.96x10^4$
PyC Poisson's ratio		0.33	0.33	0.33	0.33
PyC Poisson's ratio in creep		0.40	0.40	0.40	0.50
PyC coefficient of thermal expansion	K^{-1}	$5.50x10^{-6}$	$5.50x10^{-6}$	$5.50x10^{-6}$	$5.50x10^{-6}$
PyC creep coefficient	$(MPa - 10^{25}$ $n/m^2)^{-1}$, E>0.18 MeV	$4.93x10^{-4}$	$4.93x10^{-4}$	$4.93x10^{-4}$	$2.70x10^{-4}$
PyC swelling strain rate[1]	$(\Delta L/L)/10^{25}$ n/m^2, E>0.18 MeV	Correlation (e)	Correlation (e)	Correlation (e)	Correlation (f)
PyC mean strength	MPa	200	200	200	218
PyC Weibull modulus		5.0	5.0	5.0	9.5
SiC modulus of elasticity	MPa	$3.70x10^5$	$3.70x10^5$	$3.70x10^5$	$3.70x10^5$
SiC Poisson's ratio		0.13	0.13	0.13	0.13
SiC coefficient of thermal expansion	K^{-1}	$4.90x10^{-6}$	$4.90x10^{-6}$	$4.90x10^{-6}$	$4.90x10^{-6}$
SiC mean strength	MPa	873	873	873	572
SiC Weibull modulus		8.02	8.02	8.02	6.00
Comparison Metrics					
Comparison metric[2]		Histories as a function of burnup (% FIMA): total particle failure fraction and if calculated, the contribution from each failure mechanism; total internal gas pressure (MPa); partial internal gas pressure due to fission product gas (MPa); partial internal gas pressure due to CO (MPa); and maximum SiC tangential stress (MPa).			

Note (1): Correlations (e) and (f) follow Table 5.
Note (2): The total internal gas pressure, internal gas pressure due to CO and due to fission product gases, and the maximum SiC tangential stress histories are for a nominal particle irradiated under the same conditions as used to calculate the particle failure fractions.

Table 5. Input parameters for future irradiation experiments.

Parameter	Units	Case 13: HFR EU-1	Case 14: HFR EU-2
Fuel Characteristics			
Oxygen to Uranium ratio	atom ratio	2	2
Carbon to Uranium ratio	atom ratio	0	0
U-235 enrichment	weight %	16.7	10.6
Kernel diameter	μm	502 ± 11	508 ± 10
Buffer thickness	μm	95 ± 14	102 ± 12
IPyC thickness	μm	41 ± 3	39 ± 4
SiC thickness	μm	35 ± 2	36 ± 2
OPyC thickness	μm	40 ± 4	38 ± 4
Kernel density	Mg/m^3	10.81	10.72
Buffer density	Mg/m^3	1.01	1.02
IPyC density	Mg/m^3	1.87	1.92
SiC density	Mg/m^3	3.20	3.20
OPyC density	Mg/m^3	1.87	1.92
IPyC BAF		1.02	1.04
OPyC BAF		1.02	1.02
Irradiation Conditions			
Irradiation duration	effective full power days	600	350
End of life burnup	% FIMA	20	10
End of life fluence	10^{25} n/m^2 E > 0.18 MeV	5.4	4.5
Time-average, volume-average irradiation temperature	K	1298	1323
Ambient pressure	MPa	0.1	0.1

Notes: The ± values are one standard deviation.
Modeling of irradiation temperature, such as a constant temperature or a distribution of temperatures, is left to the decision of each participant. For example, some participants have chosen 1223 and 1373 K to represent the surface and center temperatures of a fuel sphere in HFR EU-1.

Table 5 continued. Input parameters for future irradiation experiments.

Parameter	Units	Case 13: HFR EU-1	Case 14: HFR EU-2
Material Properties			
PyC modulus of elasticity	MPa	3.96×10^4	3.96×10^4
PyC Poisson's ratio		0.33	0.33
PyC Poisson's ratio in creep		0.40	0.40
PyC coefficient of thermal expansion	K^{-1}	5.50×10^{-6}	5.50×10^{-6}
PyC creep coefficient	$(MPa - 10^{25}/m^2)^{-1}$, E>0.18 MeV	4.93×10^{-4}	4.93×10^{-4}
PyC swelling strain rate	$(\Delta L/L)/10^{25}$ n/m^2, E>0.18 MeV	Correlation (e)	Correlation (e)
PyC mean strength	MPa	200	200
PyC Weibull modulus		5.0	5.0
SiC modulus of elasticity	MPa	3.70×10^5	3.70×10^5
SiC Poisson's ratio		0.13	0.13
SiC coefficient of thermal expansion	K^{-1}	4.90×10^{-6}	4.90×10^{-6}
SiC mean strength	MPa	873	873
SiC Weibull modulus		8.02	8.02
Comparison Metrics			
Comparison metric[(1)]		Histories as a function of burnup (% FIMA): total particle failure fraction and if calculated, the contribution from each failure mechanism; total internal gas pressure (MPa); partial internal gas pressure due to fission product gas (MPa); partial internal gas pressure due to CO (MPa); and maximum SiC tangential stress (MPa).	

Note (1): The total internal gas pressure, internal gas pressure due to CO and due to fission product gases, and the maximum SiC tangential stress histories are for a nominal particle irradiated under the same conditions as used to calculate the particle failure fractions.

Correlation (e):

Fast neutron fluence (10^{25} n/m^2), E> 0.18 MeV = x

for x ≤ 6.08,

PyC radial swelling rate [$(\Delta L/L)/10^{25}$ n/m^2, E>0.18 MeV] =
$4.52013\times10^{-4}\,x^5 - 8.36313\times10^{-3}\,x^4 + 5.67549\times10^{-2}\,x^3 - 1.74247\times10^{-1}\,x^2 + 2.62692\times10^{-1}\,x - 1.43234\times10^{-1}$

for x > 6.08,

PyC radial swelling rate[$(\Delta L/L)/10^{25}$ n/m^2, E>0.18 MeV] = 0.0954

For x ≤ 6.08,

PyC tangential swelling rate [$(\Delta L/L)/10^{25}$ n/m^2, E>0.18 MeV] =
$1.30457\times10^{-4}\,x^3 - 2.10029\times10^{-3}\,x^2 + 9.07826\times10^{-3}\,x - 3.24737\times10^{-2}$

for x > 6.08,

PyC tangential swelling rate [$(\Delta L/L)/10^{25}$ n/m^2, E>0.18 MeV] = -0.0249

Correlation (f):

PyC radial swelling rate [$(\Delta L/L)/10^{25}$ n/m^2, E>0.18 MeV] =
$4.73765\times10^{-4}\,x^3 - 3.80252\times10^{-3}\,x^2 + 1.64999\times10^{-2}\,x - 2.13483\times10^{-2}$

PyC tangential swelling rate [$(\Delta L/L)/10^{25}$ n/m^2, E>0.18 MeV] =
$-1.03249\times10^{-3}\,x^3 + 5.47396\times10^{-3}\,x^2 - 3.29740\times10^{-3}\,x - 1.83549\times10^{-2}$

where x = fast neutron fluence (10^{25} n/m^2) for E> 0.18 MeV.

Note: Divide fast neutron fluences for E > 0.10 MeV by a factor of 1.10 to obtain fast neutron fluences for E > 0.18 MeV.

References

CEGA Corporation, "NP-MHTGR Material Models of Pyrocarbon and Pyrolytic Silicon Carbide", CEGA-002920, Rev. 1, July 1993.

R. Conrad, K. Bakker, H. Nabielek, D. MacEachern, W. Scheffel and P. Guillermier, "HFR-EU2 Test Specification for Irradiation Experiment of GT-MHR Compacts in the HFR Petten Within HTR-TN", Technical Memorandum HFR/01/4679 Rev. 2, April 26, 2002.

D. G. Martin, "Physical and Mechanical Properties of the Constituents of Coated Fuel Particlles and the Effect of Irradiation", HTR-F WP3 Proceedings, Lyon, France, October 2001.

G. K. Miller, D. A. Petti, and J. T. Maki, "Statistical Approach and Benchmarking for Modeling of Multi-dimensional Behavior in TRISO-coated Fuel Particles". J. Nucl. Materials, 317 (2003) p. 69.

H. Nabielek, personal communications, 2003.

D.A. Petti, J.T. Maki, J. Buongiorno, R.R. Hobbins, and G.K. Miller, "Key Differences in the Fabrication, Irradiation and Safety Testing of U.S. and German TRISO-coated Particle Fuel and Their Implications on Fuel Performance," INEEL/EXT-02-00300, June 2002.

K. Verfondern, and H. Nabielek, "Proposal for Irradiation Experiment HFR-EU1", Forschungszentrum Jülich, HTR-F-WP2-001/2000, draft revision 0.1, May 27, 2000.